Functional description of the monitoring and observability detailed concepts for the Pan-European Control Schemes

ELECTRA Deliverable D5.4. WP5: Increased Observability

Marinelli, Mattia; Pertl, Michael; Rezkalla, Michel M.N.; Kosmecki, Michael; Sobczak , Bogdan; Jankowski , Robert; Kubanek , Arkadiusz; Morch, Andrei Z. ; Reigstad, Tor Inge ; Obushevs, Artjoms

Total number of authors:
13

Publication date:
2017

Document Version
Publisher's PDF, also known as Version of record

Project No. 609687

FP7-ENERGY-2013-IRP

ELECTRA

European Liaison on Electricity Committed Towards long-term Research Activities for Smart Grids

WP 5

Increased Observability

Deliverable 5.4

Functional description of the monitoring and observability detailed concepts for the Pan-European Control Schemes

20/01/2017

ID&Title	D5.4 “Functional description of the monitoring and observability detailed concepts for the Pan-European Control Schemes”	Number of pages:	122

Short description (Max. 50 words):

Deliverable D5.4 outlines the methodology and the topics analysed in T5.4 for deriving Pan-European observables within the Web-of-Cells (WoC) concept. Observables are derived by analysing traditional instability events typical of large power systems.

Version	Date	Modification’s nature
V0.01	31/08/2015	First Draft
V0.02	02/12/2015	Revised Draft
V0.03	17/12/2015	Final Draft
V1.00	18/12/2015	Document issued for Internal Review
V1.10	15/01/2016	Comments from the Internal Review implemented
V2.00	19/01/2016	Document issued
V3.00	23/11/2016	Document extended as planned
V3.10	13/12/2016	Final version of the document issued for Internal Review
V4.00	19/01/2017	Final version

Accessibility

☒ PU, Public

☐ PP, Restricted to other program participants (including the Commission Services)

☐ RE, Restricted to other a group specified by the consortium (including the Commission Services)

☐ CO, Confidential, only for members of the consortium (including the Commission Services)

If restricted, please specify here the group:	

Owner / Main responsible:

Task 5.4 Leader:	Mattia Marinelli (DTU)	

Reviewed by:

(WP5 Leader:)	Andrei Morch (SINTEF)	18/01/2017

(Technical Project Coordinator:) (Project Coordinator:)	Helfried Brunner (AIT) Luciano Martini (RSE)	
Final Approval by:		
ELECTRA Technical Committee TOQA appointed Reviewer:	Emilio Rodriguez (TEC) Carlo Tornelli (RSE)	18/01/2017

Authors

Name	Last Name	Organization	Country
Mattia	Marinelli	DTU	Denmark
Michael	Pertl	DTU	Denmark
Michel	Rezkalla	DTU	Denmark
Michał	Kosmecki	IEN	Poland
Bogdan	Sobczak	IEN	Poland
Robert	Jankowski	IEN	Poland
Arkadiusz	Kubanek	IEN	Poland
Andrei	Morch	SINTEF	Norway
Tor Inge	Reigstad	SINTEF	Norway
Artjoms	Obushevs	IPE	Latvia
Antonio	Gatti	RSE	Italy
Silvia	Canevese	RSE	Italy
Marco	Rossi	RSE	Italy

Copyright

Consisting of:

Coordinator	
Ricerca Sul Sistema Energetico – (RSE)	Italy
Participants	
Austrian Institute of Technology GmbH - (AIT)	Austria
Vlaamse Instelling Voor Technologisch Onderzoek N.V. - (VITO)	Belgium
Belgisch Laboratorium Van De Elektriciteitsindustrie - (LABORELEC)	Belgium
Danmarks Tekniske Universitet - (DTU)	Denmark
Teknologian Tutkimuskeskus - (VTT)	Finland
Commissariat A L'Energie Atomique Et Aux Energies Alternatives - (CEA)	France
Fraunhofer-Gesellschaft Zur Förderung Der Angewandten Forschung E.V – (IWES)	Germany
Centre For Renewable Energy Sources And Saving - (CRES)	Greece
Agenzia Nazionale per Le Nuove Tecnologie, L´Energia E Lo Sviluppo Economico Sostenibile - (ENEA)	Italy
Fizikalas Energetikas Instituts - (IPE)	Latvia
SINTEF Energi AS - (SINTEF)	Norway
Instytut Energetyki - (IEN)	Poland
Instituto De Engenharia De Sistemas E Computadores Do Porto - (INESC_P)	Portugal
Fundacion Tecnalia Research & Innovation - (TECNALIA)	Spain
Joint Research Centre European Commission - (JRC)	Belgium
Nederlandse Organisatie Voor Toegepast Natuurwetenschappelijk Onderzoek – (TNO)	Netherlands
Turkiiye Bilimsel Ve Teknolojik Arastirma Kurumu - (TUBITAK)	Turkey
University Of Strathclyde - (USTRATH)	UK
European Distributed Energy Resources Laboratories (DERlab)	Germany
Institute for Information Technology at University of Oldenburg (OFFIS)	Germany

Executive summary

Task 5.4 in the ELECTRA project focuses on deriving novel observability concepts at the system-wide scale. The proposed methodology investigates typical phenomena related to power system stability and, based on the system behaviour or performance, develops observables necessary for the novel Web-of-Cells-based control methods to operate properly at cell and inter-cell level. Crucial aspects of angle, frequency and voltage stability are considered, according to the stability classification by CIGRÉ. In order to carry out the investigation, a suitable reference grid is developed.

Chapter 1 provides an overview on the task methodology and connection with other activities in the project [1], [2]. The whole framework for the analysis is explained along with the research questions that are pursued in this task.

The selected topics that will be analysed in order to derive Pan-European observables in a Web-of-Cells context are introduced in Chapter 2. For each topic an introduction is provided, followed by an explanation of the connection to the Web-of-Cells concept and its use cases and concluded by a short explanation on how the topic will be analysed in the remaining part of the task.

Chapter 3 illustrates the relevant aspects of the reference power system model developed within this task (and identified as “Pan-European single reference power system” in the ELECTRA Project). The model has been derived from the European HV Benchmark network proposed by CIGRÉ. It represents a set of cells and is intended for load flow and dynamic stability analyses; it also includes a cell with a multi-terminal DC grid to integrate a large offshore wind farm. Detailed information is given in Annex I.

Chapter 4 reports the results of the analysis taken for each topic, namely cell transient stability, cell small signal stability (with focus on inter-cell oscillations), inertia at WoC level (frequency stability), voltage stability (transmission capacity), and inter-cell loop flows.

Conclusions and lessons learned are reported in Chapter 5.

Terminologies

Definitions

The ELECTRA IRP project has a commonly coordinated strategy related to the use of terms and definitions within the project. In WP4 “Interoperable Systems” an ELECTRA Glossary activity has been created, which collects and validates specific terms and definitions. The ELECTRA Glossary is available for the project participants in the file repository at www.electrairp.eu and hence is not included in the present document.

Additionally several new terms and definitions have been introduced, which have been specifically developed in WP5 “*Increased Observability*” for the scope of the ELECTRA project, or have a meaning which may differ from the commonly used meaning. They can be found in ELECTRA deliverables D5.2 and D6.1, where they are extensively used.

Abbreviations

AC	Alternate Current
AVR	Automatic Voltage Regulator
BESS	Battery Energy Storage System
BRC	Balance Restoration Control
BSC	Balance Steering Control
CCT	Critical Clearing Time
CO	Cell Operator
CTL	Control Topology Level
DC	Direct Current
DG	Distributed Generation
DSA	Dynamic Stability Analysis
DSO	Distribution System Operator
EHV	Extra High Voltage
ENTSO-E	European Network of Transmission System Operators for Electricity
FCC	Frequency Containment Control
FRT	Fault Ride Through
HLUC	High Level Use Case

HV	High Voltage
HVDC	High Voltage Direct Current
IR	Inertial Response
IRPC	Inertial Response Power Control
LCC	Line Commutated Converter
MS	Milestone
MT-HVDC	Multi-terminal HVDC
NPFC	Network Power Frequency Characteristic
NP-RES	Non-Programmable Renewable Energy Source
OPF	Optimal Power Flow
PCC	Point of Common Coupling
PLL	Phase-Locked Loop
PMU	Phasor Measurement Unit
PPVC	Post-Primary Voltage Control
PS	Power System
PSS	Power System Stabilizer
PUC	Primary Use Case
PVC	Primary Voltage Control
PWM	Pulse-Width Modulation
RES	Renewable Energy Source
ROCOF	Rate Of Change Of Frequency
SCR	Short Circuit Ratio
SE	State Estimation
SG	Synchronous Generation / Synchronous Generator
SRPS	Single Reference Power System
STATCOM	Static Synchronous Compensator

TSA	Transient Stability Analysis
TSO	Transmission System Operator
UFLS	Under Frequency Load Shedding
VSC	Voltage Source Converter
WAMS	Wide-Area Measurement System
WECS	Wind Energy Conversion System
WLS	Weighted Least Squares
WoC	Web-of-Cells

Table of contents

List of figures and tables

1 Introduction and methodology

1.1 Increased observability needs and the ELECTRA approach

Safe accommodation of massive amounts of intermittent generation into the network, especially in a decentralized way at the transmission level and at the distribution level, requires a suitable evolution of the network structure and improvement of its control, monitoring and observing. Adequate observability of the power system operating state is therefore a more and more urgent requirement for a reliable and secure supply of electricity. Suitable subsets of observables, in turn, are the starting point for control design.

The main objective of WP5 "Increased Observability" is to develop and implement adequate concepts and methods for sufficiently observing the state of the future power system for the following “axes”:

- Pan-European, which is the focus of Task 5.4;
- Local (Horizontal/Distributed), which is the focus of Task 5.2.

The suggested observability schemes will be implemented in lab platforms programmable in advanced languages (Matlab, SciLab or similar), which will be defined and harmonised among the partners in the course of the IRP in order to transfer the results to the experimental foreseen in WP7.

On the whole, the approach adopted in ELECTRA to deal with power system control is based on regarding the power transmission and distribution system as a web of subsystems, called cells, which are operated by Cell Operators (COs). For control purposes, a CO has to act on the inner resources of its own cell and can also cooperate with other COs, in particular with the neighbouring cells COs, so that the whole power system, i.e. the whole Web-of-Cells (WoC), is stable, secure and reliable. Therefore, COs can be considered as entities similar to present TSOs (whose jurisdiction is the transmission system only, at present).

A cell can be defined simply as a group of interconnected loads, concentrated generation plants and/or distributed energy resources and storage units, all within well-defined grid boundaries corresponding to a physical portion of the grid and to a confined geographical area; neighbouring cells are connected by tie lines.

Based on operational security requirements a cell is in 'normal state' when in real-time operation:

- it is able to follow the scheduled consumption/generation set-point so that the voltage, frequency and power flows are within the operational security limits;
- it is able to activate sufficient flexible ancillary resources (active and reactive power reserves).

A cell needs to aggregate sufficient flexible resources to manage the uncertainty (variability) due to internal generation/load forecasting errors as well as generation tripping or load variations, but in case of need it can reach its balanced condition by interacting with neighbouring cells. A microgrid, instead, needs to aggregate sufficient resources to potentially allow internal generation and load to balance without any external contributions, i.e. to allow for islanded operation.

In order to keep a secure operation of a cell, or a whole Web-of-Cells, in the normal state, two main control types are needed:

- **Balance Control**, which includes all control loops (or control actions) that ensure, in real-time operation, the power system balance between generation and load;
- **Voltage Control**, which includes all control loops (or control actions) that ensure, in real-time operation, that the voltage level at each node keeps within operational limits, in order to transport the electricity energy from sending nodes (generation nodes) to receiving nodes (consumption nodes) in a stable, secure and reliable way.

Two sets of High Level Use Cases (HLUCs) – on the whole, six HLUCs – have been identified in ELECTRA deliverable D3.1 and elaborated in deliverables D5.2 and D6.1 to describe the two main control types and their control loops [1]-[4]. The six UCs are shortly recalled in the two tables below, Table 1-1 and Table 1-2. Both Balance Control and Voltage Control use cases are defined/applied/implemented at different subsystem/topology levels, ranging from a single device or an aggregation of devices, to a single cell and to a whole WoC. The WoC which is dealt with in particular in T5.4 refers to a power system with features and parameters typical of European HV transmission systems.

Table 1-1 Overview of Balance Control Use Cases and corresponding Control Aims.

Balance Control Use Cases	Control Aims
Inertia Response Power Control (IRPC)	**Objective 1**: Reacts to frequency changes over time (frequency transient plus dynamic response) **Objective 2**: Observes and regulates in real time the available amount of inertia within a Cell
Frequency Containment Control (FCC)	**Objective 1**: Reacts to deviations of the frequency value so as to contain any change and stabilise frequency to a steady-state value **Objective 2:** Observes and regulates in real time the Network Power Frequency Characteristic (NPFC) for the WoC or NPFC within a Cell
Balance Restoration Control (BRC)	Reacts to absolute frequency deviations in conjunction with the tie line power flow deviations from the scheduled interchanges so as to restore both quantities to their initial values
Balance Steering Control (BSC)	Regulates power balance within a Cell (proactively or reactively) in order to replace BRC reserves or mitigate potential imbalances in a cost effective manner

Table 1-2 Overview of Voltage Control Use Cases and corresponding Control Aims.

Voltage Control Use Cases	Control Aims
Primary Voltage Control (PVC)	**Objective 1**: Reacts in case of voltage deviations detected in any nodes of a Cells as a consequence of a severe disturbance **Objective 2**: Observes, monitors and regulates the voltage levels deviations in real-time in the grid nodes within the Cells
Post-Primary Voltage Control (PPVC)	**Objective 1**: Restores/keeps the voltage levels in the grid nodes to the set-point values within in a safe band. Simultaneously, it optimizes the reactive power flows for minimum losses in the system. **Objective 2**: Regulates the voltages in the nodes in case of generation-demand imbalances

1.2 ELECTRA Task 5.4 scope and methodology

The Web-of-Cells concept with the above six defined use cases is based on a bottom-up approach. In order to give a Pan-European approach there is the need to look at the Web-of-Cells from a top-down perspective. The idea is to analyse system stability considering the ELECTRA Web-of-Cells approach and benchmark it against the traditional way of controlling the power system. Starting from the traditional classification of stability problems, it has been decided to investigate the Web-of-Cells way of controlling the system (i.e., relying on the use cases/control triples identified in T5.1/T5.2 and T6.2) investigating the most common types of system stability. The list of topics is reported subsequently and on top of them two non-stability topics are investigated because relevant for system-wide issues (i.e., loop flows and HVDC operation) [5].

Task 5.4 focuses in particular on stability issues at Pan-European level with respect mainly to angle and frequency stability. However some elements regarding voltage stability are also included in the studies. Stability aspects will be considered according to the stability classification by CIGRÉ [6], [7].

In Figure 1-1 different stability types are depicted according to their timeframe. Moreover, the stability associated phenomena and control types are related to the respective stability type. In particular, the two figures at the top (a, b), refer to rotor angle stability and frequency stability; while the two figures at the bottom (a', b') refer to voltage stability. Furthermore, figures (a) and (a') show the conventional, or traditional, scheme of today's power system stability classification, while figures (b) and (b') show the complemented version with the proposed controls within ELECTRA project. In all the figures, the system disturbances which may cause instability are reported, together with corresponding remedial control actions.

The power system stability issues at Pan-European level will be analysed based on different topics within this task and will distinct among the mentioned timeframes. During the activity next step, simulation scenarios will be prepared in order to analyse the stability issues in a proper way.

Ultimately, the main research questions tackled in this task are:

- **Will the Web-of-Cells approach for managing and controlling the power system be as stable as the traditional one with respect to large power systems stability issues?**

- **Which are the observables needed for assessing the stability and ensuring proper operation of the system?**

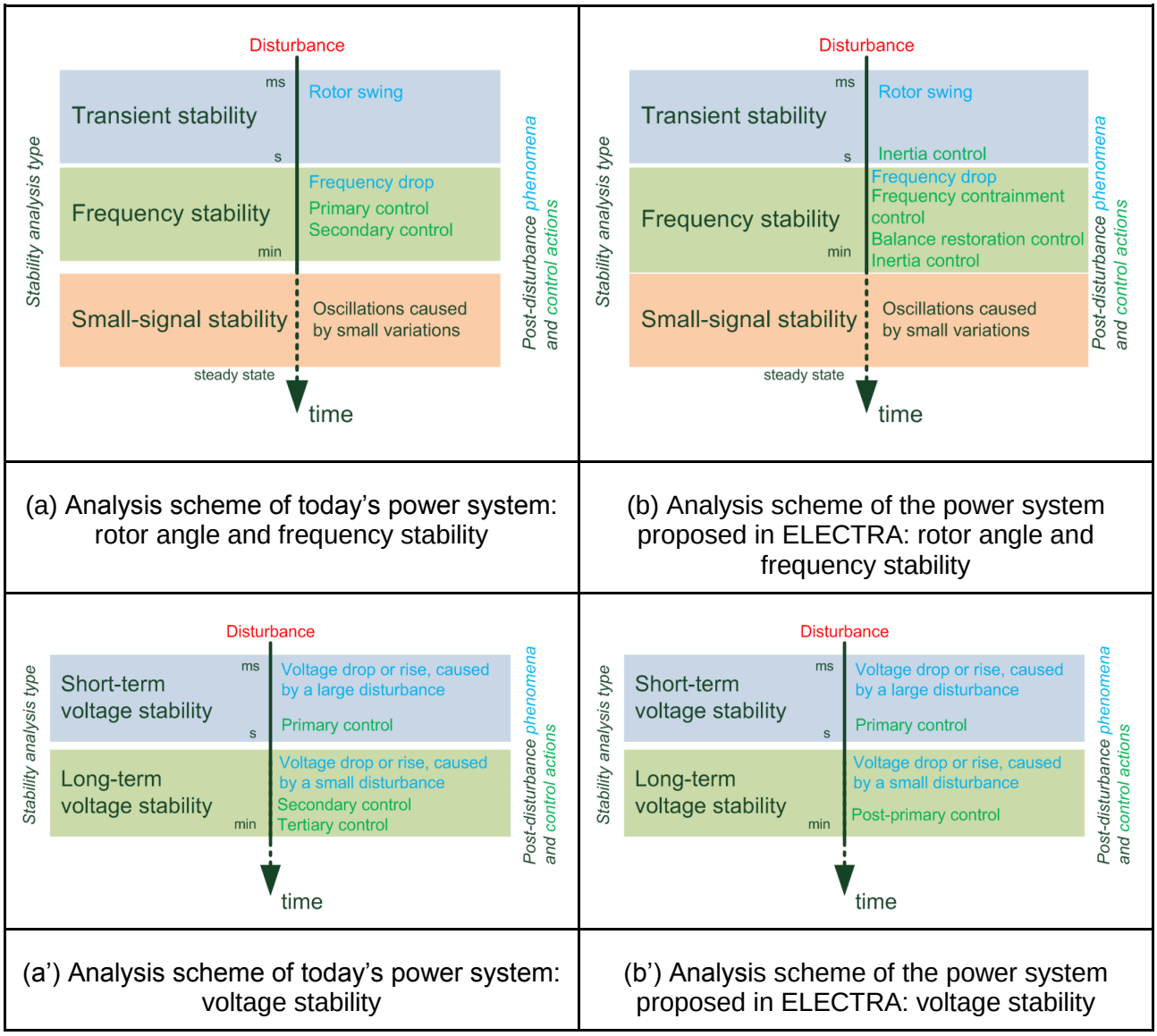

(a) Analysis scheme of today's power system: rotor angle and frequency stability

(b) Analysis scheme of the power system proposed in ELECTRA: rotor angle and frequency stability

(a') Analysis scheme of today's power system: voltage stability

(b') Analysis scheme of the power system proposed in ELECTRA: voltage stability

Figure 1-1 Comparison between today and ELECTRA power system in terms of stability issues, related phenomena and control schemes.

In order to provide extensive answer, the following elements have been identified:

1. Several relevant stability and system wide topics;
2. A common reference network model for performing the analysis, with adequate level of complexity, but at the same time reasonably simple and manageable, so that it can be transferred into different power system software platforms. This activity is highly

interconnected with the cross-task activity (T5.2-T5.3-T5.4) named Single Reference Power System (SRPS);
3. Selection of relevant observable schemes/control triples identified in T5.2/T6.2 to be applied at Pan-European level;
4. Power flow and dynamic analysis with reference to the selected topics and evaluation of main system parameters (such as maximum frequency deviation, rate of change of frequency, voltage levels, oscillation modes, angle margins, currents...). For each topic analysed, a comparison between the Web-of-Cells approach and the conventional, or traditional, approach is conducted.

Such a comparison provides information not only on the performance of the observables and control methods proposed for the WoC concept, but also on the behaviour of the future-shaped power system. This will be noticed especially with respect to generation portfolio, which can significantly differ from what is present nowadays for the assumed timeframe in ELECTRA project. For instance, the control actions proposed in ELECTRA are meant to be different from the traditional ones not only in terms of control functionalities (e.g., inertia response power control has been introduced as a true control action), but also in terms of a wider variety of devices carrying out these control actions (e.g., traditionally, large conventional generators only used to be enabled to participate in frequency control; in the future, several different kinds of flexible resources are foreseen to participate as well).

1.3 Basic and common background on power system stability

In [8], *power system stability* is defined as "the ability of an electric power system, for a given initial operating condition, to regain a state of operating equilibrium after being subjected to a physical disturbance, with most system variables bounded so that practically the entire system remains intact." Stability depends on the initial operating condition (load levels, generator power outputs, amount of ancillary service resources, key operating parameters set by TSOs, e.g. power transfer limitations on critical tie lines) as well as the nature of the disturbance (small, large). "Intact" means that the new operating condition attained is such that all components in the system have their main variables within the correct operating boundaries, and that quality, reliability and continuity of energy supply are guaranteed. When a disturbance occurs, in fact, the power system reaction includes an intrinsic, physical response (such as the inertial response of rotating masses of machines directly coupled to the grid) and the reaction of controllers (such as the classical speed droop controllers for primary frequency regulation). The traditional system stability classification is reported in Figure 1-2.

For the sake of clarity, some basic definitions and concepts about stability issues are reported below. The following ideas and quotations are taken from [6].

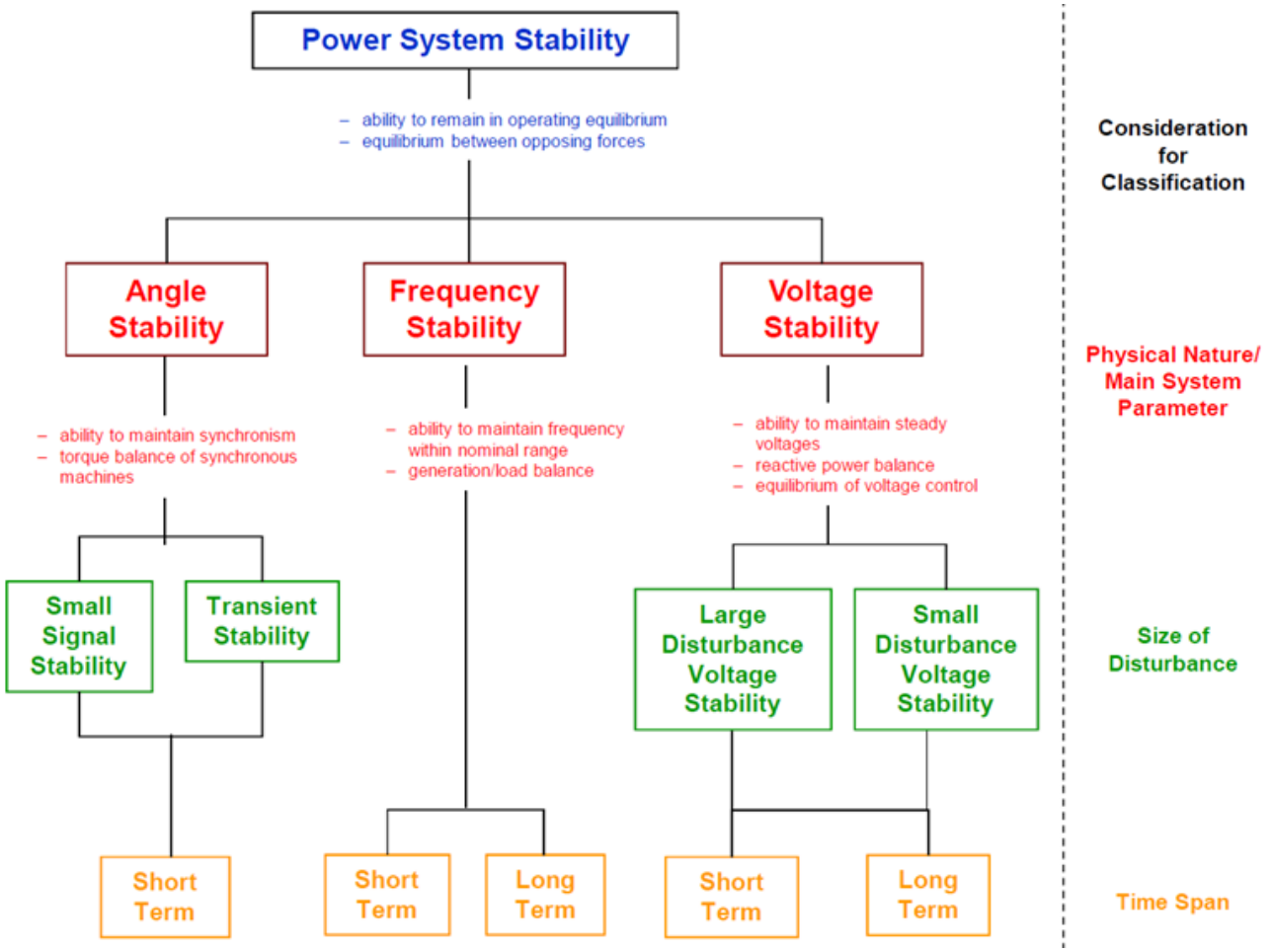

Figure 1-2 Traditional system stability classification.

1.3.1 Rotor angle stability

Rotor angle stability depends on the *ability of each synchronous machine in an interconnected power system to maintain/restore equilibrium between its own mechanical torque and electromagnetic torque*, after being subjected to a disturbance. When a system perturbation upsets that equilibrium, the rotational speed of the machine rotors can no longer be constant (variation of the mass kinetic energy). Therefore, the rotor angular position of a temporarily faster generator is in advance with respect to the angular position of a slower machine: the resulting angular difference, by means of the nonlinear power-angle relationship, transfers part of the load from the slow machine to the fast machine. This transfer, in turn, tends to reduce the speed difference and hence the angular separation. Beyond a certain limit, however, an increase in angular separation is accompanied by a decrease in power transfer such that the angular separation is further increased. In other words, instability results if the system cannot absorb the kinetic energy corresponding to these rotor speed differences, so there are increasing angular swings of some generators leading to their loss of synchronism with other generators (loss of synchronism can occur between one machine and the rest of the system, or between groups of machines, with synchronism maintained within each group after the separation).

Rotor angle stability is related to electromechanical oscillations inherent in power systems. More precisely, *the change in electromagnetic torque* of a synchronous machine has a *synchronizing torque component*, in phase with rotor angle deviation, and a *damping torque component*, in phase with the speed deviation. Following a disturbance, insufficient synchronizing torque in a synchronous machine results in *aperiodic* or *non-oscillatory instability*, while insufficient damping torque results in *oscillatory instability*.

Rotor angle stability can be usefully classified into:

- *Small-disturbance (or small-signal) rotor angle stability*, which is concerned with small disturbances (such as the typical load variation), so that linearization of system equations is affordable.
  The related problems concern a time frame on the order of 10 to 20 seconds following a disturbance and depend on the initial operating state of the system. They may be either local, usually associated with *local* (*plant*) *mode oscillations* (rotor angle oscillations of a single power plant against the rest of the power system), or *global*, involving *inter-area mode oscillations* (oscillations of a group of generators in one area swinging against a group of generators in another area).
- *Large-disturbance rotor angle stability* or *transient stability*, which is concerned with severe disturbances (e.g. a short circuit on a transmission line or the outage of a large generating/load unit), involves large excursions of generator rotor angles and is influenced by the nonlinear power-angle relationship.
  Transient stability depends on both the initial operating state of the system and the severity of the disturbance.

  Instability is usually in the form of aperiodic angular separation due to insufficient synchronizing torque, manifesting as *first swing instability*, but it can also be a result of superposition of a slow inter-area swing mode and a local-plant swing mode causing a large excursion of rotor angle beyond the first swing, and also be a result of nonlinear effects affecting a single mode causing instability beyond the first swing. The time frame of interest is usually 3 to 5 seconds following the disturbance, but it may extend to 10–20 seconds for very large systems with dominant inter-area swings.

1.3.2 Frequency stability

"Frequency stability refers to the ability of a power system to maintain steady frequency following a severe system upset resulting in a significant imbalance between generation and load. It depends on the ability to maintain/restore equilibrium between system generation and load, with minimum unintentional loss of load. Instability that may result occurs in the form of sustained frequency swings leading to tripping of generating units and/or loads.

Severe system upsets generally result in large excursions of frequency, power flows, voltage, and other system variables, thereby invoking the actions of processes, controls, and protections that are not modelled in conventional transient stability or voltage stability studies. These processes may be very slow, such as boiler dynamics, or only triggered for extreme system conditions, such as volts/Hertz protection tripping generators. In large interconnected power systems, this type of situation is most commonly associated with conditions following splitting of systems into islands. Stability in this case is a question of whether or not each island will reach a state of operating equilibrium with minimal unintentional loss of load. It is determined by the overall response of the

island as evidenced by its mean frequency, rather than relative motion of machines. Generally, frequency stability problems are associated with inadequacies in equipment responses, poor coordination of control and protection equipment, or insufficient generation reserve."

Frequency stability may be a *short-term* or a *long-term* phenomenon, since the characteristic times of the involved responding processes and devices span from fractions of a second or few seconds (under-frequency load shedding, generator controls and protections, boiler/reactor protection and controls) to tens of seconds and several minutes (prime mover energy supply systems, load voltage regulators).

Notice that not only voltage magnitudes may vary significantly when frequency changes (e.g., in islanding conditions with under-frequency load shedding), but also the load-generation imbalance is affected by large voltage magnitude variations (higher in percentage than frequency variations). "High voltage may cause undesirable generator tripping by poorly designed or coordinated loss of excitation relays or volts/Hertz relays. In an overloaded system, low voltage may cause undesirable operation of impedance relays."

1.3.3 Voltage stability

"Voltage stability refers to the ability of a power system to maintain steady voltages at all buses in the system after being subjected to a disturbance from a given initial operating condition. It depends on the ability to maintain/restore equilibrium between load demand and load supply from the power system."
In case of voltage instability, a progressive fall (most commonly) or rise of voltages of some buses shows up, and possible consequences are loss of load in an area or tripping of transmission lines and other elements by their protective systems leading to cascading outages. These outages can cause some generators to lose synchronism; this loss can also result from operating conditions that violate the field current limit.

Voltage collapse, in particular, "is the process by which the sequence of events accompanying voltage instability leads to a blackout or abnormally low voltages in a significant part of the power system. Stable (steady) operation at low voltage may continue after transformer tap changers reach their boost limit, with intentional and/or unintentional tripping of some load. Remaining load tends to be voltage sensitive, and the connected demand at normal voltage is not met."

As for voltage drop, two main "kinds" of instability can make bus voltages progressively drop: rotor angle instability (e.g., if two groups of machines lose synchronism, voltages close to the electrical centre drop fast, and then, if the two groups are not separated, voltages near the electrical centre may start fast and wide oscillations) and voltage instability.

Voltage drop related to voltage instability can be independent of rotor angle stability. It is usually a sustained fall involving loads: in fact, actions to restore load power consumption (such as those deployed by motor slip adjustment, distribution voltage regulators, tap-changing transformers, and thermostats) increase consumption of reactive power; if the load restoration attempts exceed the capability of the transmission network and the connected generation, a run-down situation is caused, leading to voltage instability. The capability of the transmission network for power transfer and voltage support is limited by the voltage drop related to active and reactive power flows through inductive reactances of the network itself, and it is further limited when some generators reach their field or armature current time-overload capability limits.

As for voltage rise, overvoltage instability "is caused by a capacitive behaviour of the network (EHV transmission lines operating below surge impedance loading) as well as by under-excitation limiters preventing generators and/or synchronous compensators from absorbing the excess reactive power. In this case, the instability is associated with the inability of the combined generation and transmission system to operate below some load level. In their attempt to restore this load power, transformer tap changers cause long-term voltage instability."
The self-excitation of a synchronous machine can also determine overvoltage instability; for instance, self-excitation can be initiated if the capacitive load of the machine is excessive.

To distinguish rotor angle stability from voltage stability, reference has to be made to "the specific set of opposing forces that experience sustained imbalance and the principal system variable in which the consequent instability is apparent." In fact, to study stability problems, stressed conditions have to be considered, when variations in active power/angle and reactive power/voltage magnitude are strongly coupled, and both kinds of stability are affected by pre-disturbance flows of both active and reactive power.

Voltage stability is usually classified into two categories (similarly to rotor angle stability):

- *Large-disturbance voltage stability*, with respect to large disturbances, such as system faults, loss of generation, or circuit contingencies. It depends on the interaction of the system and the load, with their nonlinear characteristics, and of both continuous and discrete controls and protections. The related time frame can vary from a few seconds to tens of minutes.
- *Small-disturbance voltage stability*, with respect to small perturbations, such as incremental changes in system load. It is affected by "the characteristics of loads, continuous controls, and discrete controls." Notice that, in this case, linearization of system equations is not always enough: it is enough for sensitivity analyses useful to identify factors influencing stability, while a combination of linear and nonlinear analyses is needed to deal with nonlinear effects like those in tap changer controls.

Another classification is with respect to the time frame of interest:

- *Short-term voltage stability* involves dynamics of fast acting load components (induction motors, electronically controlled loads, HVDC converters…). With respect to rotor angle stability, a similarity is that the time frame of the study is in the order of several seconds; a difference is that short circuits near loads are relevant.
- *Long-term voltage stability* involves slower acting components or devices (tap-changing transformers, thermostatically controlled loads, generator current limiters…). The timeframe of the study can cover up to many minutes. Thus, not only the effects of sudden disturbances have to be studied, but also those of slower disturbances such as sustained load variations. The size of the disturbance can be less important than the resulting outage of equipment. Instability is caused not only if the long-term equilibrium is lost (e.g., when load power restoration exceeds the transmission network and connected generation capability), but also if the steady-state operating point which can be reached after the system response to the disturbance is small-disturbance unstable, or if the post-disturbance equilibrium is stable, but there is lack of attraction toward it (as in the case of too late remedial actions).

Static analysis can often be adopted to estimate stability margins and identify factors affecting stability, but it has to be complemented by quasi-steady-state time-domain simulations when timing of control actions is important.

2 List of relevant enhanced system-wide stability topics

2.1 Chapter scope

In this chapter, a selection of relevant topics of interest for analysing system-wide stability is carried out. The topics have been chosen according to the system stability classification given in Chapter 1 and considering future trends (HVDC) and commercial issues (loop flows). For each of the topics analysed below, a description of the phenomena is now given along with related solutions used today. Connection with the ELECTRA use cases is also provided.

- Topic 1: Cell/system transient stability (large disturbance stability)
- Topic 2: Small signal cell stability with focus on inter-cell oscillation (small disturbance stability)
- Topic 3: Inertia at Pan-European level (frequency stability)
- Topic 4: Voltage stability
- Topic 5: Inter-cell loop flows
- Topic 6: HVDC operation (trip/runback)

In each topic, differences between the traditional way of controlling the power system and the proposed way to control a future power system structured as a WoC will be summarized in a picture with the following structure, illustrated in Figure 2-1.

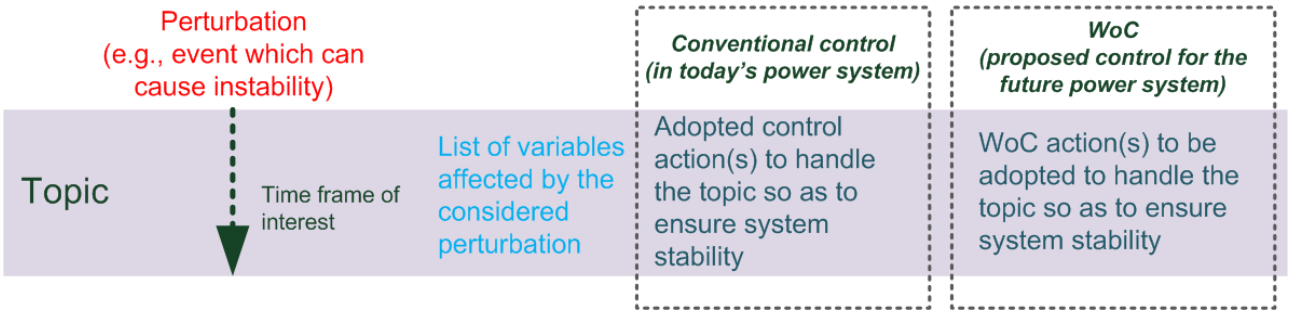

Figure 2-1 Support scheme for a detailed comparison between the traditional and the proposed ways to control the power system.

2.2 Topic 1: Cell/system transient stability (large disturbance stability)

2.2.1 Definition of transient stability

Transient stability is one out of many power system stability aspects with particular focus on the short term, typically 1 - 30 seconds after the incident [9]-[11]. Transient stability defines the ability of a power system to maintain synchronism after being subject to a severe transient disturbance such as a three-phase fault, loss of generation or loss of a large load (i.e., if the power system is able to move from one state to the next one with system variables remaining within safe limits). The power system variables like bus voltages, power flows, rotor angles as well as other system variables may deviate greatly from their nominal values after being subject to a severe disturbance. The nonlinear power system characteristics are highly influencing the stability of the power system itself while transient stability gains special interest when long distance heavy power

transmissions are involved. The load angle of synchronous generators changes due to a sudden acceleration of the rotor shaft and depending on the system conditions it will/will not reach a steady value after clearance of the disturbance, i.e. if transient stability is given or not. Due to its nonlinear character, fast evolution and catastrophic practical implications, transient stability is one of the most important and at the same time most problematic issues to assess and even more to control. When speaking about instability it can generally be said that instability occurs when at least one rotor angle becomes unbounded with respect to the rest of the system which is also known as 'going out of step'. In traditionally controlled power systems it is necessary to consider the behaviour and type of exciters, speed governors, voltage regulators, power system stabilizers and other devices influencing the system characteristics when analysing the transient stability. Therefore transient stability plays an important role in planning and operation of power systems. For the analysis of transient stability two methods are applicable. The conventional time-domain method is the most widely used where the system equations are solved to obtain the solution for a given scenario. This method can be used for any detailed model of a power system and all the information about state variables is available. However, the method has also its disadvantages as high computational effort is needed to solve the equations step by step and it is not providing any information about stability/instability margin for the condition of the system.

In contrast, a so called direct method for determining the stability of a power system has been developed.

The method, also known as *Lyapunov second method*, has its advantages in the potential of time saving at transient stability assessment and can be used in off-line tools for planning purposes as well as for on-line security assessment. The method has also its disadvantages since it is a very difficult task to construct a Lyapunov (energy) function, which is needed for the analysis, when a complex power system has to be analysed. Problems to construct this function especially appear when asynchronous machines are involved in the studies. In these systems, it is suggested to use alternative methods for stability studies [17].

2.2.1.1 Problems/needs regarding transient stability in future power systems

One of the key assumptions for the power systems of the future is that the level of distributed generation will rise significantly with respect to its present value. These fully or partially converter-interfaced energy resources tend to decrease system inertia as they potentially replace synchronous generation, which still constitutes generation base nowadays. Increasing penetration of Distributed Generation (DG) also results in a degradation of the accuracy of the above-mentioned transient stability analysis methods for large power systems. There are several factors that justify this statement. Lower or zero-inertia constant of a DG unit means lower inherent transient stability of the resource and faster oscillations in the power system after a disturbance for the scenarios with higher levels of penetration when compared to lower levels. On the other hand, higher converter-coupled resources penetration ratios usually result in lower loading of transmission lines since the generation is closer to the loads, which effectively moves the power system operating point further from the stability limit. However, depending on the method used for keeping power balance of the analysed area, transient stability can be further increased if power output of the synchronous generation is reduced or actually decreased if synchronous generation is taken out of operation [12].

Inclusion of a power converter between the rotating masses of the generator and the grid effectively decouples their dynamic response. Swing equation governing the rotor dynamics cannot

be a basis for the transient stability analysis in this case as other elements come in place. The first is the Phase-Locked Loop (PLL) which is responsible for providing information on voltage phase angle and frequency at Point Common Coupling (PCC), thus taking responsibility for proper synchronization. The second is the current control system of the voltage source inverter [13]. Both of them require the simulation time step be much less than the fundamental frequency period, which is used in standard Transient Stability Analysis (TSA). Therefore, in order to make TSA with DG possible (especially on-line TSA), special models are used [12]. PLL and internal current controllers are profoundly simplified and the focus is placed on the behaviour of the modelled DG during and after faults by incorporating fault-ride-through (FRT) functionality into the model. These so-called response models are very flexible and versatile; however they need much attention and expertise during parameterization.

FRT is a capability that allows DG to operate during a disturbance without being tripped, usually by means of a crowbar (or braking resistor) for energy dissipation, as it is commonly done in most wind turbines for instance. This is an efficient solution for DG, but not as helpful to the disturbed power system as Synchronous Generator (SG) since its does not provide inertia. Therefore, for wide scale application, substitution of SG with DG might lead to frequency problems during the transient period as a result of low inertia. As a countermeasure several methods involving so-called virtual inertia have been proposed, e.g. virtual synchronous generators [14], synchro-converters and others [15]. Such virtual inertia resources along with SG will take part in future inertia steering control proposed as of frequency control.

2.2.2 Connection to Web-of-Cells concept and use cases

Since transient stability relates to the ability of the generators in a power system to maintain in synchronism after being subject to a severe disturbance, it is crucial for the overall stability to consider this type of stability when planning and operating the power system. An instability caused by ‘going out of step’ of one or several generators within the power system can lead to subsequent stability issues as frequency stability (amongst others) due to loss of generation and thus to a partial or full blackout of the system in the worst case. In the proposed Web-of-Cells concept within ELECTRA the Cell Operator of each cell must ensure that the generators within its cell are operated within safe and acceptable limits in order to guarantee uninterrupted, safe and reliable operation of the power system with respect to transient stability.

The cell operator has to monitor the transient stability margins amongst other stability issues and take remedy actions for maintaining the safety level if problems are detected or foreseen. This assumes that the operator has the proper tools and thus the capability to monitor the transient stability and the safety margins on-line and for near future. As the previously mentioned capabilities stand for very advanced methods, an off-line assessment of transient stability should be carried out beforehand and analysed carefully. The drawn conclusions from the off-line assessment should be considered and kept in mind during planning of actions and operation of the power system in order not to drive the system in critical state by taking wrong decisions due to unconsidered or lack of information about the consequences. In the ideal case every cell operator can ensure that the margins for transient stability are sufficient within its cell and so overall transient power system stability can be achieved by sharing the responsibility amongst the cell operators.

The main use cases involved in this scenario are IRPC (Inertia response power control) and FCC (Frequency containment control). PVC (Primary voltage control) would be activated during transients as well, as indicated in Figure 2-2.

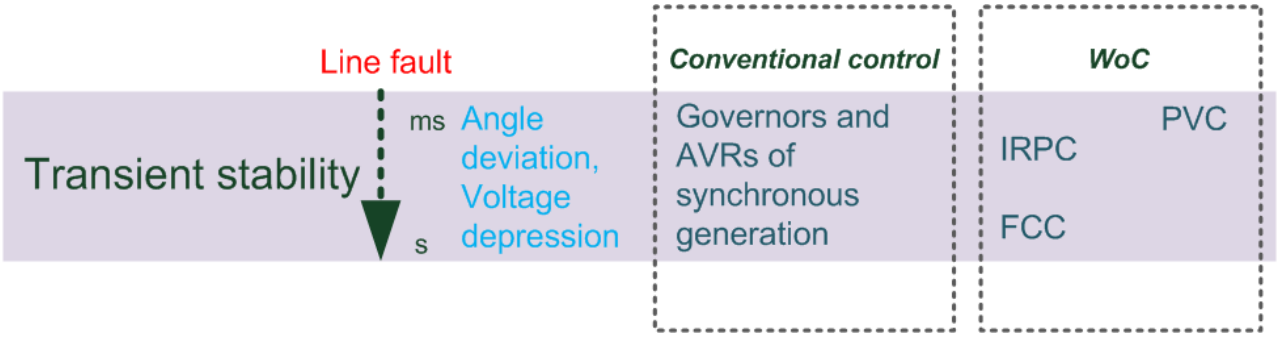

Figure 2-2 Comparison between the traditional and the proposed ways to control the power system, with reference to transient stability issues.

2.2.3 Analysis methodology and observables identification

- Model selection and preparation

SRPS of Pan-European system will be used for transient stability assessment (see Chapter 3 for more information). The model has several generation units located in different parts of the system which is both sufficient for meaningful results and flexible for parameterization and setting up initial conditions.

- Method description

The most severe disturbance allowing for transient stability assessment is a 3-phase fault applied to a network element (e.g. line or bus). The duration of the fault is changed in a way that Critical Clearing Time (CCT) is obtained, i.e. the longest duration of the fault that can be withstood without losing synchronism by any of the generators operating in vicinity. Naturally, the operating point of the generator has a crucial impact on the results, because the mismatch between mechanical power and active electric power generated during a short-circuit is driving the generator towards going out of step.

By comparing the obtained CCTs for different locations and operating conditions of the generation sources with their dynamic responses and the clearing times of the protection equipment, it can be assessed whether the system is transiently stable or not.

This procedure is adopted within the analysis of transient stability for the WoC-based power system. The whole system will be scanned so that for every relevant location CCT will be obtained, which allows for a straightforward comparison of CCTs between conventionally controlled power system and the one based on WoC.

However, two important factors have to be considered in the above analysis:

1. Percentage of inverter-coupled generation – this parameter will be varied in order to see the differences in the performance of the two control schemes; variation will be carried out by means of substituting the conventional generation with RES.

2. Loading of the generators – will also be varied in order to establish if load level has distinguishing impact on control methods.

- Parameters evaluation

The main parameter used in the comparison will be the CCT. In addition, trajectory based indices are planned to be utilized, i.e. *power angle-based stability index* describing maximum angle separation and *voltage drop/rise duration index* describing non-permissible voltage values.

- Observables identification

A pair of relative angle displacement and impedance estimation is a possible candidate for an observable which would express how stressed the system is, which in turn could be a basis for the decision making process of releasing more resources into the system in order to decrease loading of the generators.

2.3 Topic 2: Small signal cell stability with focus on inter-cell oscillations (small disturbance stability)

2.3.1 Definition of small signal cell stability

Small signal cell stability is concerned with the ability of the power system to maintain synchronism under small disturbances. These disturbances are considered to be sufficiently small that linearization of the system equations is permissible for purposes of analysis.

Instability may arise in two forms [17]:

a) Increase of rotor angle due to lack of sufficient synchronization torque, or

b) Rotor oscillations of increasing amplitude due to lack of sufficient damping torque.

While interconnections result in operating economy and increased reliability through mutual assistance, they contribute to increased complexity of stability problems and increased consequences of instability. With the growth of extensive power systems, and especially with the interconnection of these systems by ties of limited capacity, oscillations can reappear.

There are several reasons for this reappearance [18]:

1. For intersystem oscillations, the damping circuit is no longer effective, as the damping produced is reduced in approximately inverse proportion to the square of the effective external-impedance-plus-stator-impedance, and so it practically disappears;
2. The proliferation of automatic controls has increased the probability of adverse interactions among them;
3. Automatic controls are practically the only devices that may produce negative damping, the damping of the uncontrolled system is itself very small and could easily allow the continually changing load and generation to result in unsatisfactory tie-line power oscillations;
4. A small oscillation in each generator that may be insignificant may add up to a tie-line oscillation that is very significant relative to its rating;
5. Higher tie-line loading increases both the tendency to oscillate and the importance of the oscillation.

These particular oscillations, when accumulating over a certain period of time, not only limit power transfer within the network but, more crucially, could lead to power system breakdown. Thus, it is vital to properly treat the incidents in time. The frequencies of the oscillations are small, e.g. in the range of 0.1 to 1.0 Hz for inter-area oscillations (with reference damping ratio of 5% at least, in large power systems) and 1.0 to 2.0 Hz for local oscillations [19].

Local plant mode oscillations are the most commonly encountered and are associated with the swinging of units at a generating station or a small part of the power system with respect to the rest of the power system. Such problems are usually caused by the action of the automatic voltage regulators (AVR) of generating units operating at high output and feeding into weak transmission networks; the problem is more pronounced with high-response excitation systems. To prevent local mode oscillations adequate damping can be readily achieved by using supplementary control of excitation systems in the form of power system stabilizers (PSS).

2.3.2 Definition of inter-cell oscillations

Global oscillations, where a group of generators in one area is swinging against a group of generators in another area are called inter-area oscillations. This kind of electromechanical oscillations is inherent to interconnected power systems. If two similar power systems are connected by weak transmission lines the structure is prone to inter-area oscillations. The different oscillations are called oscillation modes where each mode consists of a particular frequency and an associated damping coefficient [20]. The characteristics of inter-area oscillations are very complex and therefore a detailed analysis has to be carried out. Not only the generators (excitation system, governor) have to be considered when analysing inter-area oscillations, also the load characteristics, operating point and the structure of the power system have to be taken into account in order to assess the stability of inter-area modes.

The timeframe of occurrence for inter-area oscillations can vary in a rather great range depending on various parameters but can generally set in the order of 1 to 20 seconds. To prevent global mode oscillations power system stabilizers (PSSs) can be used for instance. Inter-area oscillation assessment gained more attention in the recent years since the current power systems around the world are tending to increase, from geographical point of view, where great amounts of power are transmitted over long distances from generation to load centres. Due to that, power systems are naturally exposed to inter-area oscillations and in order to counteract these issues it is of high importance to address this problem and be aware of its consequences. The concept of inter-area oscillation can be translated into a concept of inter-cell oscillation by considering a group of generators in one cell swinging against a group of generators in another cell.

2.3.3 Connection to WoC concept and use cases

The continuing implementation of inverter-based RES will make the assessment of inter-area oscillations more and more challenging in future power systems. Therefore, as a WoC is a future power system control concept assuming a large share of renewables, the assessment of inter-cell oscillations will be a critical issue. In particular, several challenges have to be faced, like the decrease of power system inertia leading to increase of Rate-Of-Change-Of-Frequency (ROCOF), less controllable output of some generation units, e.g. wind turbines, to control the damping of oscillations and possible implemented control systems for inverters which influence the oscillations.

Thus, the main use cases involved are Inertia Response Power Control, Frequency Containment Control, Balance Restoration Control and Primary Voltage Control as shown in Figure 2-3.

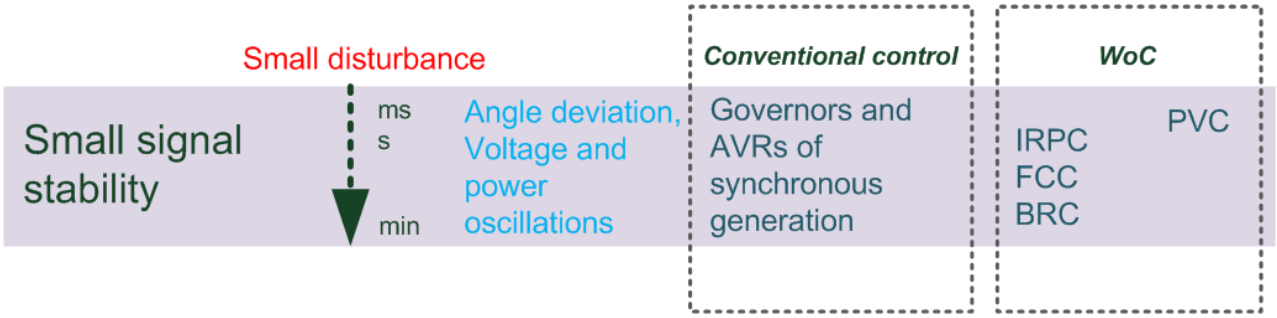

Figure 2-3 Comparison between the traditional and the proposed ways to control the power system, with reference to small signal stability issues.

2.3.4 Analysis methodology and observables identification

- Model selection and preparation

The base model is the proposed Pan-European SRPS model. However, since the existing modes are unknown, the model will have to be modified according to the specific purpose of this study, i.e. to obtain both inter-area and local modes.

The SRPS for Pan-European level is already available in PowerFactory format. A conversion is also planned to different software packages (namely DSATools) due to an excellent module for modal calculations, which would facilitate the analysis.

- Method specification

The most efficient tool for small signal analysis is modal analysis of linearized dynamic systems. Similarly to transient stability assessment, within this topic different power flow conditions need to be checked because they have considerable impact on the modes. To identify the modes a reference disturbance will be used: it can be a 5% change of reference voltage or a similar change in mechanical power.

Also influence of increasing participation of generators and loads connected by inverters will be checked in order to identify possible differences in the performance of the two control schemes. The participation will be increased and its influence on results of modal analysis, in particular frequency and damping of electromechanical modes, participation factors, mode shapes (distribution) and also controllability and observability of low-frequency badly damped modes will be analysed.

It can be suspected that decreasing participation of synchronous generation at some level will change significantly the image of small signal stability. In this point classical methods (PSS, governors) for improvement of damping will be not sufficient and new methods employed within PVC (e.g. using FACTS, HVDC or VSC connected loads and generation) will be needed to stabilize the system.

- Parameters evaluation

Characteristic parameters of modes are the parameters for evaluation. These include frequency, damping, amplitude and phase shift. Additional parameters needed for full information are participation factors for each mode and mode shapes.

- Observables identification

Useful observables would be those which refer to rated values of basic quantities, such as Δω, Δf, ΔPe, etc. (respectively, rotational speed difference, frequency difference and generated power difference). They can be constructed by using two different sources:

1. They could be defined in offline analysis carried out in the background with data supplied from a state estimator for instance: this is particularly important when oscillations observable in one part of the system are most efficiently damped by a stabilizing circuit in a different part of this system;
2. Modes could be measured in online modal analysis with use of *Prony's algorithm* for example: a priori knowledge of the system would not be required to observe small signal oscillations, however, this knowledge would be needed to control (damp) them, therefore by using information from source 1 participation factors could be identified and proper control actions could be activated.

Verifying if methods of linear dynamics will allow selecting proper signals and devices to obtain necessary level of oscillation damping is also a challenging task.

2.4 Topic 3: Inertia at Pan-European level

2.4.1 Inertia: relations with power system stability issues

The energy stored in the power system and instantly available to be exchanged is stored, for most, as kinetic energy of the connected electric machines (synchronous and asynchronous generators and motors). Inertia is an inherent mechanical feature of rotating masses and it acts as an early intrinsic countermeasure against frequency deviation after perturbations due to load-generation imbalances. More precisely, as it is well known, the present structure of the controlled power system response to a sudden change in the active power balance can be divided into five stages [21], the second of which is indeed the Inertial Response (IR):

- First of all, the magnetic field of synchronous generators releases electromagnetic energy, for about 1/3 s, to contribute to maintaining synchronism;
- After the electromagnetic release, the IR acts, for few seconds at most; IR of synchronous machines is the inherent release of kinetic energy stored in the rotors of the rotating generators;
- Within a few seconds from the event, the primary frequency reserve is activated, which should be completely deployed by a time interval which in ENTSO-E present requirements is indicated as 30 s from the event; the related control action stabilizes frequency to a steady state which is usually different from the nominal frequency value, so that a steady deviation with respect to the nominal frequency is reached; primary frequency control is typically carried out by machine governors, which are activated when frequency deviation exceeds certain limits and change the power output set point to the prime movers;

- Within (typically, according to the present ENTSO-E requirements) 15 minutes from the event, the secondary control reserve is deployed, to bring frequency back to its nominal value and free up the primary frequency reserve;
- The secondary control reserve is followed and supported by the tertiary control reserve, which frees up the previous reserves.

Therefore, when the active power balance in a power system undergoes a large disturbance, both rotor angle and frequency stability have to be considered: in fact, as also highlighted by [21], the former is concerned with keeping synchronism throughout the system, and the latter with keeping the system operating in a tolerable point of frequency equilibrium and with minimal loss of load. Inertia contributes both to rotor angle stability and to frequency stability: in fact, IR is related to the rotor angle change in synchronous machines, so it contributes to rotor angle stability, namely it contributes to keeping this angle within suitable bounds so that synchronism is preserved; besides, it contributes to frequency stability, because it affects both the ROCOF and the maximal frequency deviation: the former, in turn, influences the behaviour of protective relays (whose action can lead not only to island operation, but also to system blackout), the latter is directly connected to load shedding.

In this Section, attention will be focused on short-term frequency stability issues, in particular on those related to IR.

2.4.1.1 Problems/needs regarding inertia in future power systems

Traditionally, large synchronous generators connected to the transmission grid have supplied a large amount of inertia, thus contributing to power system stability as just described. However, as recalled in Section 2.2 Topic 1: Cell transient stability (large disturbance stability), the power system in the future decades is foreseen to be characterized by a significant increase of distributed generation, often consisting of static generators (such as PV panels) and often connected to the grid through the use of power electronics converters (such as the ones for wind turbines); such generators have already begun to displace more and more large synchronous generators in demand fulfilment. This evolution, therefore, can imply a dangerous decrease in system inertia [22]-[25], and therefore in power system stability margins. Besides, inertia decrease is accompanied by two other phenomena [23]:

- Inertia is becoming more and more heterogeneous and with a non-uniform geographical distribution, so that in an individual area different inertia constants have to be taken into account, instead of a global one as in the past; these different inertia constants depend on the number and size of converter-connected units versus conventional units online in the different areas;
- Inertia is becoming more and more time varying, in relation to the variability of the power dispatch.

Among the consequences, for frequency e.g., one can point out [23] both that frequency dynamics become differently fast in the individual grid areas, and that frequency instability phenomena are amplified (lower rotational inertia means faster frequency dynamics, so, in case of power faults, larger frequency deviations and transient power exchanges over tie-lines, therefore possible false errors and unexpected tripping of the involved tie-lines by automatic protection devices, therefore more critical conditions for the grid).

Indeed, two main concerns are underlined by ENTSO-E [26] for the near future, which can be deemed to be applicable to the ELECTRA future power system scenario as well:

1. "Inertia adequacy will have an important role in order to ensure system stability after major disturbances in future, when intermittent generation having relatively small amount of inertia is in increasing. There is need to make studies to identify the needed minimum amount of inertia in each Synchronous Area" (minimum inertia required for maintaining Operational Security at the level of Synchronous Area and to prevent violation of Stability Limits) and to "develop methodologies to fulfill this minimum inertia requirement."

2. "The power flows in Transmission System are continuously increasing due to changes in the market and increasing amount of intermittent generation. These changes together with long distance transmission paths from generation to load centers can increase the risk of wide area oscillations or other dynamic stability problems in transmission systems. To ensure that the dynamic limits are known in TSOs control centers in all situations Dynamic Stability Analysis (DSA) have to be implemented in cooperation with all TSOs in each synchronous area"; besides, emerging technologies like Wide-Area Measurement Systems (WAMS) "may in the future give possibilities to monitor or calculate the dynamic stability limits even closer to real-time."

Therefore, a multi-faceted stability analysis is necessary to assess how inertia decrease affects different aspects/issues contributing to overall power system stability. Small signal stability, inter-cell oscillations and transient stability, in particular, have already been dealt with (see topics 2 and 1, in Sections 2.3 Topic 2: Small signal cell stability with focus on inter-cell oscillations (small disturbance stability) and 2.2 Topic 1: Cell transient stability (large disturbance stability) respectively), while frequency stability issues still have to be analysed.

Moreover, as suggested by concern 1 expressed by ENTSO-E, new computational tools are needed, to enable to

- Estimate the available amount of inertia in the power system, as a function of time;
- Evaluate the needed minimum amount of inertia;
- Compute a suitable inertia time profile or "dispatch", to ensure at least the minimum amount is supplied; in turn, a request for the correct "inertia supply" has to be sent to the involved dispatched generators. If, for a certain time interval, the overall inertia need cannot be satisfied by synchronous generators (e.g. because there are not enough such generators on, due to their displacement by converter-interfaced RES generators), some inertia has to be supplied by suitably controlling other devices, such as converter-interfaced RES generators (including those connected to HVDC transmission systems), Battery Energy Storage Systems (BESSs), synchronous condensers, etc.. The amount of this "synthetic" inertia has to be computed as well, and it has to be part of the inertia dispatch.

Of course, control algorithms are needed, as just mentioned, to make non-synchronously connected generators/devices track a request for *synthetic* inertia supply. A synthetic inertia request, in particular, could mean, e.g., a set-point for the device "equivalent" inertia constant (in seconds) or a target IR, i.e. a target active power curve as a function of time (defined for a suitable time interval after a power imbalance event in the power system).

Since concern 1 can be related rather directly to the development of a simple control structure, it will be dealt with in more detail below, with reference to a Web-of-Cells scenario.

As for concern 2, one can notice that DSA is related to the power system State Estimation (SE), i.e. the determination of the most likely state, in terms of system bus voltage magnitude and phase angle, starting from topology information and remote measures of voltage magnitudes, branch power flows and bus power injections. In this regard, reviewing material can be found in [27]-[29] about very large interconnected systems composed of subsystems supervised by TSOs. As highlighted in [29], dealing with the SE problem includes/implies facing a set of sub-problems, e.g.

- What variables to measure, in terms of number and geographic location, to guarantee system observability, and what pseudo-measurements to introduce to obtain full observability in case the existing measures are not enough;
- What accuracy and timing constraints to require for measurements;
- What measuring instrumentation to use in order to meet those constraints; recent trends are towards the use of Phasor Measurement Units (PMUs) [30]-[31], both at the local and at the centralized level, because they enable effective coordination of local estimates and improve state estimation accuracy and rate of convergence;
- How to deal with bad data;
- What kinds of algorithm to use [27] to actually solve the estimation problem: this has usually a Weighted Least Squares (WLS) formulation, where an estimate state vector has to be found which fits best the measurement vector, described, in turn, by a nonlinear function of the state plus a measurement error vector, so the solution becomes more and more complex to be implemented as the power system becomes larger; complexity, however, can be reduced, and therefore dealt with, by exploiting the fact that a large power system is usually composed of smaller, regional or country-wide, interconnected areas: thus, a two-level approach can be used, by first performing local estimations on subsystems, and then coordinating them at a higher level. To this purpose, a range of numerical methods can be applied: on the one hand, the standard iterative Gauss-Newton method, which is "naturally" related to the WLS formulation; on the other hand, heuristic approaches to simplify the global WLS optimality conditions in the coordination stage; midway, relaxation-based ones iterating between local and coordination stages, or translations of the WLS formulation into an optimization problem where a Lagrangian function is usually adopted to handle equality constraints;
- What kind of computing and communication architecture to use to implement the described coordination: roughly speaking, coordination can be implemented either by hierarchical schemes, where a centralized master processor coordinates the work of slave processors and their local estimates, or by fully distributed schemes, where there are local processors only (and no master) which communicate with their neighbours, to exchange the necessary information;
- What kind of coordination scheme to adopt [27], which is an issue related to the two previous items: for instance, coordination can be carried out at the SE central level, after the local processors have carried out their iterative SE process, or at the iteration inner level;
- Last, but not least, how to improve computation robustness, accuracy and burden.

Although of the utmost importance, concern 2 is out of reach of the present analysis; we just hint at the general discussion about PMU use in [31], one the one hand, and to the *State Estimator and* Optimal Power Flow analysis (OPF) suggested in chapter 5.2.1 in [32] and run for each single cell as shown in Topic 5: Inter-cell loop flows, on the other hand.

2.4.2 Connection to WoC concept and use cases

As already remarked, the amount of "physical" inertia offered by rotating masses directly connected to the grid has been decreasing over the last years and it may become significantly varying both in time and in space [33]: these critical effects are due to the increasing diffusion of generation from intermittent RESs and, more in general, of DG, and therefore to the fact that large synchronous generators are more and more often displaced by an increasing range of generators with widely different inertia constants [34]. A Web-of-Cells structure could be beneficial to cope with not only the time distribution, but also the spatial distribution, because each Cell Operator is assumed to be aware of the inertial resources available in its cell, so that it can handle them as effectively and efficiently as possible, but, on the other hand, having cells with significantly different amounts of inertia may weaken or even threaten stability of the overall Web-of-Cells. The effects of inertia spatial distribution have therefore to be analysed, in view of ensuring overall stability; such evaluations can then be a starting point for the design of inertia control actions, at the different Control Topology Levels (CTLs) envisaged in ELECTRA, and for optimization of inertial resource procurement (before the real time, with a time horizon which could range from a day to a quarter of an hour before the real time) and management (from, say, a quarter of an hour before the real time to the real time) by the Cell Operators. In the analysis, frequency stability, in particular, will be taken into account.

The main use cases involved are Inertia Response Power Control and Frequency Containment Control, as highlighted by the dashed blue lines in Figure 2-4.

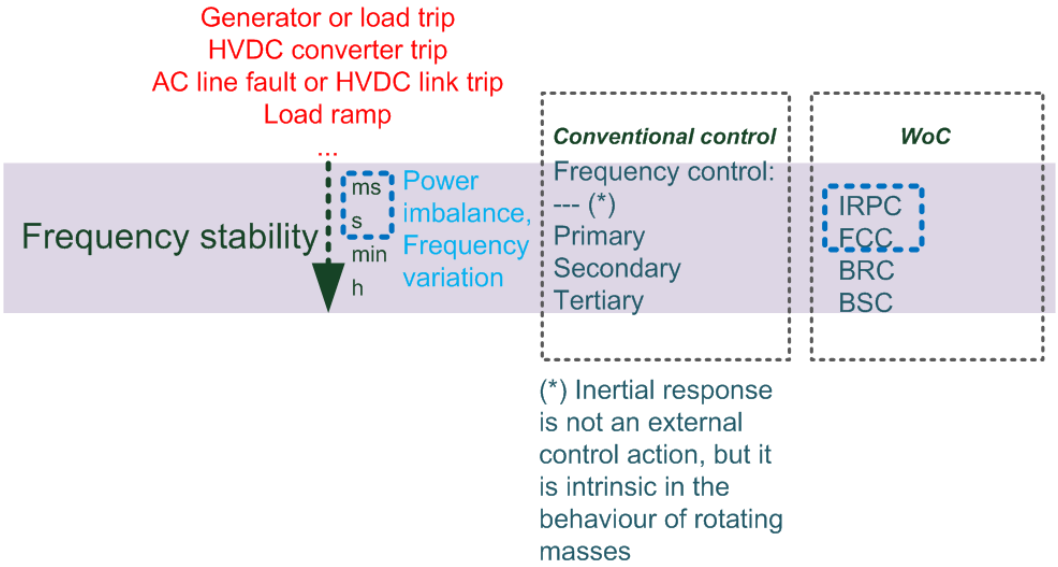

Figure 2-4 Comparison between the traditional and the proposed ways to control the power system, with reference to frequency stability issues.

Remark: frequency stability, on the whole, is influenced by events involving different time scales: for instance, slow load ramps can last hours, while an unplanned outage of a large generator is a sudden event. Correspondingly, different control actions, operating over different time spans, have been/have to be devised to control frequency. All of these controls are depicted in Figure 2-4 and should be considered for a thorough assessment of frequency stability. In this work, however, we

restrict the analysis to the first and fastest part of frequency transients, so to the scope of IRPC only, in a WoC context. Some results will also be shown with reference to the time scope of FCC, although this latter is not analysed in detail.

2.4.3 Analysis methodology and observables identification

Simulation studies aimed at frequency stability assessment can be assumed as useful tools for the identification of suitable observables for the pan-European network organized as a Web-of-Cells. For this purpose, the proposed 4-cell network model (see Chapter 3 Pan-European reference power system) will be employed, in simulations in the DigSilent PowerFactory environment. On the whole, the analysis methodology can be described as follows. For the main symbols, reference will be made to Figure 2-5, reporting the features of a typical frequency transient following a power imbalance in the form of a large power step occurring at time $t=t_{pert}$ (e.g. a relevant loss of generation or load or a relevant variation of the active power exchange between a cell and one of its neighbouring cells).

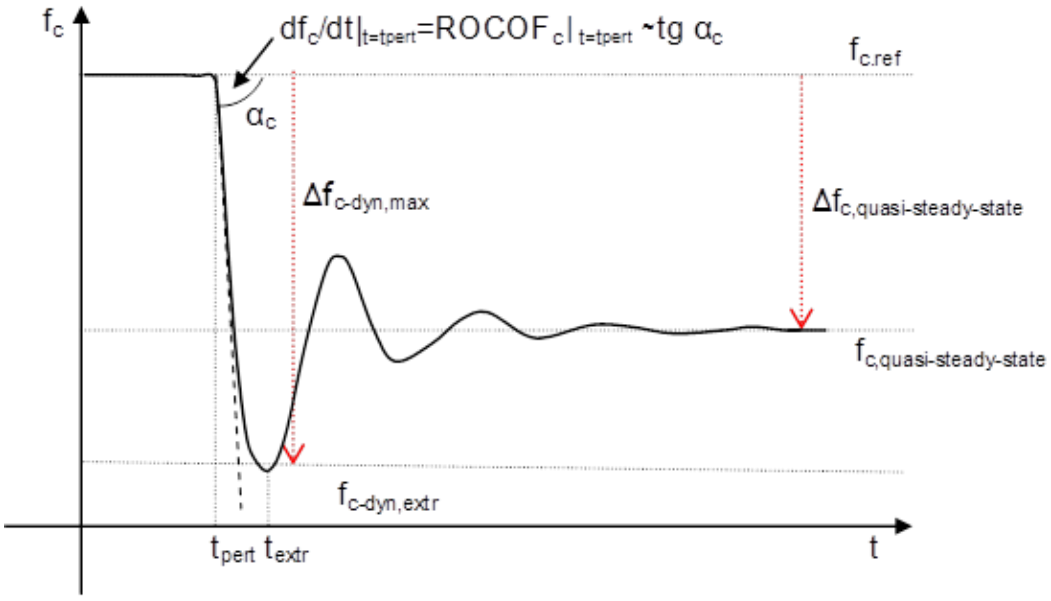

Figure 2-5 A typical frequency transient due to a step power imbalance.

A set of quantities can preliminarily be envisaged as needed to study frequency stability in a Web-of-Cells:

- The (instantaneous) average frequency of each cell, i.e. f_c (Hz); this average can be assumed, for instance, as the weighted average with respect to the inertia constant of the synchronous machines in the cell, namely as the center-of-inertia frequency of the cell;
- The rate of change $ROCOF_c$ (Hz/s) of the (instantaneous) average frequency of each cell; $ROCOF_c$ may be either the time derivative of the frequency, namely df_c/dt, typically evaluated at the time of perturbation tpert, or the incremental ratio $\Delta f_c/\Delta t$ of frequency across a suitable (i.e. sufficiently small) time interval (from 200-300 ms to 500 ms; the size of this time interval depends on how fast is the ROCOF measurement needed;

- The maximum deviation $|\Delta f_{c\text{-}dyn,max}|$ of the mentioned frequency due to a sudden and relevant change in power balance;
- The time interval t_{extr}-t_{pert}, where $t_{,extr}$ is the time instant for which $\Delta f_{c\text{-}dyn,extr}$ is attained;
- The maximal absolute value $|ROCOF_c|_{max}$ of the mentioned rate of change of frequency in the frequency transient;
- The (quasi-)steady-state deviation of frequency $\Delta f_{c,quasi\text{-}steady\text{-}state}$ from its setpoint value $f_{c,ref}$, which, in turn, can coincide with the frequency nominal value or be slightly different from it; $\Delta f_{c,quasi\text{-}steady\text{-}state}$ is obtained after the described transient has exhausted;
- The time interval, starting from t_{pert}, after which f_c reaches (quasi) steadily the value $f_{c,quasi\text{-}steady\text{-}state}$, namely after which $|f_c\text{-}f_{c,quasi\text{-}steady\text{-}state}|<\varepsilon$, where the error value ε has to be quantified as well (10-20 mHz could be a starting point for the evaluation);
- The (physical) inertia constant H_i (s) of each synchronous generator in a cell;
- The "equivalent" inertia constant H_j (s) of each device that can be used to supply synthetic inertia in a cell;
- The overall inertia constant of each cell, i.e. H_c (s); this could:
    - Either be a combination, in terms of a suitable weighted average, of all physical and equivalent inertia constants of single machines and devices; in this combination, not only the individual H_i or H_j could be relevant, but also the electrical distance, or better impedance, of the lines connecting the machines or devices;
    - Or be derived from cell frequency measurement, assuming that the Web-of-Cells working point (in terms of active power injections and absorptions, inside the cell and/or with respect to the neighbouring cells) is known and the perturbation is known;

  Of course, a comparison of the values for H_c resulting from the two methods should give indications about the consistency of the two methods and/or suggestions about the place/s where to take frequency measurements;
- The overall inertia constant of the whole Web-of-Cells, i.e. H_{sys}; again, this could be:
    - Either be a combination, in terms of a suitable weighted average, of the inertia constants H_c of all individual cells; in this combination, not only the individual H_c could be relevant, but also the electrical distance, or better impedance, of the tie lines connecting the cells;
    - Or be derived from cell frequency measurement;

The proposed simulation study will be employed to assess the effectiveness of the choice of observables from the mentioned set of quantities, in practice by assessing the impact of a relevant incident. In particular, a suitable subset of such variables, e.g. $|\Delta f_{c\text{-}dyn,max}|$, $|ROCOF_c|_{max}$, H_c or the whole H_{sys}, could be employed to define the boundaries of the Web-of-Cells frequency stability region.

Remark: inertia can be foreseen to have a sort of "pervasive", but also "tricky" role in the future power system, in that, due to the decrease of physical inertia, machine or device inertial behaviour will have direct and indirect effects on phenomena related to different forms of stability. First of all, there is a direct influence of inertia on frequency stability, as highlighted in these last paragraphs. Rotor angle stability is also affected by the variation of inertia, but in a more subtle way: for example, let us suppose that physical inertia decrease in a region jeopardizes frequency stability, and that the problem is tackled by introducing a synchronous compensator into the region, so as to

increase the region overall inertia up to an acceptable value; this measure, however, does not prevent synchronous machines in the region from having too fast and/or wide rotor angle swings, or from oscillating with respect to each other: in other words, angle stability can still be an issue (which, in turn, can be faced with other means, such as by reducing the impedance between two electrically distant generators which are oscillating with respect to each other). Therefore, once frequency stability has been obtained in terms of sufficient inertia, angle stability has to be taken into account as well. This latter problem, anyway, is foreseen to be much more complex than the former, because one average frequency can be defined and referred to, at least for each cell or for sets of AC cells connected synchronously together, while rotor angles are a large set of local variables.

2.5 Topic 4: Voltage stability (transmission capacity)

2.5.1 Definition of voltage stability

Typically, voltage stability denotes the ability of a power system to maintain voltages within limits at all buses in the power system under normal operation and after being subjected to a disturbance. It depends on the ability to maintain equilibrium between load demand and generation supply from the power system. Voltage instability that may result occurs in the form of a progressive fall or rise of voltages of some buses and may be a possible cause of a blackout.

While this definition implies that voltage stability is a global or wide-area issue, it is also among other stability types an important constraint for radial or point-to-point power transfer capability. In this respect voltage instability is caused by the incapability of the generation and transmission system to deliver the reactive power necessary to satisfy load demand, whilst keeping the voltages in permissible range. For example, for EHV lines longer than 80 km voltage drop starts to dominate as a factor limiting transfer until up to around 300 km, where small signal and transient stability are the most important limiting factors [35]. From this perspective, voltage stability analysis is a significant part of Pan-European system analysis, particularly for radial feeders and long lines.

Therefore, in the context of ELECTRA and Pan-European system analysis, the problem of voltage (in)stability can be redefined as a power supply problem specifying the limits of the power that can be supplied to the load and in this way determining stability of the supply or stability of the transfer corridor.

2.5.2 Connection to WoC concept and use cases

As described in more detail in the next subsection, voltage stability can become in peril in the wake of two types of network disturbances:

- Load increase, which can be regarded as increase of total cell demand[1] or increase of magnitude of a particular load, especially one supplied by a radial connection, would provoke counteractions from:
    - PPVC - since the process is assumed to be rather slow in pace,
    - BSC - if the load rise has not been planned and as a result has caused imbalance in the cell.

[1] Therefore later would be referred to as cell voltage stability.

This scenario might also be equivalent to a trip of a generator supplying a load (see Figure 2-6).

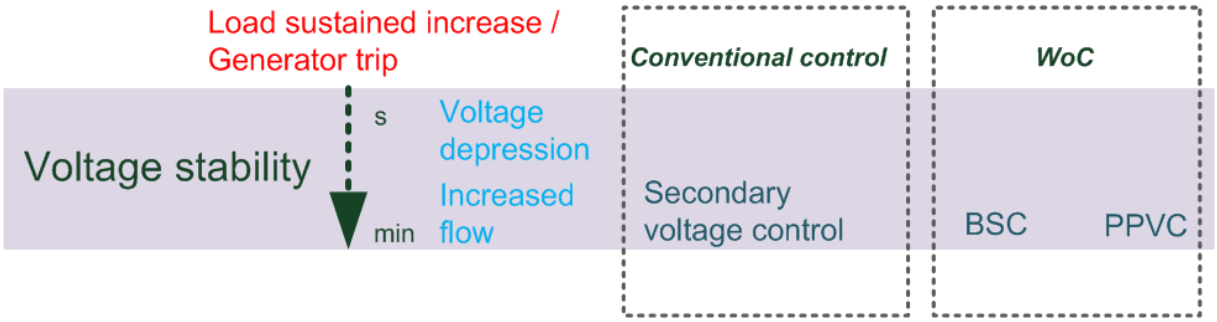

Figure 2-6 Comparison between the traditional and the proposed ways to control the power system, with reference to voltage stability issues related to load or generation variations.

- Outage of a network element, which would most likely cause PVC to react on voltage drop or rise. If the outage is far from resources operated by PVC, their influence on voltage correction might be insufficient because reactive power cannot be sent over long distances. Therefore other means of voltage improvement would have to be engaged, e.g. tap-changers of transformers under an umbrella of PPVC (see Figure 2-7).

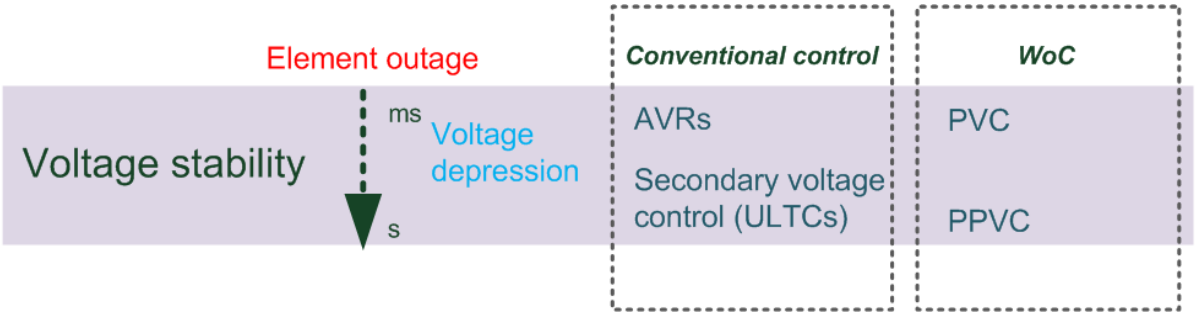

Figure 2-7 Comparison between the traditional and the proposed ways to control the power system, with reference to transient stability issues related to element outages.

2.5.3 Analysis methodology and observables identification

Voltage stability can be analysed with use of static methods based on calculating multiple load flow solutions with demand as a parameter being successively increased. As a result nose curves are obtained and by applying one of the available criteria (e.g. dQ/dV or dQ_G/dQ_L)[2] critical load power can be calculated. Then, for a given operating point the voltage stability margin is readily evaluated (P_{max}/P_0) and other stability indices can be determined.

However, solving a power flow with significant voltage deviations requires accurate load models in order to obtain meaningful results. With respect to voltage, the load models can neglect its

[2] These are classic voltage stability criteria which help to determine whether the power system is in a stable or unstable equilibrium point; dQ/dV evaluates the capability of the system to supply the load with reactive power for a given real power demand, whereas dQ_G/dQ_L helps to analyse the behaviour of the reactive power generation as the reactive power demand of the load changes.

variations (constant active and reactive power), can be directly proportional (constant active and reactive current) or can be proportional to the square of voltage (constant impedance). Different types of studies require different proportions of each type of load in a composite load model and, as can be expected, it is a crucial factor for the whole analysis. Even if the coefficients are correctly selected, static load characteristic can only approximate the real behaviour of load and can only be used for slow processes.

In practice, voltage stability is a dynamic process, in which load dynamics as well as voltage and frequency control systems play the main part [36]. Their inclusion in the analysis of PVC and PPVC operation is essential.

Within the scope of task 5.4 two typical scenarios leading to voltage instability and voltage collapse will be considered and evaluated by means of dynamic analysis:

- Load build-up
  In this typical scenario it is assumed that during a heavy demand period, load in one part of a system (e.g. a whole cell or a radially-fed load in a cell) increases close to or over the critical value determined by network parameters. The dynamics of various voltage control devices as well as the overall PPVC will have the most significant influence on this process.

  Candidates for observables resulting from this scenario are $d\Delta Q/dV$ ratio, load demand and critical load or the ratio between current load and critical load.

- Network outages
  As network parameters play a crucial role in determining the critical load it is expected that by changing the equivalent impedance between the source and sink e.g. by tripping one of the interconnectors, the voltages will drop. These circumstances may be a trigger leading to voltage collapse. In such case the pre-contingency operating point will be considered voltage insecure. On the other hand, if the n-1 contingency does not put voltages at risk, this state might be considered voltage stable.

  Candidates for observables are: network state (expressed by equivalent impedance or short circuit power) and critical load.

2.6 Topic 5: Inter-cell loop flows

2.6.1 Definition of inter-cell loop flows

An inter cell loop flow is a physical phenomenon that occurs when there is a difference between commercial schedules and physical flows of power between the producers and the customers. The power transmission between a producer and a consumer flows through all lines connecting the two, not only along the shortest distance between them (see Figure 2-8) [37].

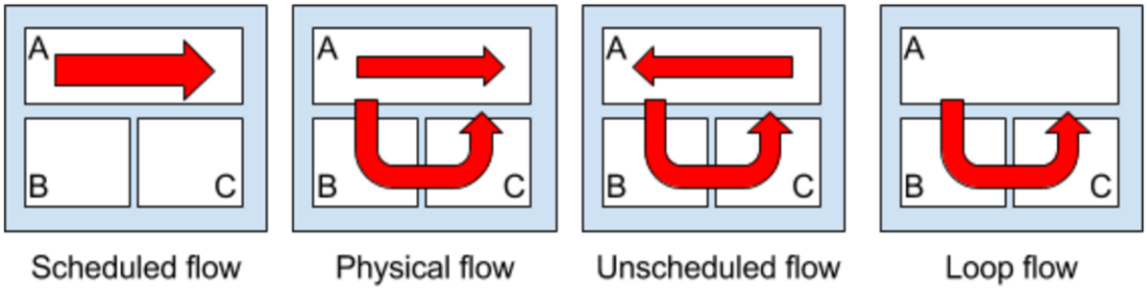

Figure 2-8 Terms explaining inter-cell loop flows.

Figure 2-8 explains the terms used for inter-cell loop flows. The scheduled flow is defined according to the market solution and describes the contracted import/export between and within the cells in the system. The physical flow is the actual power flow in the grid following Kirchhoff's first law. As seen in Figure 2-8, some of the power flows through Cell B and Cell C before going back into cell A. The unscheduled flows are the difference between the physical flow and the scheduled flow. Loop flows are the unscheduled flows through cells not part of the scheduled flow.

Power loop flows occur when a cell does not have enough internal grid infrastructures to handle new production. The power is diverted through neighbouring cells and then back into a different part of the producing cell. Germany, e.g., has increased its power production in the north by building wind power, however they have not developed the grid infrastructure to transfer the output to the loads in the south. Therefore a large share of the power flows through the grids of its neighbour countries and then back into southern Germany.

Problems related to loop flows

Problems related to loop flows are listed below:

Operational security: Loop flows are difficult to control and can damage transmission equipment: in fact, in case of transmission line overloading or under/overvoltage phenomena the voltage level at each node and power flows are out of operational security limits. In the worst case, the only way for a grid operator to avoid damage is to cut the power flow through the over loaded interconnections. This could result in a cascade effect with more over loaded interconnections resulting in large blackouts.

Market integration and efficiency: The loop flows are reducing the capacity for inter-cell trade and reduces the efficiency of the grid.

Infrastructure: Loop flows can hamper cross-border investment since these might not be beneficial for the investing country. A strong grid connection to a neighbour cell with large internal power flow could result in increased power loops from the neighbour cell.

Means of avoiding loop flow

Existing grid components could be used for redirection of the power flow and reducing or eliminating the loop flows. The most important components are listed below:

- Phase shifting transformers: The power flow between two cells can be controlled by using phase shifting transformers. The effective phase displacement between the input voltage and output voltage of a transmission line is changed, thus controlling the amount of active power that can flow in the line.
- Series compensation: Variable and controlled high-voltage series capacitors are inserted into transmission lines in order to increase the power flow across the compensated line.
- Shunt compensation: Static synchronous compensators (STATCOM) and Static VAR compensators (SVC) are usually adopted to the purpose.
- Synchronous generators: The active and reactive power production of the synchronous generators could be modified in order to adjust the power flow.
- HVDC converters: HVDC links could be used as a grid power flow controller by directing the power flow to the desired direction.

2.6.2 Connection to WoC concept and use cases

Post-primary Voltage Control (PPVC) has the commitment to bring the voltage levels in the nodes of the power system back to nominal values while minimizing the power flows in order to reduce the losses in the network. PPVC should be completed in the time frames of current secondary voltage control. Each cell is responsible for its own voltage control while a close coordination guarantees the provision of PPVC service between neighbouring cells. Since no vertical control should be applied, the cells need to cooperate in order to eliminate the inter-cell loop flows. The main task of this topic is to define the observables needed for horizontal control of the power loops. In order to achieve this task, solutions for horizontal control of power flows will be discussed.

Balance steering control (BSC) can also be used for reducing or eliminating by rescheduling power production from one cell to another cell.

Figure 2-9 compares the traditional and the proposed way to control loop flows. In the WoC, the PPVC will control the loop flows instead of the secondary/tertiary voltage control. The PPVC will use phase shifting transformers, series compensation, shunt compensation and reactive power production of synchronous generators, HVDC converters and other converters to redirect the power loop flow.

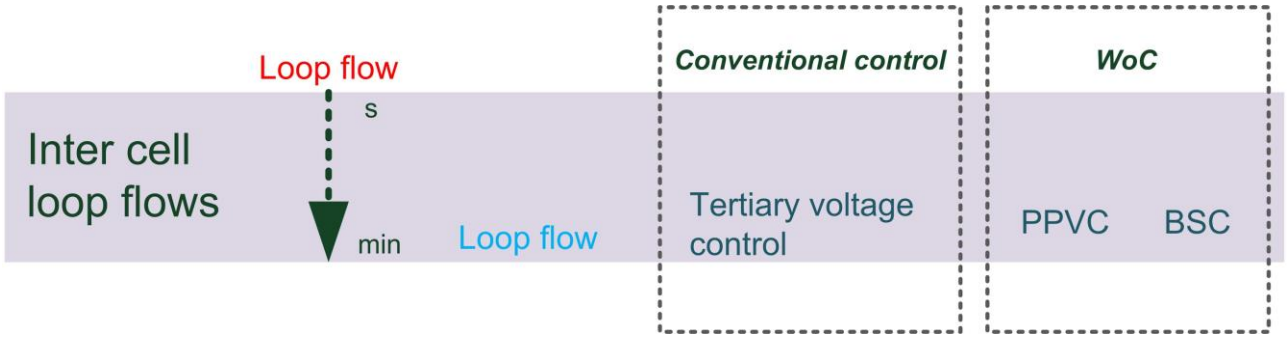

Figure 2-9 Comparison between the traditional and the proposed ways to control the power system, with reference to inter-cell loop flows.

The challenge by unscheduled flow and horizontal control or loop flows is explained in Figure 2-10. Given an unbalanced situation (a), Cell A and Cell B will agree on a power transfer from Cell A to Cell B (b). However, some of the power is actually going through Cell C and Cell D and the tie-line between Cell C and Cell D is overloaded (c). The problem could be solved in different ways:

- Cell A and Cell B handle the overload by:
  - Redirecting the power flow directly between them by using the above mentioned grid components (PPVC), or
  - Increasing power production in Cell B and reducing the power production in Cell A (BSC).
- Cell C and Cell D handle the overload, either by:
  - Redirecting the power flow back to cell A (PPVC), or
  - Increasing power production in Cell D and reducing the power production in Cell C (BSC).
- A combination of the above mentioned solutions (PPVC and BSC).

Basically, Cell A and Cell B do not know that their power transfer is causing an overload and Cell C and Cell D do not know what is causing the problem. Some information exchanges are therefore probably needed.

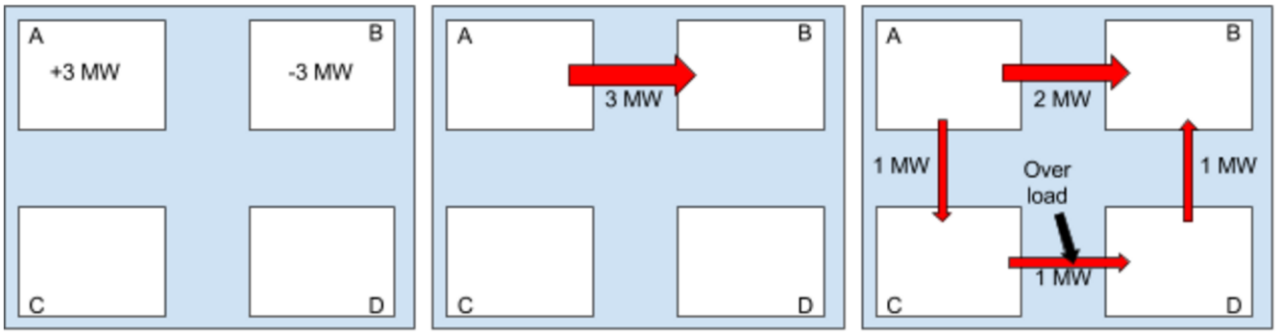

(a) (b) (c)

Figure 2-10 Loop flow case example

2.6.3 Analysis methodology and observables identification

The Pan-European SRPS presented in Chapter 3, with suitable modifications, will be used for identifying loop flows and testing control actions for reducing the loop flows. Production and loads may be moved to provoke loop flows.

The market design is not considered in this task. The defined production plan is therefore an input to the model. Improving the market design by considering the physical behaviour of the power flow between the cells could reduce the power flow problem, however a market model will not be implemented in the model.

A methodology for finding and eliminate inter-cell power loops is suggested below:

- *State Estimator and OPF: State Estimator and* Optimal power flow analysis (OPF) are executed for all the cells as shown in chapter 5.2.1 in [32].
- *Power flow analysis:* Power flow analysis is executed for all the cells.
- A disturbance (change in power production/loads, disconnected line etc.) causing inter-cell loop flows is added.
- *Identify inter-cell power loops:* The unscheduled power flow is found as the difference between the scheduled power flow and the measured power flow. Thereby the inter-cell power loops and the necessary observables are identified.

- *Reschedule the power flow:* The power flow are rescheduled by using phase shifting transformers, series compensation, parallel compensation, the reactive power of the producers and power flow of HVDC links. Necessary algorithms for this rescheduling must be developed.
- *Monitor inter-cell power loop changes:* A power flow analysis with the input from the previous point is executed and the changes in inter-cell power loop are observed.

2.7 Topic 6: HVDC operation (trip/runback)

2.7.1 HVDC fault impact on power system

Irrespective of smart-grid development pace and direction, HVDC technology will play an important role in future power system operation, either as a means for power plants (mostly offshore wind power) interconnection, bulk-power transmission corridors, or even as a backbone of a Pan-European transmission system (DC Grid). Constantly increasing power levels and attainable lengths of the HVDC connections result in increasing peril for the secure AC power system operation in case of a disturbance causing a DC link to trip. Power imbalances, i.e. surplus on sending end and shortage on receiving end, can provoke effects similar to those stemming from tripping out aggregated generation or load. In such an event, active power imbalance would most likely be accompanied by reactive power flow change, resulting in further aggravation of voltage problems. What is more, if the tripped HVDC link was operating between two parts of a synchronous system also connected by other tie lines, these could become overloaded and eventually tripped.

Occasionally, when a DC link is a main transmission corridor for power delivery to an islanded power system (e.g. Gotland, Corsica-Sardinia), an abrupt termination of transmission might also cause frequency fluctuations and, depending on the current operating state of the islanded power system, activation of special protection schemes (e.g. UFLS – Under Frequency Load Shedding) in order to restore the power balance. Therefore, from the stability slant, HVDC malfunction can have impact on almost all stability-related aspects of a power system.

2.7.2 Connection to the WoC concept and use cases

The devised and elaborated use cases do not explicitly redefine the role of HVDC systems in the future. One can assume, however, that having capability of very fast control of active and reactive power, HVDC systems can take part as an actor or flexibility resource in all HLUCs, particularly in situations where an HVDC link connects two separated cells. Therefore, it is important to assess whether a malfunction in operation of a DC link will have different impact on the operation of the WoC than it has on a traditionally operated power system.

It should be stressed that from the viewpoint of the WoC-based system analysis it is expected that both leading technologies used in HVDC transmission, namely LCC and VSC, would have similar level of impact on the power system, as far as an interruption of AC power delivery is concerned. Therefore, this abrupt change in delivered/sent active power will cause cell imbalance, which will activate BRC and BSC. Depending on the ratio of the size of the system and amount of transmitted power, frequency deviation might occur entailing action from FCC and IRPC for large ROCOF. Also, the Cell Operator in whose cell an HVDC link acts as an inertia resource has to take actions to restore the response power present in the cell.

With respect to reactive power, VSC is much more flexible, being able to control voltage at PCC in a STATCOM-like manner, whereas LCC is aimed at operating close to unity power factor [38]. Thus, subsequent to a converter trip, this event would cause a reactive power imbalance and a voltage deviation at PCC in a power system with VSC HVDC, while a system with LCC HVDC would experience temporary overvoltage due shunt capacitor banks which just after the event would still remain connected. In both cases, nearby PVC would be initially triggered in order to restore voltage to a proper level and then PPVC action would be required in a degree depending on the reactive power imbalance level.

The progress of each of the above-mentioned phenomena is highly dependent on short circuit ratio (SCR) [39], which in turn is subject to constant variations, especially due to generation portfolio changes and system load changes. Lower SCR means more problematic operating conditions and thus higher requirements for cell control systems.

In a typical HVDC configuration, once the fault has been cleared a runback procedure is initiated in order to bring back the converters as quickly as possible. Usually this process is finished within a few hundreds of milliseconds, which makes it virtually invisible from the AC system perspective, particularly for slower acting systems like turbine governors and part of AVRs. However, for a low-SCR converter location the recovery time is longer so that the situation is not aggravated even more. In this case an attempt to re-establish a pre-fault power transfer on the link might be problematic for the new control systems (HLUCs) if they are too fast, as they might interpret this procedure as another disturbance and act in an opposite way. Thus depending on SCR and response speed of the control loops each fault might be seen as a no-fault scenario (fast systems, high SCR) or double-fault scenario (slow systems, low SCR).

The relationship between HVDC type and the involvement (and importance) of different high level use cases has been summarized in Table 2-1. The involved time frames are reported in Figure 2-11.

Table 2-1 Expected level of engagement of HLUC for different loading levels of HVDC links

HVDC type	Transfer level	High level use case (control mechanism)					
		IRPC	FCC	BRC	BSC	PVC	PPVC
VSC	high	low[1] to high	low[2] to high	high	high	medium to high[3]	medium to high[3]
	low	low[1]	low[2]	medium	medium	low to high[3]	low to high[3]
LCC	high	low[1] to high	low[2] to high	high	high	high[4]	high[4]
	low	low[1]	low[2]	medium	medium	low	low

[1] If the HVDC link is used as a flexibility resource for Inertia Control then other resources might be needed in order to substitute for the faulted link.

[2] If the receiving end system is small compared to the bandwidth of frequency support provided by the HVDC link, then FCC involvement after HVDC fault might be higher.

[3] STATCOM capability might be lost during the fault.

[4] Especially for low SCR location.

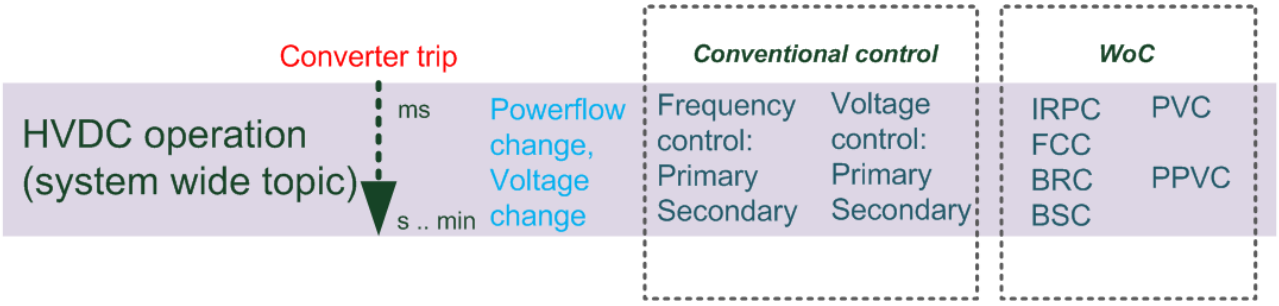

Figure 2-11 Comparison between the traditional and the proposed ways to control the power system, with reference to HVDC operation.

The chosen reference power system model contains several HVDC links constituting a part of a DC grid, which was planned to form one cell of a WoC. By means of simulation, this model allows to evaluate the impact of HVDC technology on WoC operation.

2.7.3 Analysis methodology and observables identification

- Model selection and preparation

The chosen power system model is expected to be adequate for the purpose of HVDC impact analysis provided that minor changes are introduced. For the purpose of inclusion of the most common HVDC technology, i.e. LCC, the existing AC line 1.2 - 2.5 (b), between cell 1 and cell 2, will be changed to DC. Simultaneously, the remaining line can be switched off to consider asynchronous operation of the two cells or remain unchanged for synchronous operation with parallel DC line. The existing DC network is suitable for the purpose of VSC-type converter operation analysis.

- Method specification

Firstly, desired operating conditions need to be established. This step includes setting up the right power flow by changing load and generation in the model, as well as the ordered power flow in the HVDC link. Two cases regarding loading level and other two regarding SCR level will be prepared for each technology, which in total gives eight cases to be validated (see Table 2-2).

Table 2-2 HVDC analysis cases

Case No.	**1**	**2**	**3**	**4**	**5**	**6**	**7**	**8**
HVDC Technology	LCC	LCC	LCC	LCC	VSC	VSC	VSC	VSC
Load level	High	High	Low	Low	High	High	Low	Low
SCR	High	Low	High	Low	High	Low	High	Low

In each case a disturbance leading to a converter trip will be simulated. This can be for example a DC fault or an AC fault (especially on inverter side). Impedance and duration of the fault will be selected in such way, that the transfer will be terminated due to DC voltage collapse and/or DC overcurrent protection, which will be determined by the response model of the HVDC link.

With DC current terminated, AC voltage and current will undergo a transient which will trigger high-level control loops involved in balance and voltage control, as described in Subsection 2.7.2.

Since the response models are planned to be used, a runback procedure can be easily included in the analysis and simulation tests can be repeated.

- Evaluation parameters

Since the proposed method constitutes a kind of a benchmark test for a WoC-based power system, there is no focus on a particular stability type, but rather on global, generic operational parameters of the power system. These include: maximum voltage deviations, time needed to reach a new equilibrium point, maximum angle deviations, etc.

- Analysis procedure

The analysis will be carried out for all the eight cases. For each of them, simulation tests with disturbances causing converter trip will be run, including the runback procedure, and the mentioned benchmark parameters will thus be evaluated.

The procedure allows for a straightforward comparison with a traditionally controlled power system.

- Observables identification

Since SCR is a critical parameter for proper HVDC operation, this parameter is a candidate for an observable. Also a ratio between cell generation and HVDC power transfer to/from that cell might be important.

3 Pan-European reference power system description

3.1 Scope

The scope is to define a single reference power system which is suitable for the stability and system-wide studies at the Pan-European level. The complexity of the modelled power system depends on the kind of analysis being carried out and can be adjusted according to that. The structure of the model and all relevant parameters are given in the following section in order to be able to use different modelling software. The original model is realized in Powerfactory version 15.2.6 and depending on the partners' needs, it will be translated into other simulation packages (for instance Simulink-SimPowerSystem or PSCAD).

The model is actually a work-in-progress, meaning that, although the current status constitutes the basis for running the analysis in the different topics, nevertheless, depending on specific topic needs, the model may be subject to revisions or different operating points. For instance the generation centres, represented so far with synchronous machines, will be partially replaced with inertia-less units (such as type 4 wind turbines or photovoltaic units) or reduced inertia units (such as type 3 wind turbines [40]-[41]) in order to create a realistic scenario for investigating the topics mentioned in chapter 2.

3.2 European HV benchmark network proposed by CIGRÉ synthetic overview

The European HV Benchmark network proposed in the CIGRÉ report [43] laid the foundation for the derived Pan-European test grid for ELECTRA Task 5.4. A synthetic overview of the original CIGRÉ network is reported below while the so called “Pan-European” network is described in the following section.

The network transmission voltages used are 220 kV and 380 kV, which are typical in European transmission systems. Generation bus voltages are 22 kV, and the system frequency is 50 Hz. The system is a balanced three-phase HV transmission network, and assumes ideal line transposition. The HV transmission network benchmark is shown in Figure 3-1: it consists of 13 buses and covers three geographical areas, referred to as Areas 1, 2, and 3, denoted by dashed lines. Area 1 is predominantly a generation centre. Area 2, situated about 500 km from Area 1, is a load center with a small amount of generation available. Area 3 is situated between the main generation Area 1 and the main load centre Area 2. Three voltage levels exist in the network: generation bus voltage of 22 kV, primary transmission high voltage of 220 kV, and a long line connecting Areas 1 and 2 at the extra high voltage (EHV) level of 380 kV. Bus 6a in Area 2 is a suitable location for studying the incorporation of large-scale renewable energy sources such as wind energy conversion systems.

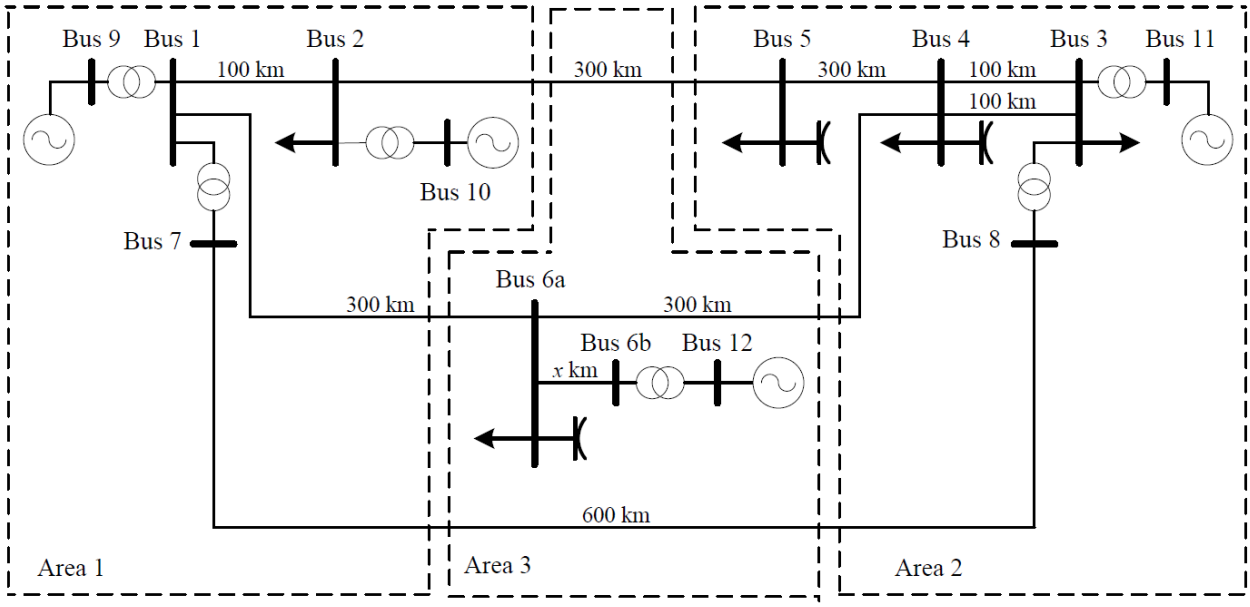

Figure 3-1 Topology of European HV transmission network benchmark [38].

3.3 Pan-European network synthetic description

Since the CIGRÉ grid only represents a pure AC grid and ELECTRA focuses on the future power grid, the grid has been extended with a DC part and also subject to a revision of the AC side in order to improve load flow convergence. Furthermore, the grid topology has been modified in order to create a more diverse and flexible model while trying to keep it as simple as possible. The network includes a 220 and 400 kV (note that the 380 kV level has been updated to 400 kV) AC grid together with a meshed DC 725 kV grid. The DC voltage level has been chosen so that it allows direct connection of HVDC VSC converters without need of internal transformers for stepping down the AC side. The generation units are connected to the 20 kV AC bus (it has been chosen to change the 22 kV level with the more common 20 kV level). Most of the buses have both conventional and renewable units, because the network is representing an equivalent transnational grid, where load and generation units are aggregated. It has been decided to equip conventional units with either a gas turbine governor or a hydraulic governor; the excitation system is similar for all of them. Renewable units are mainly wind turbines type 3 (i.e., doubly fed induction generator based) and 4 (i.e., full converter based). At this stage no PV is included, however from stability point of view, the transient behaviour of a PV system can be compared to the one of type 4 wind turbine, being both units connected with PWM converter. It has to be noted that the generation capacity in the system exceeds what is required to cover the demand, so that it is not possible for the generation units to produce full power at the same time. In this way it is possible to investigate several renewable penetration scenarios, having conventional plant progressively displaced (i.e. physically disconnecting synchronous machines from the network) in order to make room for renewable resources. Loads are modelled according to the classic ZIP theory [8]: active power consumption is linearly dependent on voltage value, while it is not dependent on frequency (this takes in account that more and more asynchronous motors are being replaced with inverter driven motors, which present a constant power characteristic during frequency variations); reactive power consumption is quadratically dependent on voltage and it is assumed not being dependent on frequency.

Four cells are identified and the main information for each cell is reported in the Table 3-1. The grid is presently under testing and therefore changes/modifications of both static and dynamic models are foreseen in order to accommodate the analysis intended in the different topics.

Table 3-1 overview of the cell generation and consumption level

	Cell 1	**Cell 2**	**Cell 3**	**Cell 4**
Voltage levels (kV)	20; 220; 400; 725	20; 220; 400	20; 220	400; 725
AC/DC	AC and DC	AC	AC	AC and DC
Nominal generation power	2x400 MVA 2x500 MVA synchronous machines (gas turbine governor) 100x6 MW (type 3 wind turbines) 100x6 MW (type 3 wind turbines)	1x700 MVA synchronous machine (gas turbine governor) note: this machine is used as slack for LF calculations	2x500 MVA synchronous machines (hydraulic governor) 100x6 MW (type 3 wind turbines)	1x600 MVA equivalent wind generation (type 4)
Nominal consumption power	2x1000 MW + j 2x165 MVAr loads (load P consumption is linearly dependent on voltage and constant on frequency; load Q is quadratically dependent on V and constant on frequency)	3x400 MW + j 3x130 MVAr loads	1x400 MW + j 1x130 MVAr;	no load
Number of tie-lines	Cell 1-2: 2 AC 220 kV tie lines Cell 1-3: 2 AC 220 kV tie lines Cell 1-4: 1 AC 400 kV tie line; Cell 1-4: 1 DC 725 kV tie line	Cell 2-1: 2 AC 220 kV tie lines; Cell 2-4: 2 AC 400 kV tie lines; Cell 2-3: 1 AC 220 kV tie line	Cell 3-2: 1 AC 220 kV tie line; Cell 3-4: 1 220/400 kV transformer 1 tie line Cell 3-4: 1 AC 220 kV tie line;	Cell 4-1: 1 AC 400 kV tie line; Cell 4-1: 1 DC 725 kV tie line; Cell 4-2: 2 AC 400 kV tie lines; Cell 4-3: 1 220/400 kV transformer Cell 3-4: 1 AC 220 kV tie line
Number of internal lines	2x220 kV line	4x220 kV lines	3x220 kV line	3x725 kV lines
Nominal HVDC capacity	1x500 MVA PWM converter	no PWM	no PWM	3x500 MVA PWM converters

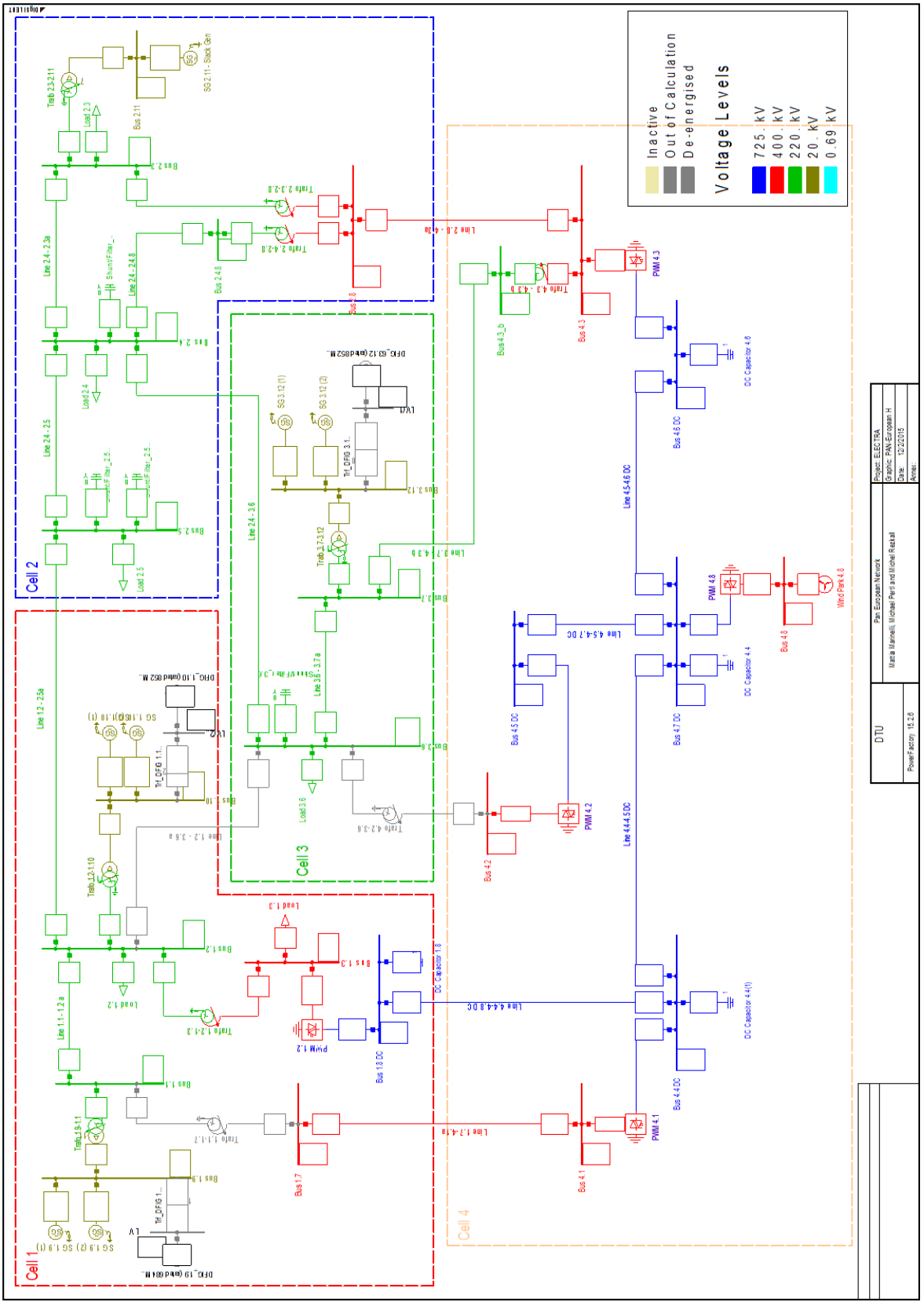

Figure 3-2 Topology of the proposed Pan-European Single Reference Power System.

3.4 Modelling assumptions

In order to achieve realistic results with time domain simulations, some important considerations have to be made prior to the analysis. This includes, but is not limited to the models of (a)synchronous machines, transformers, converters and loads. Load modelling has to gain special attention due to its large impact on the results. The loads are representing the aggregated behaviour of the underlying distribution system. Thus, the loads are modelled as voltage and frequency dependent. However, the load characteristics have to be adjusted according to the load distribution of the considered system.

3.4.1 Simulation Model

The simulation model comprises four cells with different properties in terms of generation portfolio, load and voltage level/type. The key features of the model are summarized in Table 3-1. The synchronous generators in cell one and two are representing gas turbines while the synchronous generators in cell three are hydraulic turbines. All the generators are equipped with excitation systems, which are suggested by ENTSO-E [44].

The multi-terminal DC (MT-DC) grid in cell four connects a static generation unit with the AC grid at four different locations via voltage source converters (VSC). The VSCs are controlled according to a master/slave principle, i.e. Converter 4.3 controls the AC and the DC voltage at its terminals and, thus, acts as the master while the other grid connected converters control their AC terminal voltage and the active power flow through them and are therefore called slaves. Converter 4.8 connects the static generation unit with the MT-DC grid and controls the AC voltage and frequency at the remote AC Bus 4.8. The static generation unit can represent any kind of converter connected generation, such as wind power or PV.

The DFIG models are originating from the PowerFactory library and are available as templates with rated powers from 1 - 6 MW. The 6 MW-type with 65 parallel units was used in the analysis as indicated in Table 3-1. This configuration of wind parks with 65 6 MW units is installed at three different locations which correspondents to a total installed capacity of 1170 MW (3 x 65 x 6 MW) DFIG generation.

Loads are modelled as dynamic loads, i.e. the active and reactive power consumed by the loads is sensitive to changes in voltage and frequency. This behaviour is usually described by ZIP models (Z = const. impedance, I = constant current, P = constant power) for voltage dependence and extended by a term to account for frequency dependence. The exponential model for voltage dependence extended with a linear model for the frequency dependence is shown in Eq. 3-1 and Eq. 3-2 and (2) for active and reactive power consumption, respectively.

$$P=P_0(\underline{V}^{\alpha})(1+K_{pf}\Delta f) \qquad \text{Eq. 3-1}$$

$$Q=Q_0(\underline{V}^{\beta})(1+ K_{qf}\Delta f) \qquad \text{Eq. 3-2}$$

Where:

$$\underline{V}=V/V_0 \text{ and } \Delta f=f-f_0 \qquad \text{Eq. 3-3}$$

P, Q - actual active/reactive power drawn by the load

P_0 , Q_0 - nominal active/reactive power of the load

V - actual voltage

V_0 - nominal voltage

α, β - exponential coefficients for characterization of ZIP (0 = const. power, 1 = const. current, 2 = const. impedance)

K_{pf}, K_{qf} - linear coefficients for frequency dependence of active and reactive power, respectively

The voltage dependence for active power is set to constant current (α = 1) and to constant impedance (β = 2) for reactive power. The set up for voltage dependence applies for voltages between 0.7 and 1.2 pu and is changed to constant impedance if the voltage exceeds this limits to avoid computational problems. The frequency dependence is set to K_{pf} = 1.5 and K_{qf} = -1 for active and reactive power, respectively. The coefficients for voltage and frequency dependence are set according to the common practice for stability studies which is also recommended in [45]. Table 3-2 summarises the used parameters for voltage and frequency dependence of the loads.

Table 3-2 Summary of Load Model Parameters

Voltage Dependence		Frequency Dependence	
α=dP/dV	β=dQ/dV	K_{pf}=dP/df	K_{qf}=dQ/df
1	2	1.5	-1

The calculation of aggregated system inertia (acceleration time constant rated to $S_{r,i}$) 2H for n generators is calculated according to Eq. 3-4.

$$2H = 2\frac{\sum_{i=1}^{n} H_i S_{r,i}}{\sum_{i=1}^{n} S_{r,i}} \qquad \text{Eq. 3-4}$$

Where:

2H - total aggregated system inertia (s)

H_i - inertia time constant of the i-th generator (s)

$S_{r,i}$ - rated power of the i-th generator (VA)

3.4.2 Simulation Scenarios

To analyse the transient stability eight simulation scenarios with different levels of RES penetration have been assumed. The generation from RES ranges from 0 to 90 % with respect to the total load. To set up particularly challenging simulation scenarios, a heavily loaded system was assumed, since generally the stability of highly loaded systems is lower than in lightly loaded systems. This is mainly caused by operating SGs closer to their limits. The total load of the system corresponds to 2600 MW with cos(φ) = 0.95 (ind) as shown in Table 3-1.

Table 3-3 summarizes the key aspects of the eight simulation scenarios such as RES penetration level P_{RES} in relative and absolute values, number and set point of active synchronous generators and the system inertia 2H. Scenario 1 builds the base case without penetration of RES and exclusively generation from SGs, i.e. all eight SGs are in service which correspondents to the total system inertia of 2H = 10 s. In the following scenarios, the RES penetration continuously increases while the share of synchronous generation is simultaneously decreased. SGs are consecutively decommissioned to keep the active power setpoint at a reasonable level. The total system inertia decreases with increasing RES share due to the decommissioning of SGs.

The share of RES generation indicated in Table 3-3 is split into 50% of DFIG and 50% of full converter generation.

Table 3-3 Summary of the Defined Scenarios

	P_{RES} w.r.t. total load (%)	P_{RES} (MW)	number of conventional generators in service	SGs set point P_{SG} (MW)	Loading of SGs % Pgen	Total system inertia 2 H (s)
Scenario 1	0	0	8	325	76	10
Scenario 2	25	650	8	244	57	10
Scenario 3	25	650	6	325	76	7.5
Scenario 4	50	1300	6	217	51	7.5
Scenario 5	50	1300	4	325	76	5
Scenario 6	75	1950	3	217	51	3.75
Scenario 7	75	1950	2	325	76	2.5
Scenario 8	90	2340	2	130	31	2.5

4 System stability and system wide studies results and identification of the relevant observables

The results of the analysis taken for each topic, namely cell transient stability, cell small signal stability (with focus on inter-cell oscillations), inertia at WoC level (frequency stability), voltage stability (transmission capacity), and inter-cell loop flows are reported in this chapter.

4.1 Topic 1: System-Wide Transient Stability Assessment and Visualization

In the past, the equal area criterion, the single machine equivalent method, Lyapunov's direct approaches and critical fault clearing time (CCT) approach were usually used to assess the transient stability. Since these methods are limited to SGs, they cannot be applied to converter based generation units which may also induce active power swings into the system and therefore provoking rapid voltage drops at several buses. Hence, a method which allows to assess the transient stability of SGs and possible active power swings of converter based units on a cell-wide basis has to be developed. Furthermore, the results of the assessment have to be visualized properly in order to facilitate the perception of critical conditions for control room operators.

The introduced method includes assessment and visualization of transient stability on a cell-wide basis. It is also able to capture active power swings induced by converter based generation units, which may cause voltage issues. A time domain (TD) approach is used to assess the transient stability. Opposed to traditional methods, voltage angles at the buses are used to determine whether the grid in its current operational state can sustain a particular large disturbance. The justification why voltage angles at the buses, instead of rotor angles, are used to examine the transient stability is explained by means of the two-machine system in Figure 4-1. The rotor angle φ_{GM} between the two machines is determined by the power transfer P, the sum of the reactances X_T and the two internal machine voltages V_G and V_M. This highly nonlinear relationship, given in (5), is valid for high voltage grids due to the high X/R ratio, but obviously it will deviate significantly for multi-machine systems considering automatic voltage regulators and other effects. However, the general form is similar. The vector diagram of the two-machine system in Figure 4-2 shows that the internal generator voltage is leading the internal motor voltage by the angle φ_{GM}. A greater power transfer leads to an increased angle displacement. Consequently, also the angle φ_L between the two buses increases which enables an assessment of transient stability by utilizing the voltage angles. When the angle between two machines or groups of machines reaches 180° during transient conditions, a loss of synchronism is most likely. That will cause large fluctuations in voltage, current and consequently in the power output of the generator, which eventually leads to voltage angle swings in the system. Additionally, rapid voltage drops at the intermediate point in the network could occur due to the large angle displacement. Since there is no rotor angle in converter based generation, the voltage angle at their buses can be used to evaluate the transient stability on a grid-wide basis. The voltage angle displacement of the bus voltages will indicate whether the power system can sustain a particular contingency without losing synchronism and furthermore indicate if large power swings of converter based generation units occur.

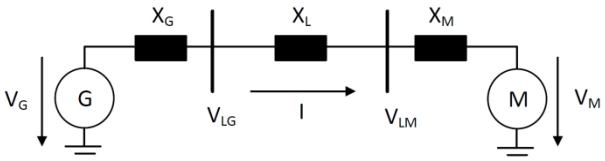

Figure 4-1 Two-machine system, which shows the internal machine voltages V_G and V_M and the synchronous reactances X_G and X_M as well as the line reactance X_L. The sum of the reactances is referred to as X_T.

$$P = \frac{V_G V_M}{X_T} \sin(\varphi_{GM}) \qquad \text{Eq. 4-1}$$

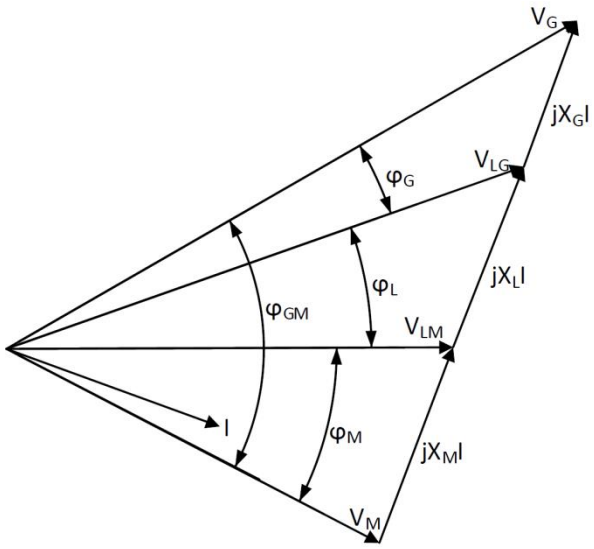

Figure 4-2 Vector diagram for the two-machine system

When a generator falls out-of-step, it has a pole slip which means the rotor angle displacement between the critical generator and the other generators in the system exceeds 180°, which will also be reflected in the voltage angle at the generator bus. If no pole slip occurs, the rotor angle displacement does not exceed this value, and following that, the voltage angles at the buses neither do. Unfortunately, no fixed limit for the maximum voltage angle displacement can be set which guarantees that the rotor angles are not reaching the critical limit but it is suggested that the maximum voltage angle displacement should not exceed 120° to maintain some security headroom.

In the following paragraphs, the proposed procedure of the transient stability approach is explained in detail. A flow chart of the approach is shown in Figure 4-3 where the red frame highlights the focus of this work. Parts outside the red frame are not covered in particular, but mentioned due to their importance for the approach.

System snapshot: There are three possibilities to obtain a snapshot of the state of the system. Either, the data about the current state of the grid are extracted from the SCADA system or they are obtained from PMU measurements, which assume full observability of the power system by PMUs. As a third method, a hybrid approach using both SCADA data and PMU measurements to obtain a full system snapshot could be used. The data include breaker status, generation dispatch, activation of capacitor banks and further relevant data for the assessment.

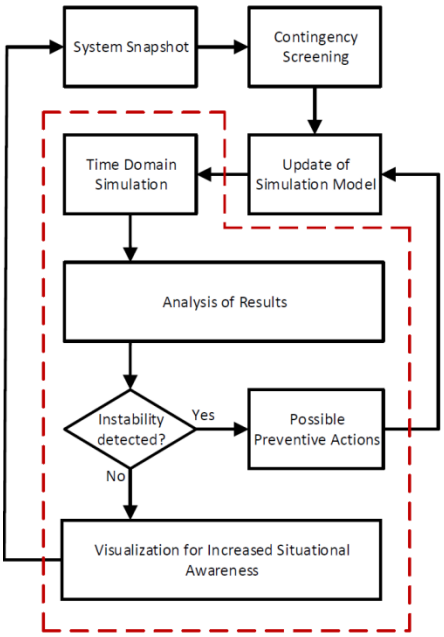

Figure 4-3 Flow chart of the transient stability approach

Contingency screening: To assess the transient stability, a contingency has to be applied in the TD simulation. Theoretically, every potential contingency which could perturb the system has to be analysed to guarantee transient stability. Certainly, it is not possible to include every possible contingency in the assessment since a TD approach is used and computational effort should be kept within reasonable limits. Therefore, a contingency screening to determine the most critical buses with regard to electrical faults is needed. Within this work only one three-phase fault was used since the contingency screening is beyond the scope of this work.

Update of simulation model: the simulation model which represents the real system has to be updated to comply with current system state before starting the TD simulation. Generator dispatch, breaker status, activated capacitor banks and generation from RES have to be refreshed.

Time domain simulation: Time domain simulations are carried out for the most severe contingencies determined in the preceding screening. The duration of the simulation is flexible, but the computational effort grows with increasing simulation time. Therefore, a fixed simulation time up to a few seconds depending on available computational power and security level should be set to capture first swing instabilities. An early stop of the assessment when detecting instability on the fly could be implemented to reduce the computational power even more.

Analysis of the results: In the TD simulation the voltage angles are referenced to the voltage angle of the slack bus. In order to make the voltage angle calculation independent from the slack bus definition, the average voltage angle $\varphi_{U,avg}$ is calculated to serve as an artificial reference, similarly to the definition of the center of inertia. Then the voltage angles $\varphi_{U,Bus\ i,nref}$ are calculated with the new reference according to Eq. 4-2.

$$\varphi_{U,Bus\ i,nref} = \varphi_{U,Bus_i} - \varphi_{U,avg} \qquad \text{Eq. 4-2}$$

Following the calculation of the slack-independent voltage angle, the absolute maximum of the voltage angle for every bus is determined. The concept is visualized in Figure 4-4. The dashed

lines are the original voltage angle results from the TD simulation which are referenced to the slack bus. The black line represents the calculated average of the original voltage angles. The solid lines are the calculated voltage angles with reference to the average.

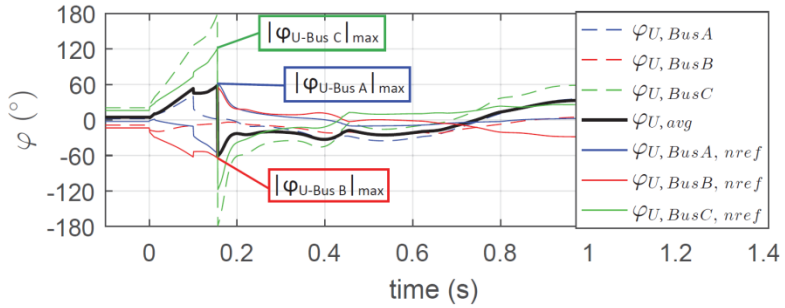

Figure 4-4 Example of the concept to obtain the slack-independent maximum absolute voltage angle deviation for three buses

Instability detection: If voltage angles exceed 120°, instability is detected. Since voltage angles are used rather than the rotor angles the limit for transient stability is set to this limit.

Possible preventive actions: Available counteractions to return the system in a transient stable condition highly depend on the properties of the particular power system. The following counteractions are of interest from an operational perspective: installed capacitor banks, demand response, load shedding capability, generation re-dispatch possibility and temporary increase of voltage set points.

Visualization for increased situation awareness: The visualization is one of the key points of the procedure. It has to be informative by highlighting the most important information which should be communicated. The results are visualized as bar plot with the bus notation on the x-axis, scenario number on the y-axis and the height of the bars is determined by the maximum absolute voltage angle, as seen in Figure 4-5. The bars are coloured according to their height, i.e. the highest bars are coloured red and the lowest are coloured blue. This type of colouring eases the recognition of the highest deviations across the power system. The highest deviations are seen at the first glance.

To evaluate the assessment method four scenarios (1, 3, 4 and 6) from the predefined ones have been used. The predefined scenarios are shown in Table 3-3. Of course, in a real implementation the y-axis would not reflect the scenario number, but the results of the assessment for consecutive system snapshots. This means, that the evolution of the system, with respect to transient stability, can be monitored and compared to results for previous evaluations.

It is clearly visible that the differences between scenarios 1, 3 and 4 are marginal while the results of the sixth scenario differ significantly. Four significant peaks at Bus 4.1, 1.7.1.3 and 1.2 can be seen. Peculiarly, the maximum angle deviation of the faulty Bus 1.10 is not the largest. Instead, the (critical) buses, mentioned before, are highly affected. Since the maximum angle deviation exceeds the defined limit, the contingency is likely to cause a transient instability. However, no SG is connected at Bus 4.1 but a converter (PWM 4.1) which injects active power into the AC grid. The large angle excursion is caused by a large active power swing of the converter during the disturbance which is also seen at the adjacent Buses 1.7 and 1.9. This is clearly an undesired condition and has to be avoided by taking countermeasures.

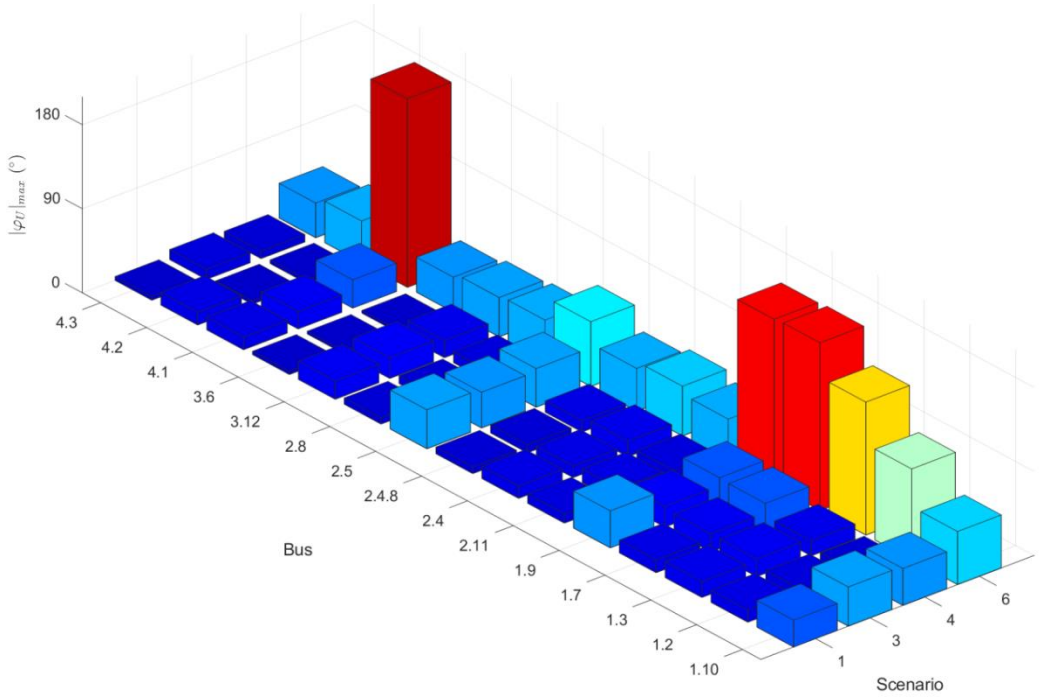

Figure 4-5 Results of a TD simulation for a bolted three-phase short circuit for 200 ms at Bus 1.10 in the Pan-European reference grid for four different scenarios

Summing up, the introduced transient stability assessment method enables a grid-wide transient stability assessment and visualization. It eases the visual examination of transient stability issues on a grid-wide basis through the use of a colouring which facilitates the perception of the communicated information. The maximum absolute voltage angle deviation at the buses across the grid are plotted in a bar plot, with the colours set according to their height. One of the advantages of the method is that it is not dependent on the rotor angles of synchronous machines. Thus, it can also be applied under the presence of high share of converter based generation to detect large active power swings that may be induced by converter based units [46].

However, work concerning the contingency screening has to be carried out. The most critical buses of the grid, where a fault would have the largest impact on the grid, have to be determined in order to reduce the computational effort needed. Moreover, the effectiveness of possible preventive actions has to be studied in terms of technical feasibility and from economical perspective to allow an appropriate counteraction to return the power system into a transient stable operating point. Additionally, it has to be studied if the preventive actions are interfering with other operational objectives.

4.2 Topic 2: Small signal cell stability with focus on inter-cell oscillations (small disturbance stability)

Inter-cell oscillations need to be monitored and accurate estimation of frequency and damping of the oscillations in real time is vital as they provide considerable insight into system stability. These oscillations are characterized by a group of synchronous machines swinging against another group of synchronous machines in an interconnected power system. If these oscillations are not sufficiently damped, unstable operation may occur, potentially leading to uncontrolled separation of the power system into islands and consequently blackouts. Modal frequency and damping indicate the stability of the system and hence accurate estimation of these parameters are critical. A modal

analysis by linearizing the system around an operating point is a powerful tool for small signal stability analysis. However, this method is limited by the large size and model of power system. Operating conditions keep changing due to variations in load, generation, switching and control actions. Model based methods are computationally expensive as they require development and update of power system models to facilitate change in operating conditions. Hence, measurement-based modal analyses are extensively studied [69]-[75].

Estimation of electromechanical mode properties can be carried out from PMU measurements. Different methods have been developed over the last two decades. These methods utilize different types of dynamic responses which can be captured by PMUs. The dynamic response of a power system is product of different inputs to the system. Power system responses are product of random load variations as unknown input noise (ambient response), and network switching/disturbances from known and unknown components (transient response). The methods developed for the estimation of mode properties use either type of data, methods that use ambient data have the advantage that they can be continuously applied, while methods that use transient responses can only be applied when a large enough switching (such as a disturbance) occurs in the network.

Due to the stochastic nature of power systems, the accuracy of any mode estimation method is limited. However, it is possible to improve the estimation process by exciting the system with a known signal, through “known switching” and by “μ(t) (known probing input)”. An example of a “known switching” is a transmission line opening and closing. Signals “μ(t) (known probing input)” can also be injected through different kinds of actuators, such as generator excitation or modulation of HVDC links. This practice has been successfully applied in particular in the Western Electricity Coordinating Council power system [76].

The ability to control inter-cell oscillations helps to increase power transfers when networks are operating close to their dynamic operational constraints. Different measurements from PMUs can be used to generate cell-wide signals, such as bus voltage angle differences. Therefore, the exploitation of PMU signals is desirable for inter-cell mode control. Inter-cell mode control can be effective by using cell-wide signals as inputs to generator excitation systems, static VAR compensators (SVCs), other FACTS and HVDC in the form of a supplementary damping control. One major challenge in damping control design is the selection of feedback input signals. With the availability of signals from PMUs, choices of inputs are not only limited to those local but now include cell-wide signals. However, the main issue is which signal, among all the available signals, would give satisfactory damping performance. Available “dominant inter-area paths” [77]-[79] concept could be used to design controls for inter-cell mode control effectively using PMU signals.

4.2.1 Mode Frequency Estimation

For power networks that have operation constraints limits imposed by the existence of low-damped electromechanical oscillations, the estimation of electromechanical mode properties is of crucial importance for providing power system control room operators with adequate indicators of the stress of their network. Application of different spectral analysis techniques can be used for the estimation of electromechanical mode properties using data emerging from real PMUs located at both the medium- and low-voltage distribution and high-voltage transmission networks.

It is not uncommon for PMU data to suffer from data quality issues. Before using phasor measurement data for mode estimation purposes, the data must be pre-processed to remove flawed and redundant data and, when possible, to add estimates of missing samples. Moreover, spectral analysis techniques require data from a stochastic process to be able to work properly. To

this aim, deterministic components in the signals must be removed. The use of raw measurements from PMUs can lead to ambiguous results due to:

1) Possible errors in some of the measured samples;
2) Ill conditioned auto covariance matrices in the case of PMUs with high sampling rates;
3) Existing trends in the signal which do not carry any information about system dynamics.

Before applying any of the spectral estimators, available data must be pre-processed. The main goals of the pre-processing stage are removal of erroneous data, trend removal, down sampling and data parcelling [80]. By estimating the power spectral density (PSD) from a stochastic process, periodicities which are related to the dynamical behaviour of a system may be detected. Modal frequencies will show up as peaks in the PSD, so if the PSD can be estimated, this will in turn give an estimate of mode frequencies. There exist many methods for PSD estimation [76], [81], [82].

4.2.2 Mode Damping Estimation

There exist many methods for damping estimation from transient data [74]; the Eigenvalue Realization Algorithm and Prony's Method are often used for this. However, if a data set has more ambient characteristics and does not contain any transients of significant size, these methods will perform poorly. To overcome this, all the minor transients from the data can be collected and used to construct a transient of sufficient size for the methods to perform properly. To detect and collect minor transients in the data, a threshold is set and every time the signal exceeds this threshold the data sequence is collected. The collected data sequences will then be averaged to create a transient:

$$y(k) = \frac{1}{N}\sum_{i=1}^{N} y_{i,k} \qquad \text{Eq. 4-3}$$

where y is the data sequence (3 seconds time period), N is the number of collected sequences (10 sequences) and n is the number of samples in each sequence (30 samples, 0.1 second each). With the transient, Prony's Method can be used to extract the mode amplitude, frequencies, energy and damping. Figure 4-6 presents the power system model used with the method flow chart of small signal inter-cell stability assessment.

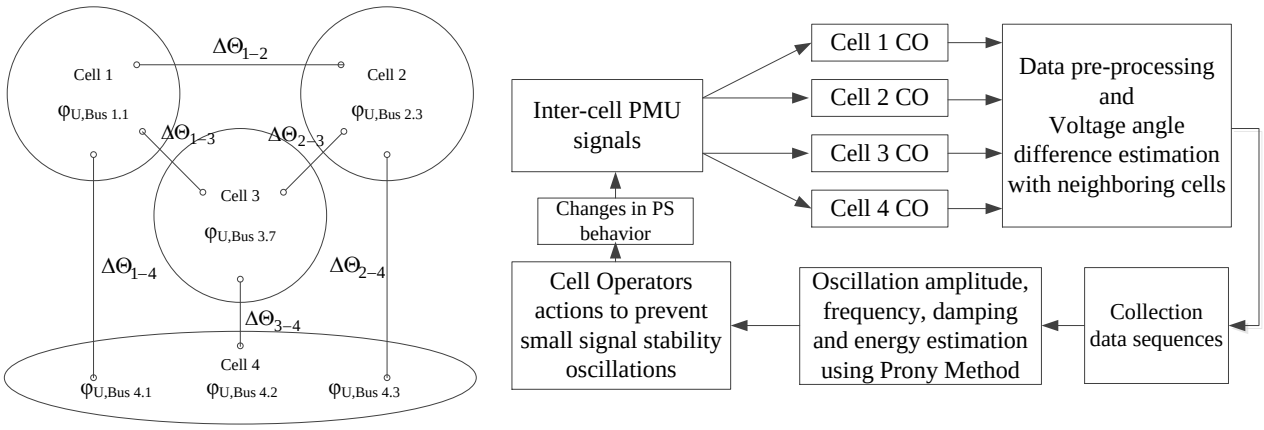

Figure 4-6 Used power system model with method flow chart of small signal inter-cell stability assessment

4.2.3 Simulation results

For the validation of the proposed method, three case studies of the Pan-European power system model are used, to derive small signal stability modes in real time. Table 4-1 presents the list of events for the small signal cell stability simulation and proposed real-time oscillation detection method.

Table 4-1 List of events for the small signal cell stability analysis of the Pan-European reference power system model

Study case	Events	Simulation time
2: 25% RES – 8 Gen	Line 1.2 – 2.5a, 3.7-4.3: Out of service; load increase in bus 1.2 by 10%	30 s
2: 25% RES – 8 Gen – Loaded system	Lines 1.2 – 2.5a, 2.4-2.3b, 3.6-3.7a, 3.7-4.3, 1.2–3.6a: Out of service; load increase in bus 1.2 by 20%	100 s
8: 90% RES – 2 Gen	Line 1.2 – 2.5a: Out of service; load increase in bus 1.2 by 10%	30 s

Study case 2 – 25% RES – 8 Gen

Starting from the system steady state at time t = 0 s, after 2 seconds a 10% load increase at bus 1.2 is simulated (simulation time period 30 s).

Simulation results are presented in Figure 4-7, where frequency and voltage angles variations are plotted for the observed time period (30 s) after the events occur. After small disturbances in load 1.2 small signal stability modes with 0.83 Hz between cells 1 and 2 occur and become attenuated in the considered period of time.

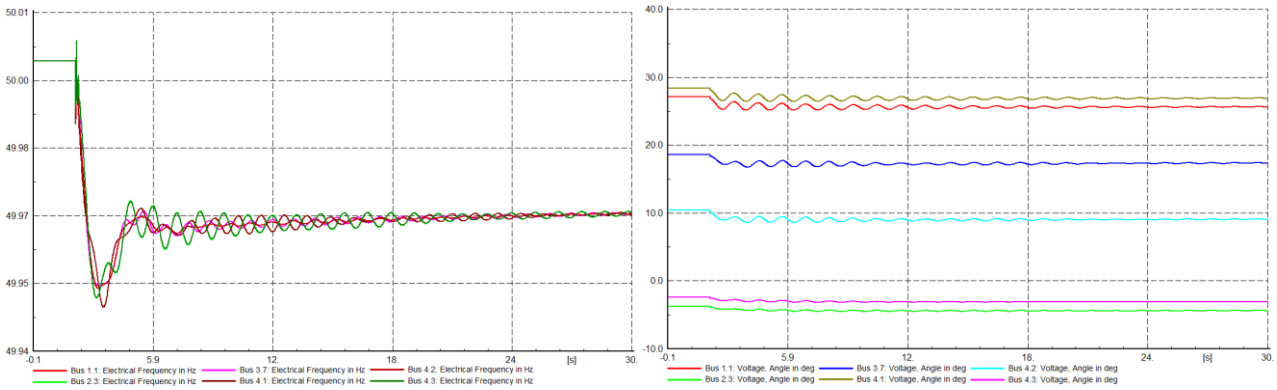

Figure 4-7 Scenario 2, Frequency and Voltage Angle variations at Pan-European reference power system model buses

For damping estimation from transient data, PMU voltage angle signals from bus 1.1 and 2.3 are used. Figure 4-8 presents voltage angle difference variation between buses with 3 seconds time period window.

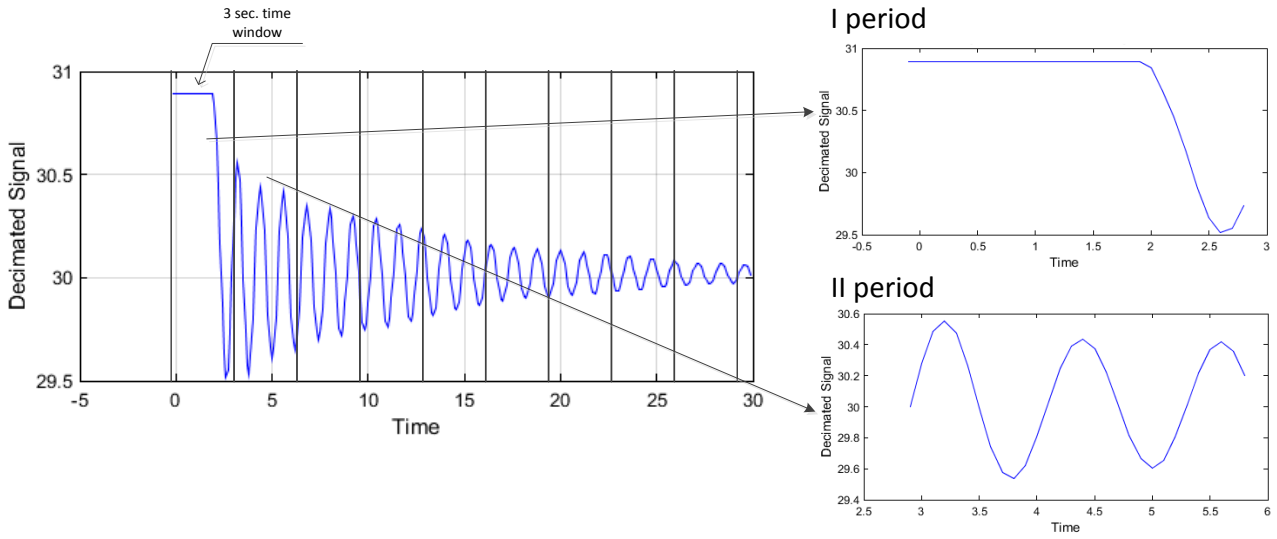

Figure 4-8 Scenario 2, Voltage Angle difference variation between bus 1.1 ($\varphi_{U,Bus1.1}$) and bus 2.3 ($\varphi_{U,Bus2.3}$) in different time frames

Each time period frame is analysed using Prony's method to extract the mode amplitude, frequencies, damping and energy characteristics. The Prony's analysis based controller output curve is shown in Figure 4-9 for the 1st and 2nd time windows.

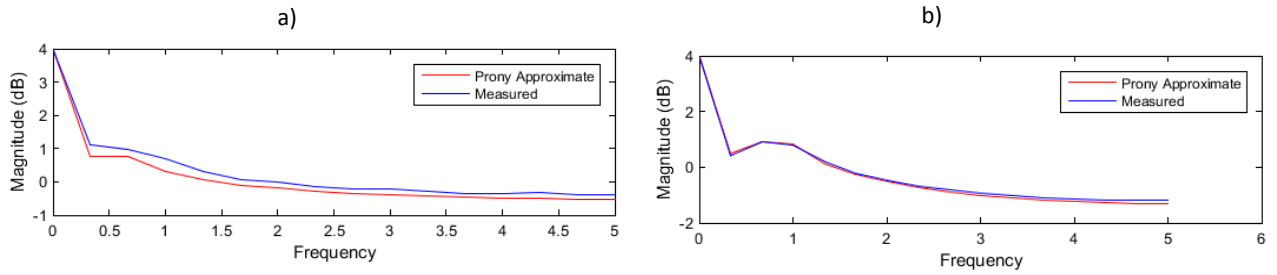

Figure 4-9 Prony's Analysis of Model in Frequency Domain for a) I period, b) II period

For providing power system control room operators with adequate indicators of the stress of their network useful observables could be derived from Table 4-2, where analysis results for 30 seconds time period and 10 periods using Prony's method are presented.

Table 4-2 Scenario 2, Voltage Angles difference between bus 1.1 ($\varphi_{U,Bus1.1}$) and bus 2.3 ($\varphi_{U,Bus2.3}$) analysis using Prony's method

Scenario 2 Modes:	Amplitude	Damping	Frequency	Energy
Before event 1.	$6.2 \cdot 10^{1}$	$8 \cdot 10^{-7}$	0	$2.1 \cdot 10^{4}$
2.	$1.6 \cdot 10^{-5}$	$-1 \cdot 10^{1}$	0	$7 \cdot 10^{-11}$
3.	$6.8 \cdot 10^{-6}$	-1.3	3.6	$1 \cdot 10^{-11}$
I period 1.	$6.2 \cdot 10^{1}$	$-8.5 \cdot 10^{-3}$	0	$2.9 \cdot 10^{4}$
2.	$5.3 \cdot 10^{-2}$	$5.8 \cdot 10^{-1}$	$7.1 \cdot 10^{-1}$	$2 \cdot 10^{-1}$
II period 1.	$6 \cdot 10^{1}$	$6.2 \cdot 10^{-4}$	0	$2.8 \cdot 10^{4}$
2.	$6.1 \cdot 10^{-1}$	$-1.8 \cdot 10^{-1}$	$8.4 \cdot 10^{-1}$	$1.8 \cdot 10^{0}$
III period 1.	$6 \cdot 10^{1}$	$2.2 \cdot 10^{-4}$	0	$2.8 \cdot 10^{4}$
2.	$3.7 \cdot 10^{-1}$	$-8.5 \cdot 10^{-2}$	$8.3 \cdot 10^{-1}$	$8.3 \cdot 10^{-1}$
IV period 1.	$6 \cdot 10^{1}$	$-1.1 \cdot 10^{-4}$	0	$2.8 \cdot 10^{4}$
2.			$8.4 \cdot 10^{-1}$	$5 \cdot 10^{-1}$

	$2.7 \cdot 10^{-1}$	$-4.8 \cdot 10^{-2}$		
V period 1. 2.	$6 \cdot 10^{1}$ $2.4 \cdot 10^{-1}$	$-5.9 \cdot 10^{-5}$ $-1.1 \cdot 10^{-1}$	0 $8.4 \cdot 10^{-1}$	$2.8 \cdot 10^{4}$ $3.2 \cdot 10^{-1}$
VI period 1. 2.	$6 \cdot 10^{1}$ $1.7 \cdot 10^{-1}$	$-2.1 \cdot 10^{-5}$ $-1.2 \cdot 10^{-2}$	0 $8.3 \cdot 10^{-1}$	$2.8 \cdot 10^{4}$ $1.7 \cdot 10^{-1}$
VII period 1. 2.	$6 \cdot 10^{1}$ $1.2 \cdot 10^{-1}$	$2.7 \cdot 10^{-5}$ $-5.2 \cdot 10^{-2}$	0 $8.3 \cdot 10^{-1}$	$2.8 \cdot 10^{4}$ $1 \cdot 10^{-1}$
VIII period 1. 2.	$6 \cdot 10^{1}$ $1 \cdot 10^{-1}$	$4.9 \cdot 10^{-5}$ $-8.5 \cdot 10^{-2}$	0 $8.4 \cdot 10^{-1}$	$2.8 \cdot 10^{4}$ $6.6 \cdot 10^{-2}$
IX period 1. 2.	$6 \cdot 10^{1}$ $8.1 \cdot 10^{-2}$	$-1.1 \cdot 10^{-5}$ $-1.4 \cdot 10^{-1}$	0 $8.3 \cdot 10^{-1}$	$2.8 \cdot 10^{4}$ $3.5 \cdot 10^{-2}$
X period 1. 2.	$6 \cdot 10^{1}$ $5.4 \cdot 10^{-2}$	$-1.8 \cdot 10^{-5}$ $-6.7 \cdot 10^{-2}$	0 $8.3 \cdot 10^{-1}$	$2.8 \cdot 10^{4}$ $1.9 \cdot 10^{-2}$

After the small disturbance in load 1.2, small signal stability modes with 0.83 Hz frequency between cells 1 and 2 occur. Analysis using Prony's method in 1st period shows appearance of a new mode with 0.71 Hz frequency, amplitude 0.053 and 0.2 energy. The 2nd period of time represents transient process with 0.84 Hz frequency, higher mode amplitude 0.61 and 1.8 energy. The 3rd period represents decrease of mode amplitude till 0.37 and energy 0.83, as a consequence of the damping of the observed mode in the considered period of time.

Study case 2 – 25% RES – 8 Gen – Loaded system

Starting from the system steady state at time t = 0 s, after 2 seconds load increases at bus 1.2 by 20% (simulation time period 100 s).

Simulation results are presented in Figure 4-10, where frequency and voltage angles variations are plotted for observed time period. After disturbances in load 1.2 small signal stability modes occur and power system start swing.

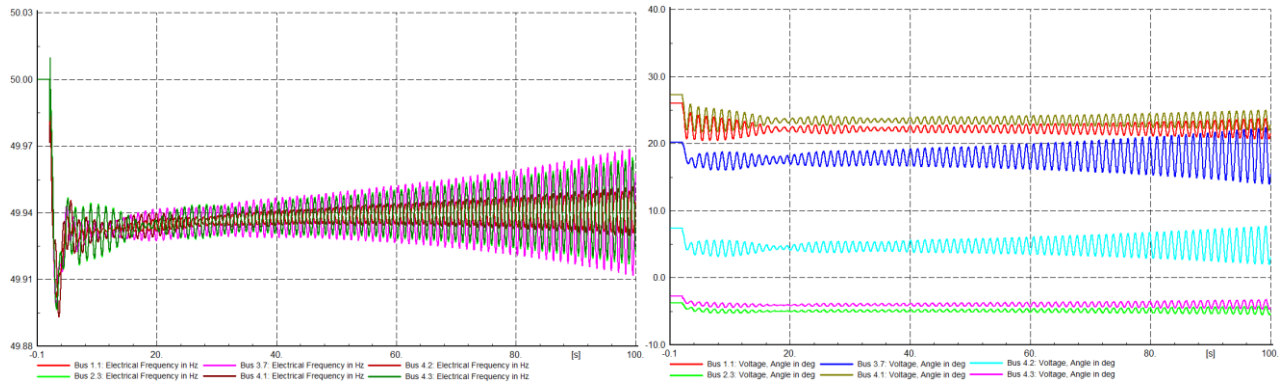

Figure 4-10 Scenario 2: Loaded system, Frequency and Voltage Angle variations at Pan-European reference power system model buses

For damping estimation from transient data, PMU voltage angle signals from bus 1.1 and 3.7 are used. Figure 4-11 presents analysis using Prony's method: frequency, amplitude, damping and energy change for simulated time period.

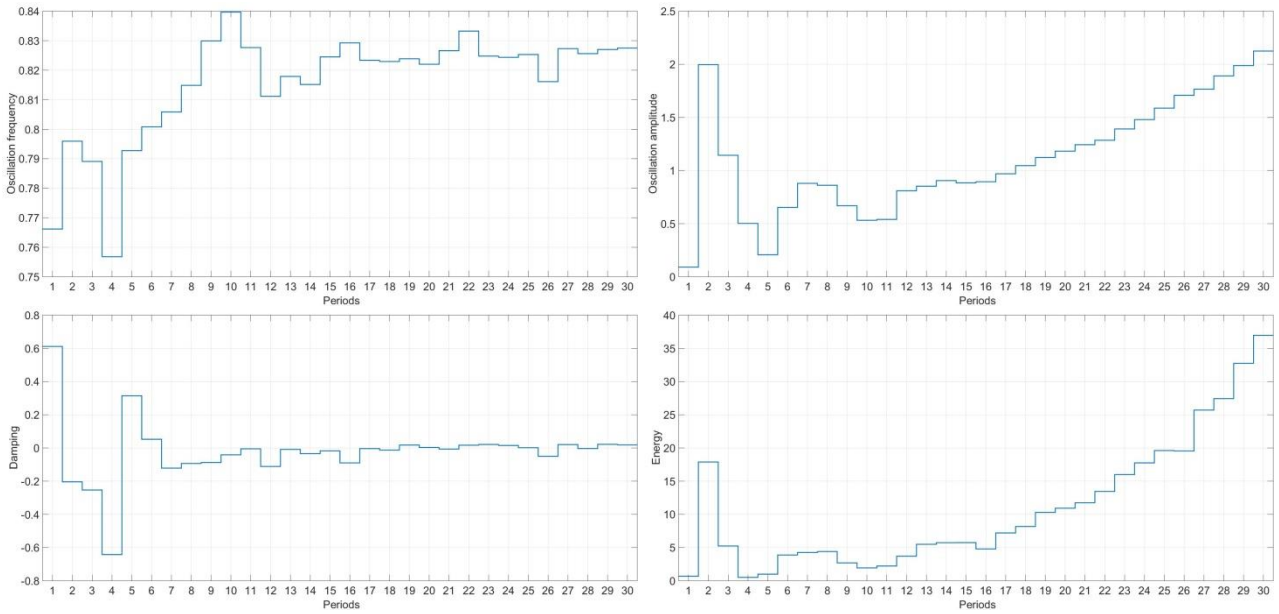

Figure 4-11 Scenario 2: Loaded system, Voltage Angles difference between bus $\varphi_{U,Bus1.1}$ and bus $\varphi_{U,Bus3.7}$ analysis using Prony's method: frequency, amplitude, damping and energy

After disturbance in load 1.2 small signal stability modes occur. 1st period shows appearance of new mode with 0.765 Hz frequency, amplitude 0.009 and 0.694 energy. The 2nd period of time represents transient process with 0.796 Hz frequency, higher mode amplitude 2 and 17.88 energy. Subsequent periods represent system swing, especially after 17 periods, where oscillation frequency fluctuating near 0.825 Hz and damping is close to zero, oscillation amplitude and energy start increasing, as consequence to more system swing and leading to the collapse. Figure 4-12 presents similar simulation with 3rd cell operator action, switching line 3.6-3.7a on service at 20th period, due to indicators (observables) of the stress of their network.

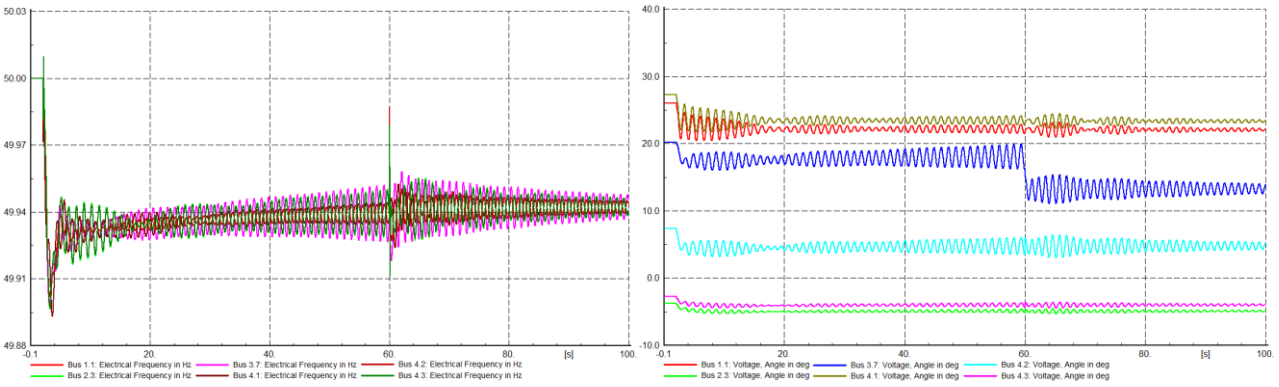

Figure 4-12 Scenario 2: Loaded system, Frequency and Voltage Angle variations in case line 3.6-3.7a is on service at 20 period

Study case 8 - 90% RES – 2 Gen

Starting from the system steady state at time t = 0 s, after 2 seconds load increases at bus 1.2 by 10% (simulation time period 30 s).

Simulation results are presented in Figure 4-13, where frequency and voltage angles variations are plotted for observed time period (30 s) after event occur. After small disturbances in load 1.2 small signal stability modes are not observed in this case. Table 4-3 presents analysis results for 12 seconds time period and 4 periods using Prony's method.

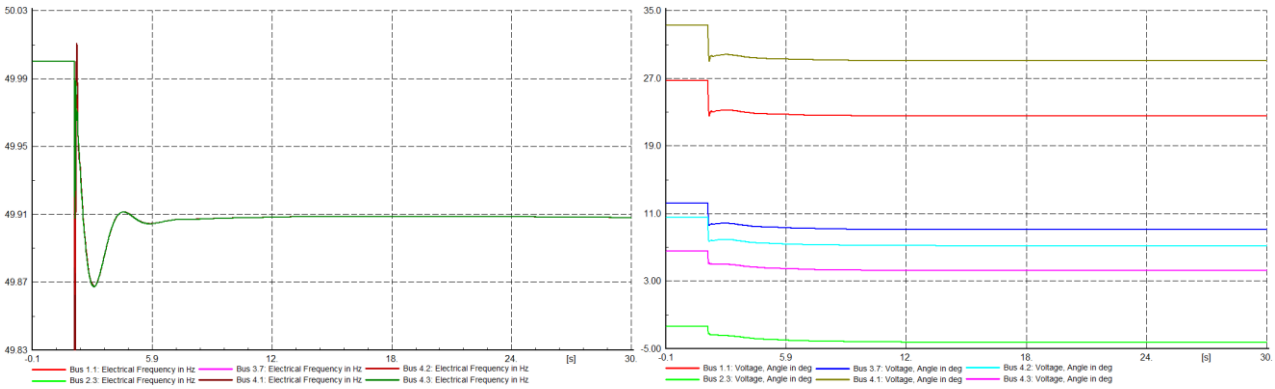

Figure 4-13 Scenario 8, Frequency and Voltage Angles variation at Pan-European reference power system model buses

Table 4-3 Scenario 8, Voltage Angles difference between bus 1.1 ($\varphi_{U,Bus1.1}$) and bus 2.3 ($\varphi_{U,Bus2.3}$) analysis using Prony's method

Scenario 8 Modes:	Amplitude	Damping	Frequency	Energy
I period 1.	$5 \cdot 10^{1}$	$-3.6 \cdot 10^{-2}$	0	$1.6 \cdot 10^{6}$
2.	$1.3 \cdot 10^{-1}$	$-1.4 \cdot 10^{1}$	0	$1.5 \cdot 10^{-1}$
3.	$5.6 \cdot 10^{-4}$	$-2 \cdot 10^{3}$	0	$8.1 \cdot 10^{-8}$
II period 1.	$4.6 \cdot 10^{1}$	$-6.9 \cdot 10^{-4}$	0	$1.6 \cdot 10^{6}$
2.	$1 \cdot 10^{-1}$	$-3.8 \cdot 10^{0}$	0	$1.5 \cdot 10^{-1}$
3.	$1.5 \cdot 10^{-5}$	$-1.7 \cdot 10^{3}$	$1.3 \cdot 10^{2}$	$8.1 \cdot 10^{-8}$
III period 1.	$4.5 \cdot 10^{1}$	$-4.6 \cdot 10^{-4}$	0	$1.5 \cdot 10^{6}$
2.	$8.8 \cdot 10^{-5}$	$-8.7 \cdot 10^{1}$	0	$1.2 \cdot 10^{-1}$
3.	$4.7 \cdot 10^{-5}$	$-1.6 \cdot 10^{3}$	$1.3 \cdot 10^{2}$	$5.7 \cdot 10^{-10}$
IV period 1.	$4.5 \cdot 10^{1}$	$2.8 \cdot 10^{-4}$	0	$1.6 \cdot 10^{6}$
2.	$3.4 \cdot 10^{-4}$	$-8.5 \cdot 10^{1}$	0	$1.9 \cdot 10^{-7}$
3.	$6 \cdot 10^{-5}$	$-1.8 \cdot 10^{3}$	$1.1 \cdot 10^{2}$	$9.1 \cdot 10^{-10}$

4.2.4 Applications of PMUs for Control of Inter-Cell Oscillations

One goal of a WAMS is to have tracking tools for oscillatory dynamics in interconnected power grids, particularly those which are critical to operational reliability, i.e., inter–cell oscillations. Insufficient damping of low-frequency inter-cell oscillations arises as weak interconnected power systems are stressed to meet up with increasing demand. This inadequacy may lead to oscillatory instability, resulting in system collapse. A characteristic of power oscillations is that, for every mode of oscillation, there exists a series of connecting corridors in which the highest content of the mode would propagate. The path is termed “dominant inter-area oscillation path”, or “dominant inter-cell oscillation path” here, a concept based on the notion of interaction path. These dominant inter-cell oscillation paths are deterministic and algorithms for their identification using both models and measurements are available [77]-[79]. Signals from the dominant path are the most observable and have the highest content of inter-cell modes. This suggests that by using well-selected dominant path signals for wide-area control, adequate damping performance can be achieved [74].

4.2.5 Topic 2 conclusions

This section has shown how spectral analysis techniques can be applied to PMU measurements to estimate low-frequency electromechanical oscillations. For mode damping estimation, Prony’s

method is used with simulation data. The performance of this estimator was evaluated through three different cases. The most important realization here is that to improve the quality of mode estimates and in order to be able to obtain reliable damping estimates, methods that can detect and remove the effects of forced oscillations in the measurements need to be developed. The selection of the "right" input signals from PMUs is critical for effective damping control. The use of the signal type and location is crucial to ensure that control design specifications are maintained and damping is maximized. In the case of signal loss, due to communication failures, the controller must be adjusted even if new signals are used to replace a lost signal. Derived observables, as oscillation mode amplitude, frequency, damping and energy could be used for providing power system control room operators with adequate indicators of the stress of their network and prevent power system swing with proper actions.

4.3 Topic 3: Inertia at Pan-European level

4.3.1 Simplified equivalent dynamic model of the power system

We recall that the dynamics of each Synchronous Machine (SM) connected to a power system can be described in a simplified way by the following swing equation [8]:

$$M_i \cdot \frac{df_{sys}}{dt} \simeq P_{m,i} - P_{e,i}\ [MW] \qquad \text{Eq. 4-4}$$

where $P_{m,i}$ is the turbine mechanical power and $P_{e,i}$ its electric power, M_i the machine mechanical inertia. In turn

$$M_i = \frac{2 \cdot H_i \cdot S_{n,i}}{f_n}\ \left[MW \cdot \frac{s}{Hz}\right], \quad H_i = \frac{J_i \cdot \omega_{n,i}^2}{2S_{n,i}}\ [s] \qquad \text{Eq. 4-5}$$

where $S_{n,i}$ is the machine nominal apparent power, H_i its inertia time constant, J_i its moment of inertia, $\omega_{n,i}$ its nominal rotational speed. f_n is the nominal frequency.

Considering the set α_G of the Synchronous Generators (SGs) connected to the network as one equivalent SM, the overall swing equation is

$$M_{sys} \cdot \frac{df_{sys}}{dt} \simeq P_{m,sys} - P_{e,sys} \qquad \text{Eq. 4-6}$$

where

$$M_{sys} = \frac{2 \cdot H_{sys} \cdot S_{n,sys}}{f_n} = \sum_{i \in \alpha_G} M_i, \quad S_{n,sys} = \sum_{i \in \alpha_G} S_{n,i} \qquad \text{Eq. 4-7}$$

With reference to a WoC, this simplified model can be assumed for each cell, by introducing a Centre-Of-Inertia (COI) frequency in each cell *k* [58]:

$$f_{COI,cell\ k} := \frac{\sum_{i \in \alpha_{G,k}} H_{i,k} f_{i,k}}{\sum_{i \in \alpha_{G,k}} H_{i,k}} \qquad \text{Eq. 4-8}$$

$$M_{cell\ k} \cdot \frac{df_{COI,cell\ k}}{dt} \simeq P_{m,cell\ k} - P_{e,cell\ k} \qquad \text{Eq. 4-9}$$

where $f_{i,k}$ is the frequency at the i-th generator bus in cell k and $\alpha_{G,k}$ is the set of SGs in cell k. Similarly, for the whole WoC, Eq. 4-6 can be employed.

Eq. 4-6 and Eq. 4-9 can be easily employed to estimate the instantaneous Rate Of Change of Frequency (ROCOF) after a power imbalance. For the WoC, in particular, one has

$$ROCOF(t=0^+) = \frac{df_{sys}}{dt}(t=0^+) \simeq \frac{P_{m,sys} - P_{e,sys}}{M_{sys}} \; [Hz/s] \qquad \text{Eq. 4-10}$$

where $P_{m,sys} - P_{e,sys}$ is the instantaneous imbalance occurring at $t = 0$.

From primary regulation point of view, the Network Power Characteristic (NPC) and the Relative NPC in quasi-steady state conditions can be defined as follows [59]:

$$NPC = \frac{\Delta P_{sys}}{\Delta f_{sys}} \left[\frac{MW}{Hz}\right], \quad RNPC = \frac{\Delta P_{sys}/P_{n,sys}}{\Delta f_{sys}/f_n} \; [p.u.] \qquad \text{Eq. 4-11}$$

where $P_{n,sys}$ is the system nominal rated power. The NPC (and the RNPC) can be related to the contribution of both generators and loads. If, for simplicity, generators only are considered, then one can introduce the corresponding droop as

$$\sigma_i = \left(\frac{\Delta f_{sys}}{f_n}\right) / \left(\frac{\Delta P_i}{P_{n,i}}\right) \qquad \text{Eq. 4-12}$$

for the i-th SG contributing with ΔP_i to ΔP_{sys}.

4.3.2 Simulation description, reference requirements and preliminary results

Table 4-4 recalls the scenarios considered in the Pan-European SRPS, while Table 4-5 lists the inertia constant and mechanical inertia of each cell and of the whole WoC in each scenario, obtained with the simplified system model described above. We recall that each i-th SG is characterized by nominal apparent power $S_{n,I}$ = 500 MVA, nominal power $P_{n,I}$ = 425 MW and inertia constant H_i = 5 s. The speed droop is assumed as 4% for hydro generators, 4.47% for gas turbine generators.

In this Section focus is on scenarios 1, 3, 5 and 7 only, because they are characterized by the same generation for each SG. In other words, in those scenarios the power generation of the conventional generators out of services is replaced exactly by the RES generation. The same imbalance, more precisely the loss of generator SG 2.11(2) at time t = 2 s, is simulated for each of these four scenarios, in order to have comparable events. The event is a power injection step decrease equal to 325 MW. This is rather critical, because cell 2 is a mainly importing area. Besides, it can be considered as a relevant incident within this SRPS, which can be considered as a model of a very small power system: indeed, 325 MW is 12.5% of 2600 MW, which is the WoC total load. For completeness, the loss of generator SG 2.11(2) is also simulated in the other scenarios, thus having smaller power injection step decreases: 244 MW in scenario 2, 217 MW in scenarios 4 and 6, 130 MW in scenario 8. Detailed results are not reported here.

Table 4-4 Summary of the defined scenarios

Scenario	RES [%]	P-RES [MW]	Number of SG in service	SG out of service	P_{set} for each SG [MW]
1	0	0	8	-	325
2	25	650	8	-	244
3	25	650	6	1.9 (2); 1.10 (2)	325

4	50	1300	6	1.9 (2); 1.10 (2)	217
5	50	1300	4	1.9 (1/2); 1.10 (2); 3.12 (2)	325
6	75	1950	3	1.9 (1/2); 1.10 (2); 3.12 (1/2)	217
7	75	1950	2	1.9 (1/2); 1.10 (1/2); 3.12 (1/2)	325
8	90	2340	2	1.9 (1/2); 1.10 (1/2); 3.12 (1/2)	130

Table 4-5 Simplified bus-bar dynamic model: inertia constant and mechanical inertia evaluation

Scenario	H_{cell1} [s]	H_{cell2} [s]	H_{cell3} [s]	H_{sys}, i.e. H_{WoC} [s]	M_{cell1} [MW·s/Hz]	M_{cell2} [MW·s/Hz]	M_{cell3} [MW·s/Hz]	M_{sys}, i.e. M_{WoC} [MW·s/Hz]
1	5	5	5	5	400	200	200	800
2	5	5	5	5	400	200	200	800
3	2.5	5	5	3.75	200	200	200	600
4	2.5	5	5	3.75	200	200	200	600
5	1.25	5	2.5	2.5	100	200	100	400
6	1.25	5	0	1.875	100	200	0	300
7	0	5	0	1.25	0	200	0	200
8	0	5	0	1.25	0	200	0	200

Regarding the Operating Reserve for Frequency Containment (FCR) in the considered SRPS, one can observe that each unit working at 325 MW could supply up to 100 MW, since its rated nominal power is 425 MW. Therefore, since the SGs in operation are 8, 6, 4 and 2 in the four considered scenarios, but one generator is lost in each scenario, then the total operational reserve is 700 MW, 500 MW, 300 MW and 100 MW respectively.

The frequency transient response to the simulated event can be evaluated by taking into account the Frequency Quality Defining Parameters specified by the ENTSO-E Network Code [60]: maximum instantaneous frequency deviation equal to ±800 mHz for the Continental Europe system and the Great Britain system, ±1000 mHz for Ireland and for the Nordic system; maximum steady-state frequency deviation equal to ±200 mHz for the Continental Europe system, ±500 mHz for the other systems. As for the ROCOF behaviour, maximum values following incidents in real power systems can range from some mHz/s up to 3 Hz/s, depending on the size of the imbalance and of the system itself .

Table 4-6 shows for the whole Power System the estimation of mechanical inertia, Network Power Characteristic (NPC), initial ROCOF (estimated according to the approximated swing equation for the whole WoC) and estimated steady-state frequency deviation for all the scenarios: it also reports, for each SM, the instantaneous power output after the power imbalance. The stabilizing effect of load dependency of the frequency (few percent per Hz, as it is typical in interconnected systems) is not considered in these computations, but it is included in the SRPS simulation model. The initial ROCOF and the steady-state frequency deviation just computed will be taken as comparison values for the simulation results, shown in the next subsection.

Table 4-6 Simplified bus-bar dynamic model: estimated values of main parameters of the PS

Scenario	Mechanical Inertia [MW·s/Hz]	NPC [MW/Hz]	Initial |ROCOF| estimate [Hz/s]	|Freq_Dev| Steady-state [Hz]	Initial power variation of SGs [MW]
1	800	1360	0.4063	0.239	40.63
2	800	1360	0.3050	0.179	30.50
3	600	1020	0.5417	0.319	54.17

4	600	1020	0.3617	0.213	36.17
5	400	680	0.8125	0.478	81.25
6	300	510	0.7233	0.425	72.33
7	200	340	1.6250	0.956	162.50
8	200	340	0.6500	0.382	65.00

4.3.3 Detailed simulation results

In Figure 4-14, results in terms of the frequency transient response at all the buses in the WoC are reported, for the four analysed scenarios (1, 3, 5 and 7); a zoom around the first second after the imbalance event is also shown, to highlight the frequency spatial distribution inside each cell. The COI frequency in each cell and for the whole WoC are also depicted.

One can observe that a new steady state is attained in a few seconds. In particular, in scenarios 1, 3 and 5, the system is close to the new steady state after 5-6 s after the event; in scenario 7 only the transient is slower, taking about 15 s to reach the new regime. Besides, in the first three scenarios the steady-state frequency deviation values differ slightly from the ones obtained from the simplified model, while a significant difference shows up in scenario 4, since the simplified model is no longer enough to describe the system behaviour. From the zoomed graphs, one can deduce that the very initial ROCOF absolute values are rather high, due to superposition of two effects: the interactions between the SGs and the network, and the fact that bus frequency is heavily affected by the fast dynamics of voltage; therefore, in the very first fractions of a second after the event, the bus frequency exhibits an initial spike, lasting 100-500 ms. One can also see that ROCOF values more similar to the ones from the simplified linearized model can be found after the initial frequency spike. The interactions between the machines and the network also cause a spatial spread among different bus frequencies. Finally, due to the mentioned interaction again, the cells electrically more distant from the one where the event occurs have a less steep descent of the frequency. The ROCOF behaviour is depicted in more detail in Figure 4-15, which reports the values output by PowerFactory. Of course, the initial ROCOF impacts on the initial part of the frequency transient, so that the minimal frequency value decreases as the initial ROCOF decreases (i.e. increases in absolute value); e.g., in scenario 1 the frequency nadir is around 49.68 Hz (-320 mHz with respect to 50 Hz, the pre-event value), in scenario 7 the frequency nadir is around 47.45 Hz (-2.55 Hz with respect to 50 Hz, the pre-event value). Obviously, if the intervention threshold for protection systems is set at 47.5 Hz (a typical value), in scenario 7 due to the protections there would be the tripping of all the generators, and consequently a blackout.

The COI frequencies and their derivative can also be adopted to describe the transient phenomena, because their values are rather similar to the ones at the buses in each cell or in the whole WoC. The use of a COI has a meaning if inside each cell there exist generation units with a rotating mass, or some devices emulating the behaviour of rotating masses (synthetic inertia). However, if this is not the case, it is necessary to find suitable points inside the cells or at their borders (on the tie-lines connecting cells together; for instance, tie-lines are crucial for monitoring of the power flows and of the voltage amplitude and phase angle, so measures of the frequency along them or at their ends have to be present), where to measure the frequency. We also recall that the rotational speed of the SGs is related only to the mechanical power imbalance and therefore to the electromechanical response of the system; thus, it is insensitive to the network voltage variation. Therefore, an approximate but simple, way to account only for the electromechanical interactions among the synchronous machines can be computing the COI

speed, the consequent frequency and the ROCOF of such a frequency (this last ROCOF is shown in Figure 4-16, where it is computed in three ways: as the incremental ratio of the frequency with respect to time, as the slope of the frequency from the event, as the slope of the frequency from an instant just after the event; the sampling interval used in these computations is 10 ms). This way, the voltage effect on frequency and therefore on ROCOF should be filtered out. Alternatively, comparing the ROCOF computed from the COI frequency and the COI speed should highlight the voltage effect, which could be a relevant issue from the measurement process point of view. In fact, as stated in [62], “System faults (short circuits) cause transients in the sine wave of the system voltage. Zero crossings of the voltage will shift even when the system frequency, based on the speed of the generators supplying the grid, does not change. Also switching operations in the grid will cause a sudden phase shift of the voltage at the moment of switching. As a result, the time between zero crossings will be longer or shorter and the calculated frequency will be lower or higher than the actual system frequency. Therefore a longer allowed time for a measurement is required to distinguish between a fault or switching event and a genuine ROCOF event. The ROCOF device must be stable under such circumstances and not be triggered.” For the SRPS under consideration, to obtain a reliable measure of the ROCOF, due to “a genuine ROCOF event” (i.e. a relevant active power imbalance and not to the local perturbation of voltage), could require a minimal time window, on the order of 200-500 ms.

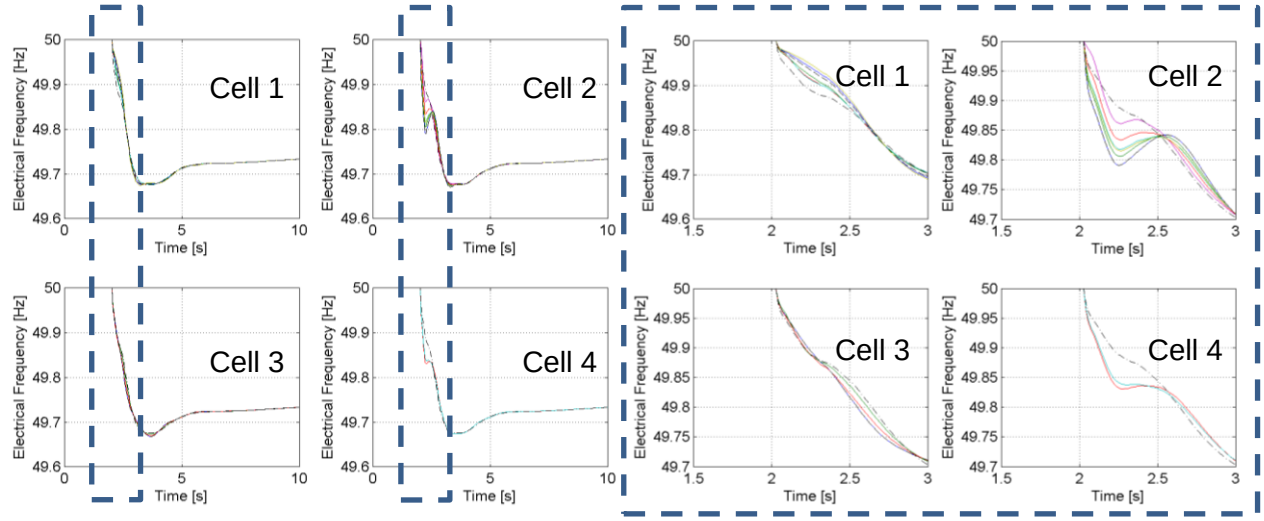

Scenario 1

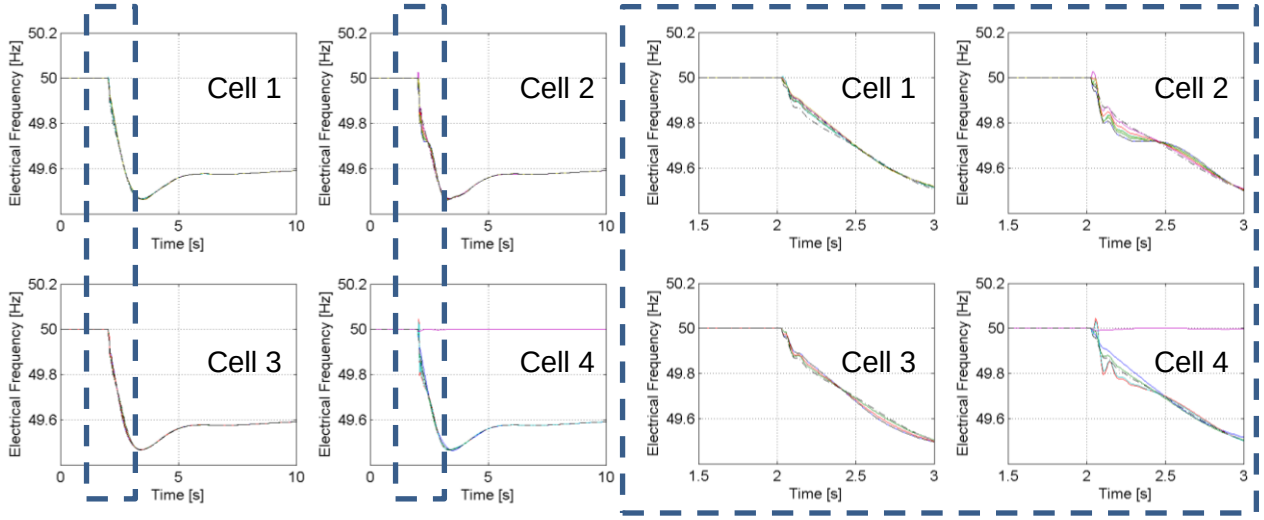

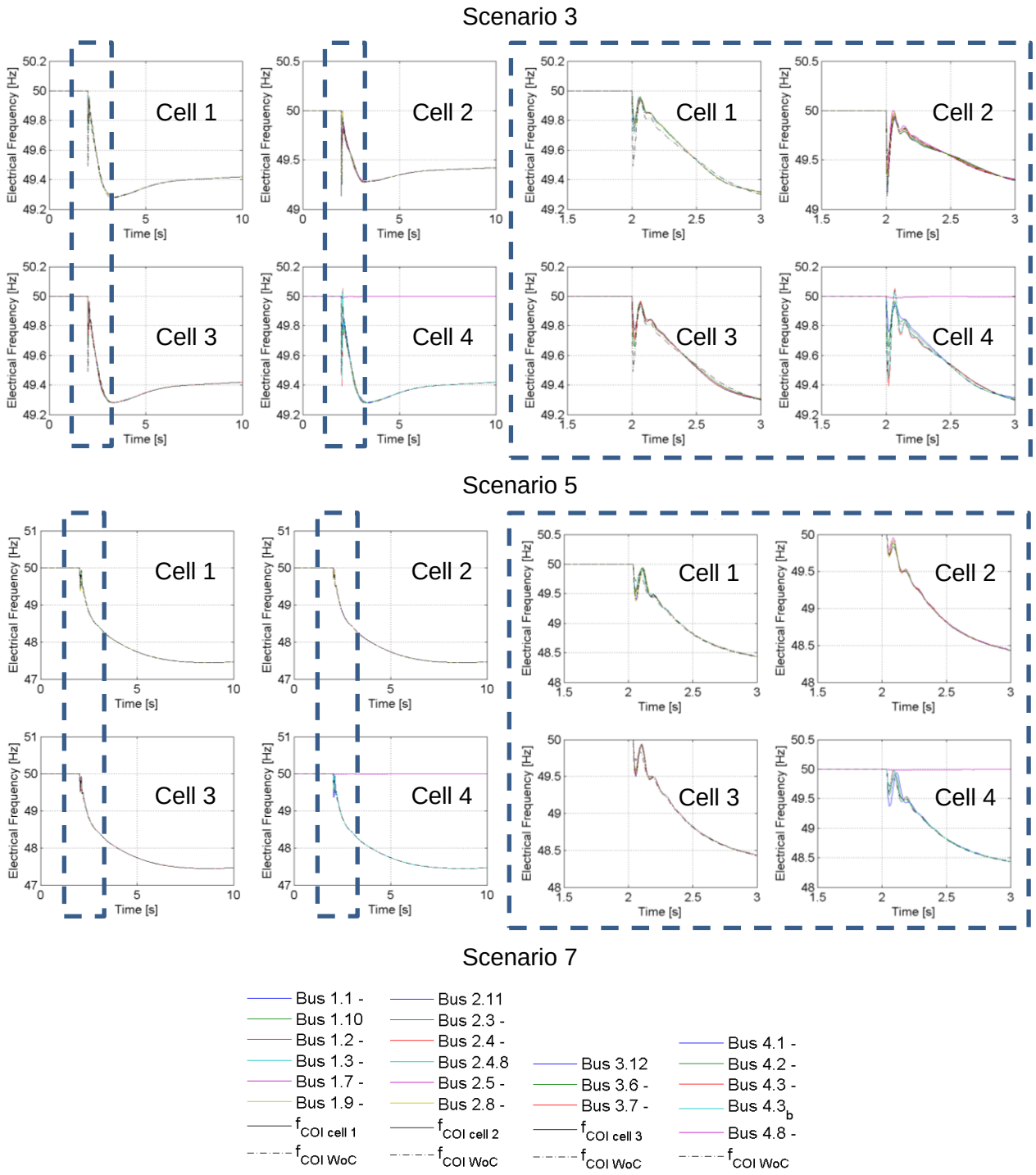

Legend for the four cells: Cell 1, Cell 2 , Cell 3, Cell 4

Figure 4-14 Frequency transients for the four different scenarios chosen

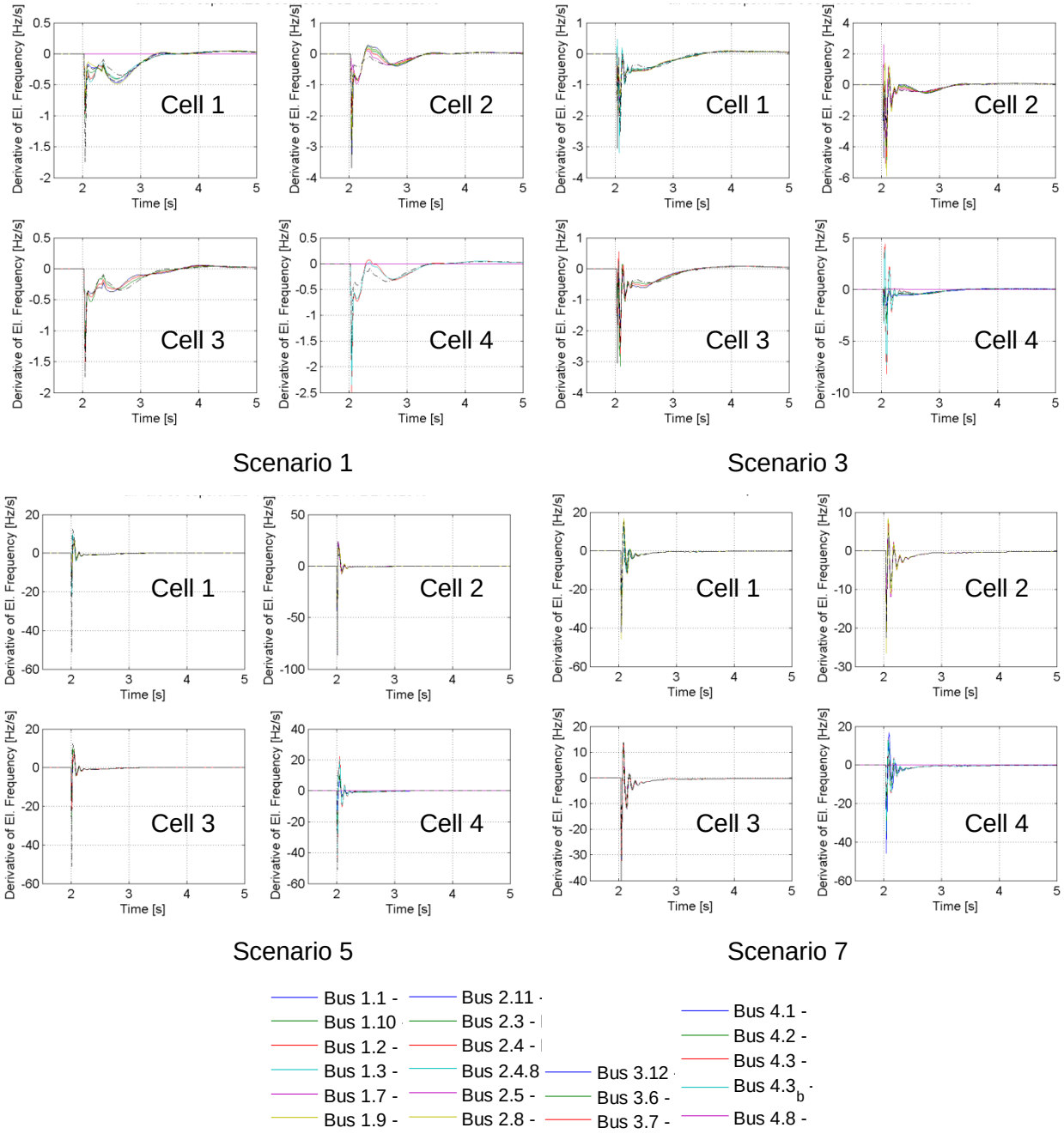

Legend for the four cells: Cell 1, Cell 2 , Cell 3, Cell 4

Figure 4-15 Frequency transients for the four scenarios chosen: ROCOF

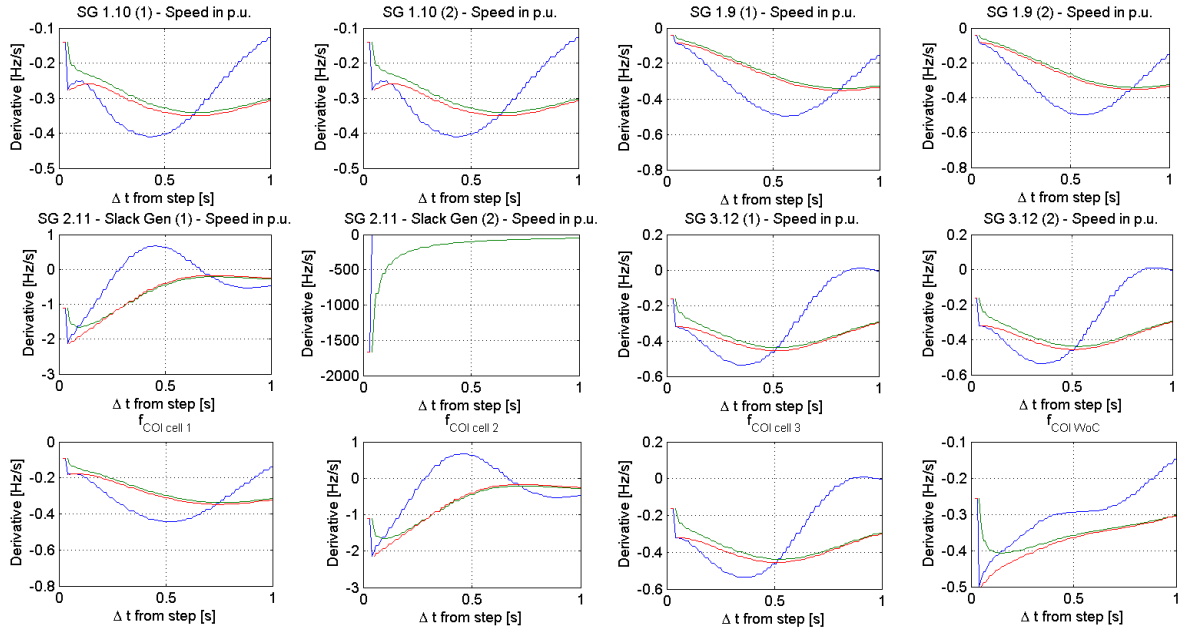

Scenario 1

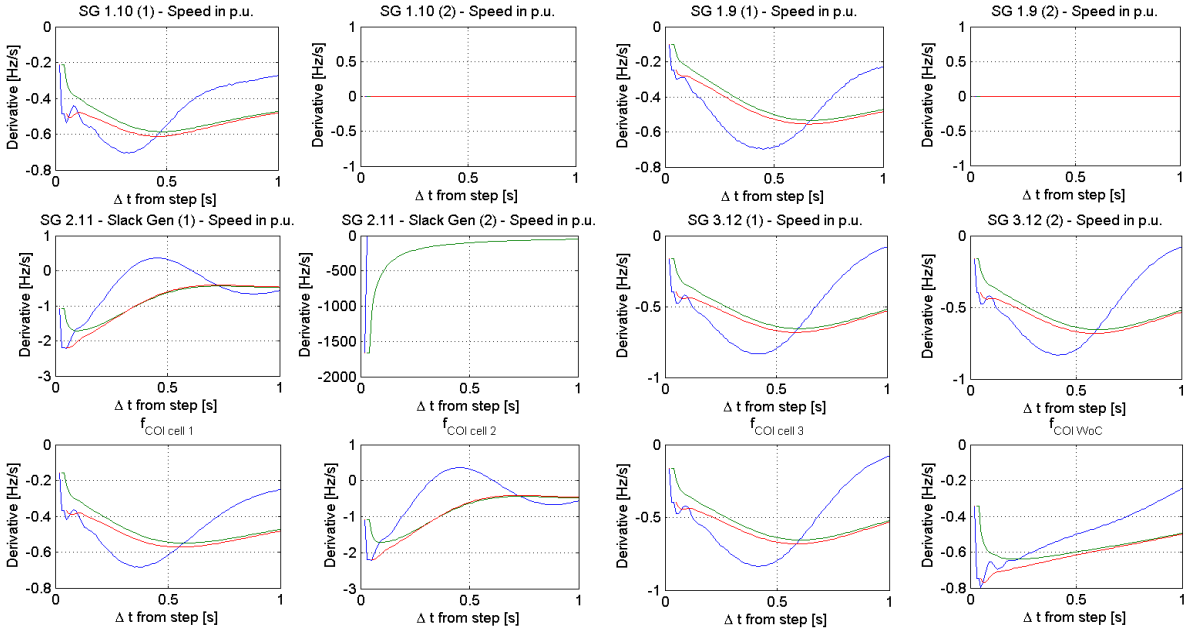

Scenario 3

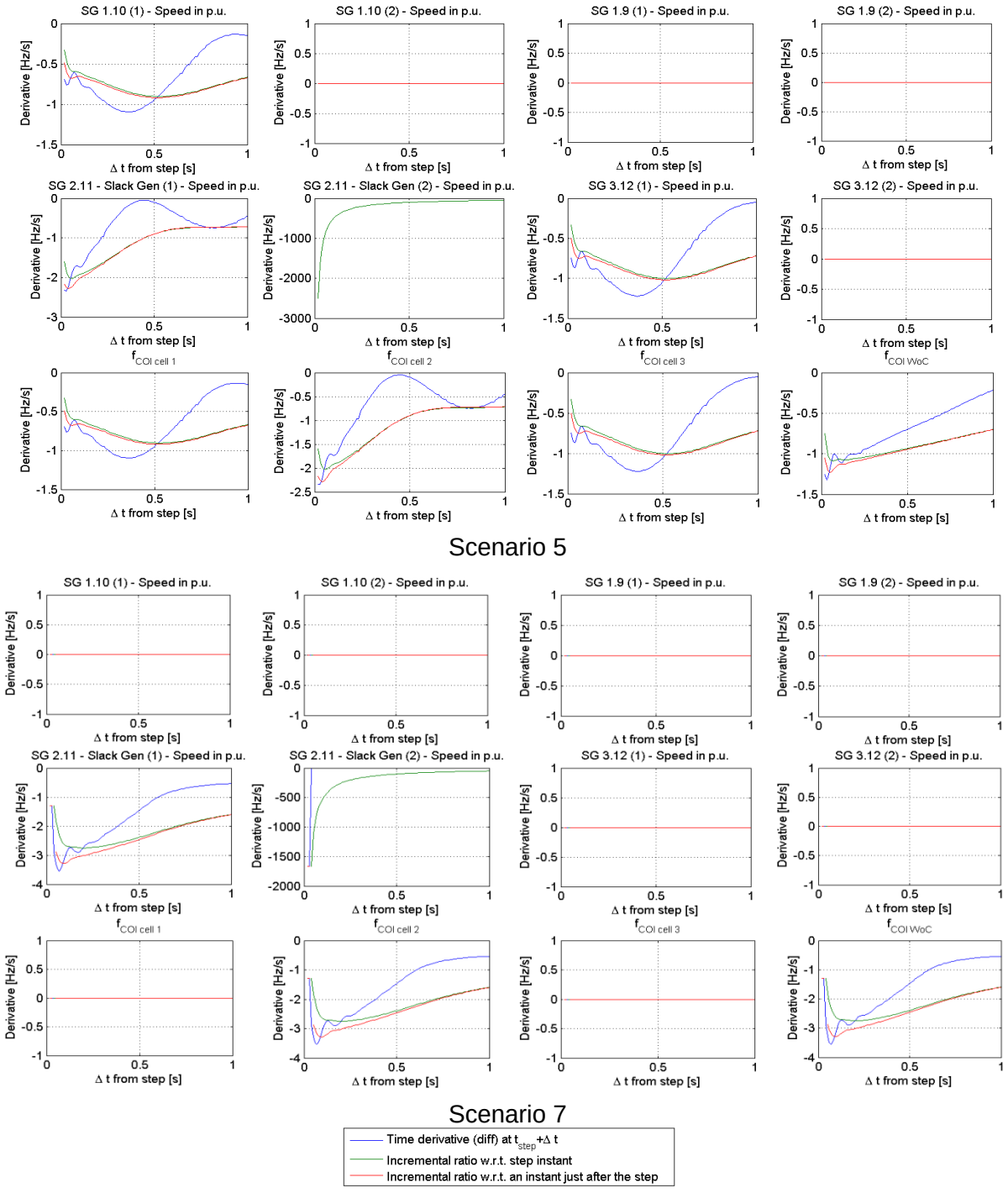

Figure 4-16 ROCOF computed from SG speed, in the four scenarios

From the results just obtained, one can deduce that different options can be envisaged for the choice of a set of relevant observables for a WoC, such as:

- **in each cell, frequency and ROCOF at all the buses where synchronous machines are connected**, or were connected in case synchronous machines are taken away from the network due to NP-RES penetration; new flexible resources supplying synthetic inertia could indeed be placed at the same buses or near them, in order to obtain frequency transients similar to the ones in the original no-RES scenario;

- **in each cell, frequency and ROCOF at a chosen set of buses**; such buses could be the ones found in simulations as the most critical ones, in that they exhibit the largest variations in frequency and ROCOF; again, new flexible resources supplying synthetic inertia could indeed be placed at those buses or near them;

- **in each cell, the COI frequency and its ROCOF; in addition, an overall WoC COI frequency and its ROCOF**; such values could be computed either from the SGs bus frequencies or from the SG rotor speeds;

- **the inertia of each cell and of the whole WoC**; inertia can be estimated, e.g., as the weighted sum of the cell, or WoC, inertia constants of the online SGs and of the equivalent inertia constants of the resources supplying synthetic inertia; alternatively, if continuous measurements of the ROCOF and continuous knowledge of power imbalances were available, they would allow to estimate, almost in real time, the online inertia. In both cases, inertia estimates, in turn, could be adopted for cell inertia procurement, i.e. to size the minimal amount of inertia needed in each time slot related to the market, for instance a quarter of an hour or even five minutes; then, local control actions, in terms of FCC or IRPC, can be given by resources connected to the buses already described.

Each option has to compare to measurement issues, which are mentioned in the next subsection.

4.3.4 Observing the system frequency and ROCOF

4.3.4.1 Mathematical model of AC quantities

According to the previous sections, it is clear that the system frequency and the related ROCOF are fundamental observables for the provision of inertial response, as well as frequency containment control. In AC power systems these two quantities cannot be directly measured, but they have to be extracted from other quantities by means of dedicated observers. A generic three-phase quantity can be expressed by means of the following formula (also extendable to single-phase signals):

$$\bar{X}(t) = x_m(t) \cdot e^{\delta(t)} + \epsilon \qquad \text{Eq. 4-13}$$

where $x_m(t)$ and $\delta(t)$ are the magnitude and phase angle of $\bar{X}$ (space vector[3] of the measured quantity) and ε is the effect of noise/distortion/inverse components present on the measured signal. Looking at this formula, it can be noticed that the frequency $\omega(t) = 2\pi f(t)$ attributable to the measured signal can be extracted only from the phase angle:

$$\delta(t) = \delta_0 + \int_{T_0}^{t} \omega(t)dt \qquad \text{Eq. 4-14}$$

and the same can be concluded for the ROCOF $\dot{\omega}(t)$, for which:

$$\omega(t) = \omega_0 + \int_{T_0}^{t} \dot{\omega}(t)dt \qquad \text{Eq. 4-15}$$

Normally $\bar{X}(t)$ is directly measurable and, according to Eq. 4-13, it can be noticed that $\delta(t)$ can be extracted by means of non-linear processes. As it can be deduced from Eq. 4-14 and Eq. 4-15, this

[3] A space vector is a common representation of three-phase quantities which can be obtained by operating the Clarke's transformation on the phase values. The value of the space vector can be also expressed for rotating reference systems by processing the phase quantities with the Park's transformation.

is valid also for the estimation of frequency and ROCOF since $\omega(t)$ and $\dot{\omega}(t)$ are linear functions of $\delta(t)$.

4.3.4.2 Mathematical modeling of frequency and ROCOF observers

The measurement of the system frequency is a well-known problem and literature reports many methods for its estimation (a survey is reported in [66]). Some estimation processes are based on the extraction of the phase angle $\delta(t)$ and on the computation of its derivative while some others directly return the frequency value by elaborating the time-domain signal $\bar{X}(t)$. The most common architectures adopted for the extraction of $\omega(t)$ from a generic real-world measurement of $\bar{X}(t)$ can be basically divided into two categories (Figure 4-17):

- Closed-loop observers [67]
  These functions guarantee a real-time and fast estimation of the system frequency and the most common observers are based on the reconstruction of the phase angle (Phase Locked Loop – PLL) or also on the direct extraction of the frequency signal (Frequency Locked Loop). Because of the stability requirements of closed-loop observers, the latency in reconstructing the frequency signal is generally smaller than open-loop estimations and, in general, this negatively affects the accuracy of the reconstructed observable.
- Open-loop observers [66]
  These functions elaborate the measured signal $\bar{X}(t)$ by means of signal processing techniques aimed at extracting the frequency in an accurate way. Even in this case, direct estimation of the system frequency or phase angle processing are possible. The advantage of open-loop observer is that the internal parameters of the observer can be tuned in order to achieve the desired accuracy since no particular restrictions in terms of processing latency are required.

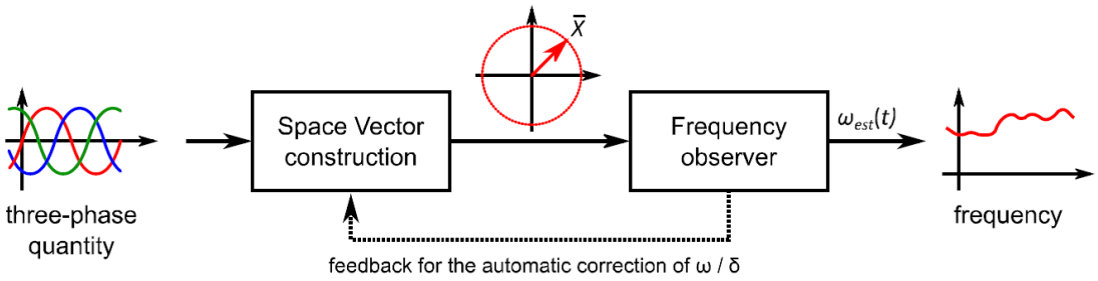

Figure 4-17 Frequency observer architecture

Concerning the observation of the ROCOF (Figure 4-18), the normally adopted procedure is based on the application of a derivative operator on the estimated frequency signal $\omega(t)$ (or second order derivative on the input signal phase angle). This process can be generally classified as an open-loop system and, since it starts from the frequency/phase angle estimation, the observation of the signal ROCOF can have significant latencies. Therefore, as it happens for the extraction of the frequency, a trade-off between ROCOF accuracy and estimation delays has to be carried out.

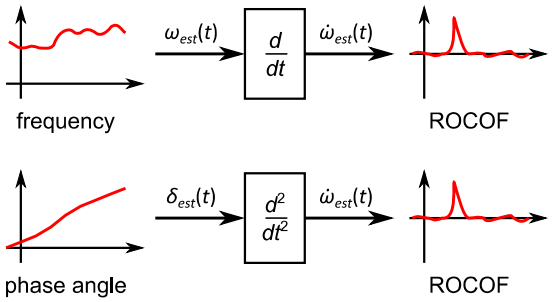

Figure 4-18 ROCOF observer architectures

As it is clear from Eq. 4-13, the performance of a frequency/ROCOF observer is strictly influenced by its ability in extracting the profile of $\delta(t)$ from $\bar{X}(t)$. Therefore, the estimation process has to filter out the variations of the space vector magnitude $x_m(t)$ and of the noise ϵ:

- In order to minimize the observation disturbances introduced by the uncontrolled time evolution of $x_m(t)$, the voltage is normally selected as the directly measurable quantity from which to extract $\delta(t)$. In fact, because of the quality-of-supply requirements, voltage should be subjected to limited variations with respect to other electrical variables of the system.
- Quantities measured in real systems are subjected to noise and distortion and the observers have to be selected in order to mitigate the effect of these non-idealities. The sensitiveness of frequency/ROCOF estimations to ϵ (but also to variations of $x_m(t)$) is typically reduced by tuning the parameters responsible of observers dynamics, in order to make the observers act as low-pass filters (Figure 4-19). This guarantees an accurate estimation of the frequency/ROCOF but the reduction of observers bandwidth necessarily means a consequent increase in the latency.

Having considered the operation characteristics and the services that a cell is called to guarantee, two main roles can be assigned to the observation of the frequency and of the ROCOF:

- Provision of FCC and IRPC contribution by energy units
- Observation and monitoring of Cell total contribution to FCC and IRPC

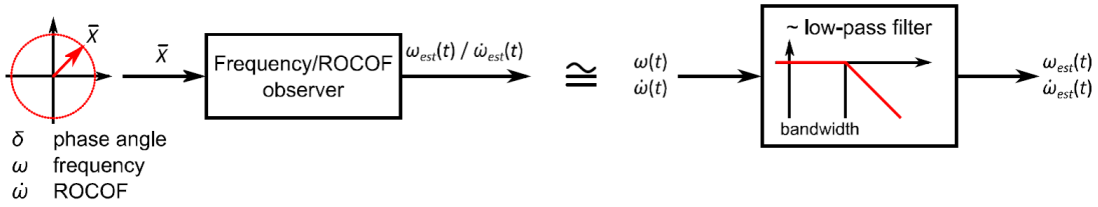

Figure 4-19 Approximated dynamic response model of typical frequency/ROCOF observers

4.3.4.3 Provision of FCC and IRPC contribution by energy units

The overall reaction of a cell to a frequency transient is built up, in the first seconds, by the activation and response of flexible resources supplying FCC and IRPC.

Of course, flexible energy resources participating in the system frequency and inertia control within a cell need the observation of $\omega(t)$ and $\dot{\omega}(t)$; these are normally derived from the estimation of

$\delta(t)$ which is used for the synchronization of static generation units. Because of the response promptness required for the FCC and IRPC (and their high level of reliability requirements), it is preferable to estimate frequency and ROCOF by means of local observers (operating on board of flexible resources controllers and measuring the voltage at their physical terminals – Figure 4-20). In this case, closed-loop estimation functions are most likely the best trade-off between latency and accuracy.

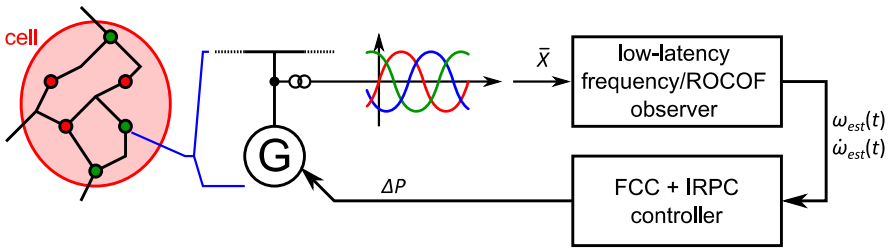

Figure 4-20 Energy units on-board observer for frequency and ROCOF estimation

4.3.4.4 Observation and monitoring of Cell total contribution to FCC and IRPC

According to the Web-of-Cells concept, each cell of the power system is called to procure a predefined amount of reserve for the FCC and IRPC, in order to have resources enough to provide such regulation actions in real time. Of course, because of the system losses and non-idealities and load and RES generation forecast errors, the effective reserve of the entire cell is not always easily predictable. In order to overcome this problem, the total reserve in FCC and IRPC can be deduced by monitoring the current state of the network and running (sufficiently fast) dedicated dynamic simulations that take into account the non-linear behaviour of the network as well as the response of energy units to critical events (Figure 4-21).

In particular, the current state of the cell can be monitored, e.g., by observing the frequency and the ROCOF in correspondence of the tie-lines (which are for sure monitored) and the power response of each flexible energy unit inside the cell. In this case, since no particular requirements in terms of latency have to be respected, highly accurate estimations of $\omega(t)$ and $\dot{\omega}(t)$ can be obtained from tie-line observables; besides, it can be useful to compare the (active) power response monitored in correspondence of same tie-lines with the one the FCC and IRPC participating units (Figure 4-21). Since multiple observables have to be collected, their time-synchronization is fundamental and the employment of PMUs is the preferred option.

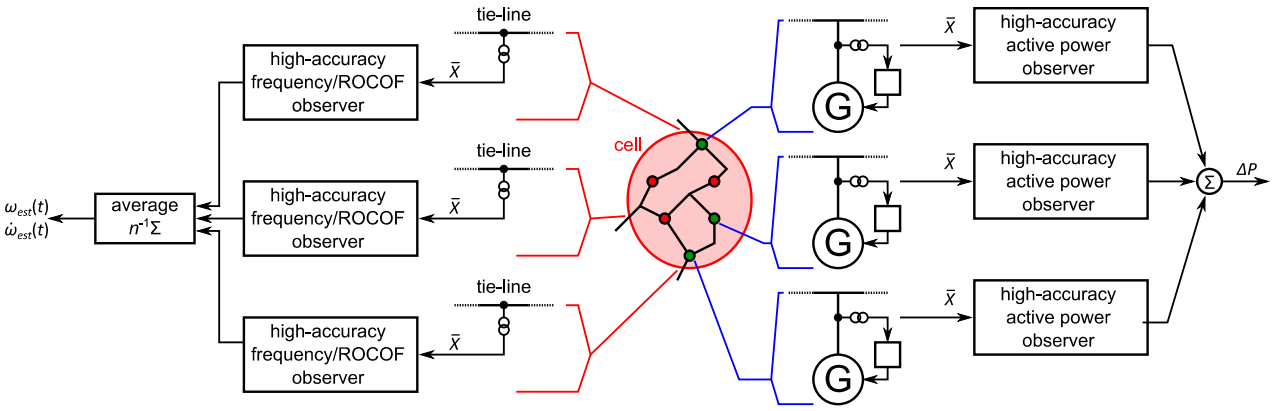

Figure 4-21 Observation of the cell total contribution to FCC and IRPC

For long-term offline analyses, the contribution of a cell in terms of frequency and inertial response can be monitored in correspondence of large perturbations of the system [68]. In fact, failures of large generation/load units determine an energy imbalance and a consequent noticeable transient in the frequency signal (see the simulation results in Section 4.3.3). Because of the magnitude of these perturbations, the cell frequency/inertial response can be accurately characterized (in terms of suitable parameter indexes, such as the NPFC, the overall inertia constant, the frequency nadir…) as well as the one of each single flexible unit participating in FCC and IRPC.

4.4 Topic 4: Voltage stability

Proper voltage profile at the transmission grid level has been maintained primarily by large synchronous generators. These are connected to network by step-up transformers and deliver the necessary amount of reactive power to the network. As new renewable generation is being connected to the power system and new bulk power transmission corridors are commissioned, voltage control is also performed by non-synchronous generation like large wind farms and HVDC converters with AC voltage control capability as required by the network codes [47], [48].

Effective voltage control requires the operational points of the participating resources be far from their limits. The resulting margin can be readily acquired from the PQ plane, in which the boundaries are set by circuit rating (thermal) constraints as well as other acting limiters. Consequently, the boundaries in the PQ plane are not constant, but depend on current state of the power system, mainly on voltage as in synchronous generators and power electronic converters of wind turbines, but also on voltage and AC system strength and system impedance characteristics as in VSC converters used in HVDC applications [49]. On the other hand, the current position of the operating point is a result of power system conditions, voltage set point as well as voltage controller type and parameters.

Despite the number of factors influencing voltage control process, it can be assumed as a rule of thumb that if typical system variables and parameters are close to their rated values, then the power system runs normally and is far from stressed conditions. Conversely, when the system becomes stressed subsequent to a significant contingency, several system variables will deviate from their usual values, even though stable operation of the power system is still assured. These system variables have indicative meaning for the assessment of the current operating conditions and can provide valuable insight useful for dispatching the power system.

This report proposes an approach to utilize one of the indicative system parameters not only for evaluation of current state of the power system, but also as means for direct voltage stability assessment. A modification of the method described in [50] using reactive power reserves as a system indicative parameter is presented and evaluated based on the Pan-European reference grid model elaborated within this task.

4.4.1 Principle of the method

Case 1: local load and local generation

As explained in [50], the reactive power reserve can be associated with voltage stability quantitatively expressed by the voltage stability margin (VSM). According to Eq. 4 16 the margin is defined as the relative amount of system load rise until voltage collapse [51]. The relation between reactive power reserve and VSM is illustrated by the following example. In the power system of Figure 4-22, load 1.2 is supplied from three generators; 1.9, 1.10 and 2.11. The stability of the

current operating point of the power system is evaluated by calculating the voltage stability margin for the present state of the grid as well as for the defined set of contingencies. The result is presented in Figure 4-23 where reactive power reserve of each generator is plotted against VSM. Each point represents each contingency and the base case is marked with an ellipse.

$$VSM = \frac{P_{Max} - P_{Init}}{P_{Init}} \qquad \text{Eq. 4-16}$$

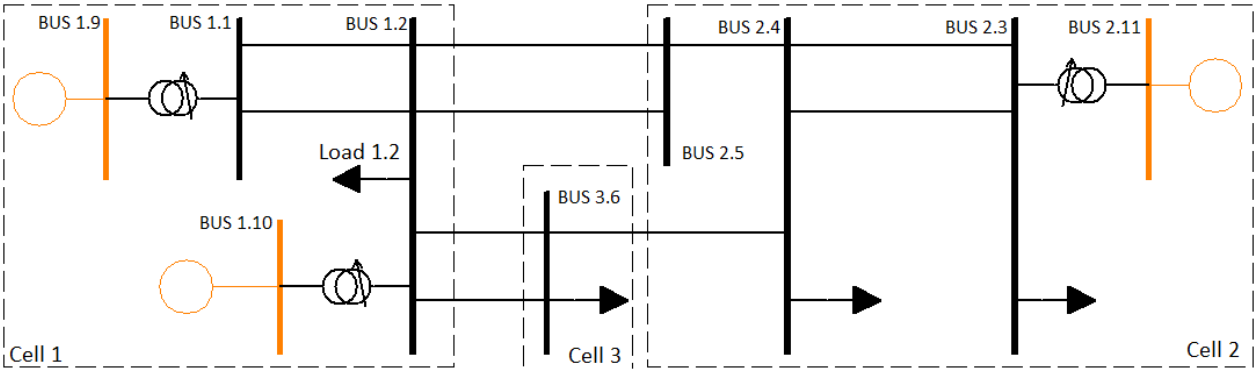

Figure 4-22 Part of the Pan-European reference power system model used for method development

Table 4-7 List of contingencies for the voltage stability analysis of load at bus 1.2

Contingency No.	Tripped element
0	Base case (no tripped elements)
1	Line 1.2 – 1.1
2	Line 1.2 – 2.5
3	Line 1.2 – 3.6
4	Line 1.2 – 1.1 & Line 1.2 – 3.6
5	Line 1.2 – 1.1 & Line 1.2 – 2.5
6	Line 1.2 – 2.5 & Line 1.2 – 3.6

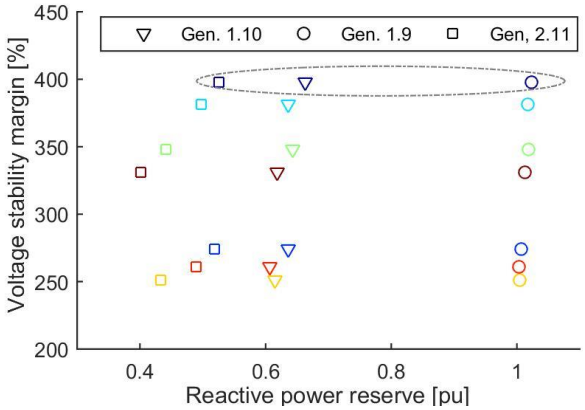

Figure 4-23 Scenario 1, voltage stability margin as a function reactive power reserves of the three generators for a set of contingencies

In Scenario 1 depicted in Figure 4-23, the results from both the base case and the contingencies imply very secure conditions. The most significant contingency can lower the VSM down to 250%. Since generators operate in different electrical proximity from the load, their contribution to satisfy its demand in active and reactive power in different contingencies varies, however patterns can be

identified. Reactive power reserves of generators 1.9 and 1.10 align almost linearly with a very high gradient, whereas for generator 2.11 it is difficult to identify a pattern.

For the situation depicted above, a curve fitting technique can be used in order to find the correlation between the points and the VSM. Next, by using extrapolation, a critical reactive power reserve, i.e. the one for which VSM approaches zero, can be calculated. By using this prediction, it could be evaluated that the system would become voltage unstable when the reserves of generator 1.10 decreased down to 50% and in the same time the reserves of generator 1.9 decreased only to 96% (Figure 4-24) of the base case level. It is also evident that generator 2.11 is irrelevant for the assessment of VSM as it is remote from load 1.2.

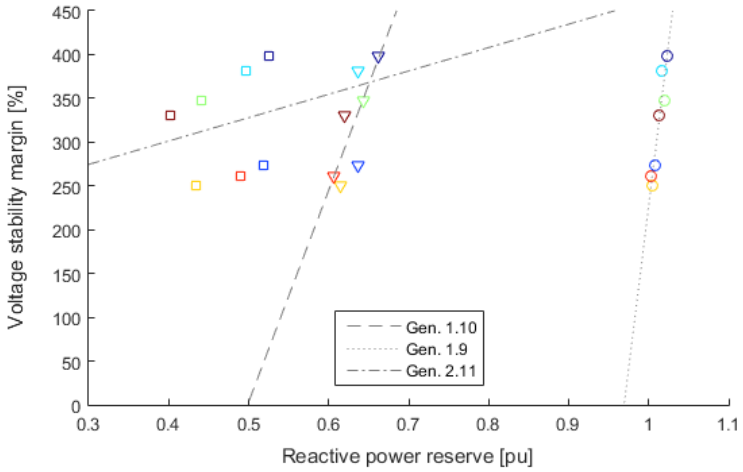

Figure 4-24 Linear approximation of the points

However, the base case scenario can be considered not only as a current operating point of the power system, but also as a starting point for a consecutive assessment of voltage stability margin as the load increases. It can be achieved by evaluating VSM for numerous operating points with different level of load. The results are depicted in Figure 4-25.

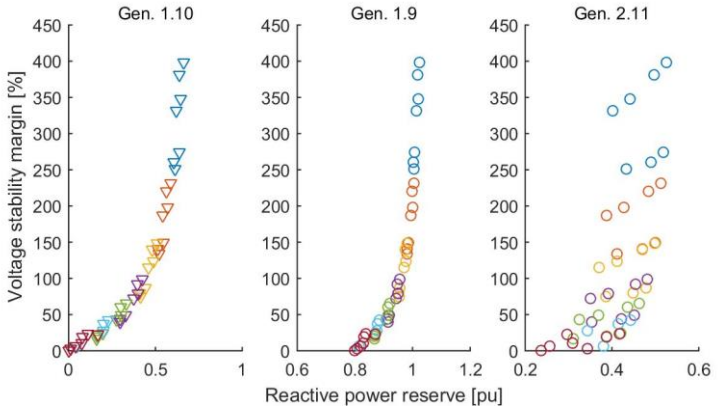

Figure 4-25 Distribution of operating points for increasing load levels; each load level is marked with different color starting from top blue

Patterns for generators 1.9 and 1.10 can be easily approximated by power or exponential functions as depicted in Figure 4-26. Due to horizontal spread of reactive power reserves of generator 2.11 in different contingencies, this unit is not taken into consideration in the evaluation of VSM.

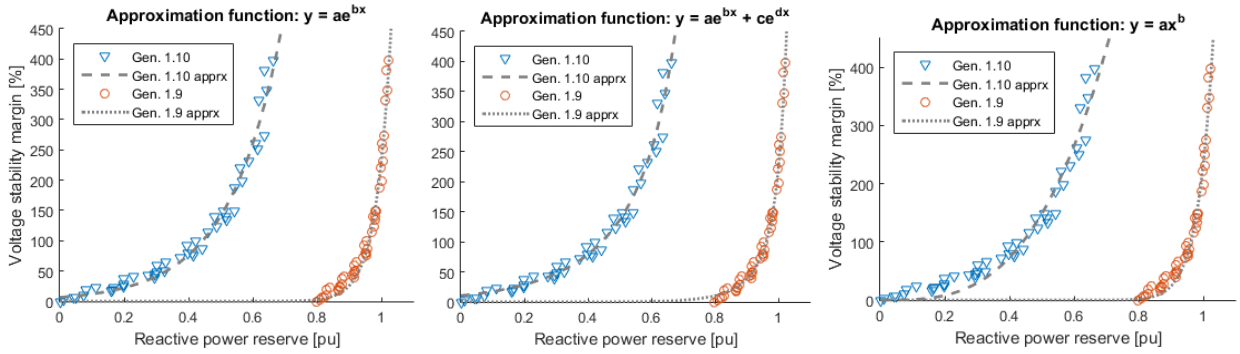

Figure 4-26 Comparison of different curve fit types for all points

Table 4-8 Quantitative evaluation of selected curve fit types

Approximation function	$y = ae^{bx}$	$y = ae^{bx} + ce^{dx}$	$y = ax^{b}$
R^2 for Gen 1.10	0.973	0.976	0.955
R^2 for Gen 1.9	0.980	0.989	0.977

Both visual inspection of plots depicted in Figure 4-26 and quantitative assessment with use of coefficient of determination (R^2) indicate that the best fit is provided by the exponential function with two terms ($y = ae^{bx} + ce^{dx}$), however a single-term exponential function ($y = ae^{bx}$) offers almost as good results and is easier to use, therefore the subsequent analysis is limited only to this function. For the examined case, $a = 6.584$ and $b = 6.125$ for generator 1.10, and the voltage stability margin can be readily calculated for any value of the reactive power reserve of this generator using the following formula:

$$VSM = 6.584e^{6.125Q_{Reserve}} \qquad \text{Eq. 4-17}$$

Eq. 4-17 can also be used to set alerts and/or limits for the current operating points of the resources in the power system. After transformation, a minimum reactive power reserve Q_{ResMin} is obtained for a predefined critical VSM_{Crit}:

$$Q_{ResMin} = \frac{1}{b} ln \frac{VSM_{Crit}}{a} \qquad \text{Eq. 4-18}$$

In practice, reaching the low level of reactive power reserve given by Eq. 4-18 could trigger protection actions such as load limitation, generation re-dispatching, activation of additional resources or special protection schemes.

In this simple example the only information needed for the assessment of the current operating conditions in terms of voltage stability is reactive power reserve of a single generator. The generator located closest to the load is the most suitable for this purpose. The rest of the information (e.g. power system operating conditions, contingencies, etc.) has been taken into account in the preparation process of the formula Eq. 4-17 and is not required for the on-line assessment.

Case 2: concentrated load, system generation

The analysis is extended to cover a less favourable case, in which there is no single dominant generator supplying the load and the contingencies may affect a wider part of the grid. This situation is illustrated with an increase in the load at bus 3.6. The contingencies are listed in Table 4-7 and Table 4-9.

Table 4-9 List of additional contingencies for the voltage stability analysis of load at bus 3.6

Contingency No.	Tripped element
7	Line 2.4 – 2.5
8	Line 2.4 – 3.6
9	Line 2.3 – 2.4
10	Line 1.2 – 2.5 & Line 2.3 – 2.4
11	Line 1.2 – 3.6 & Line 2.3 – 2.4

The results depicted in Figure 4-27 indicate that there is a subset of contingencies causing release of reactive power reserves of generators 1.9 and 1.10 as compared with contingencies with similar voltage stability margin. It can be further investigated that the reactive power reserve is larger for generators 1.9 and 1.10 when the contingency affects direct connection between these generators and the load. In the same time these contingencies engage generator 2.11 to a larger extent. The horizontal spread of points appearing in the plots for generator 1.9 and 1.10 would bring a significant error if a curve-fitting solution was applied as in the previous example and therefore direct application of this method is not suitable without prior data preparation.

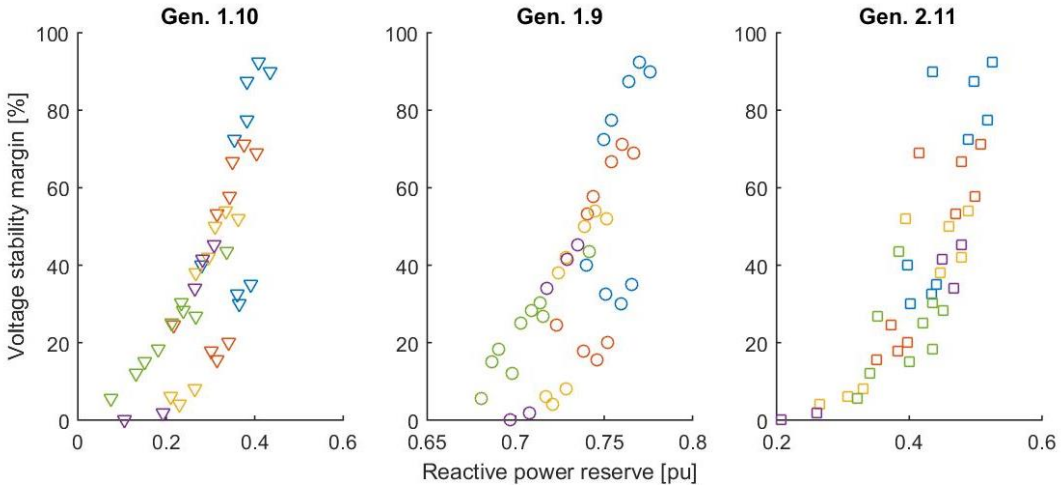

Figure 4-27 Distribution of operating points for increasing load levels; each load level is marked with different colour starting from top blue

In Figure 4-27 the points for generator 2.11 are distributed in a different way than the points of the two other generators, i.e. they tend to spread more widely as the VSM increase. In general, whenever a contingency causes one generator to be weakly connected with the load (and hence deliver less reactive power), the other generator has to cover for this difference. The interdependence of the generators can be captured via an indicator called equivalent reactive power reserve, in which particular reserves take part. The key issue in calculating the equivalent reserve is to find the weighting factors expressing correlation between the generators and the equivalent reserve. Two methods are considered:

1. By assuming the weighting factors arbitrarily and finding for which scope of points they would apply. For example from the graphical results (of Figure 4-27) or by using statistical methods, it can be identified that for VSM above 35%, generators 1.9 and 1.10 offer good correlation between Q reserves and the VSM. On the other hand for VSM lower than 20%, generator 2.11 should be used. Then, a simple rule can be applied:

$$\bigwedge_{G\in(1.9,1.10)}\ \bigwedge_{C\in\langle 1\ldots N_C\rangle} w_{G,C} = w_{High} \Leftrightarrow VSM_{G,C} \geq 35\%$$

$$\bigwedge_{G\in(2.11)}\ \bigwedge_{C\in\langle 1\ldots N_C\rangle} w_{G,C} = w_{High} \Leftrightarrow VSM_{G,C} \leq 20\% \qquad \text{Eq. 4-19}$$

$$\bigwedge_{G\in\langle 1\ldots N_G\rangle}\ \bigwedge_{C\in\langle 1\ldots N_C\rangle} w_{G,C} = w_{Low} \Leftrightarrow w_{G,C} \neq w_{High}$$

$$Q_{ReserveEquiv_C} = \frac{w_C Q_{Reserve_C}}{\sum_{i=1}^{N_G} w_{i,C}} \qquad \text{Eq. 4-20}$$

where:

N_G is the number of generators (reactive power reserves),
N_c is the number of contingencies,
w is the weighting factor for a particular reserve,
w_{High} is arbitrarily assumed high weight,
w_{Low} is arbitrarily assumed low weight,
$Q_{ReserveEquivC}$ is the equivalent reserve for contingency C,
w_C is the N_G-element vector of weighting factors for contingency C,
$Q_{ReserveC}$ is the N_G-element vector of reactive power reserves for contingency C.

The effect of applying this assignment rules is plotted in Figure 4-28.

2. By calculating the weighting factors with use of an optimization algorithm. The optimization problem is defined as minimizing an error between the input data defined as the *VSM* calculated by the voltage stability program for a given set of contingencies and an estimated voltage stability margin, VSM_e, given by the same equation (Eq. 4-21) as proposed in Case 1. Nonlinear least-squares optimization method is used for calculating coefficients in this equation so that one curve can fit the points in an optimal way.

$$VSM = ae^{bQ_{ReserveEquiv}} \qquad \text{Eq. 4-21}$$

where $Q_{ReserveEquiv}$ is an equivalent reserve defined as:

$$Q_{ReserveEquiv} = wQ_R \qquad \text{Eq. 4-22}$$

where w is the N_G-element vector of weighting factors, Q_R is the N_GxN_C matrix of reactive power reserves.

The first method requires user intervention or effective statistical methods in order to select the right VSM thresholds for differentiating the weighting factors. However, it also offers flexibility and control as additional rules can be easily added and used. On the other hand, the second approach is fully automatic and involves no manual assistance. Comparison of the two methods is depicted in Figure 4-28 and Figure 4-29.

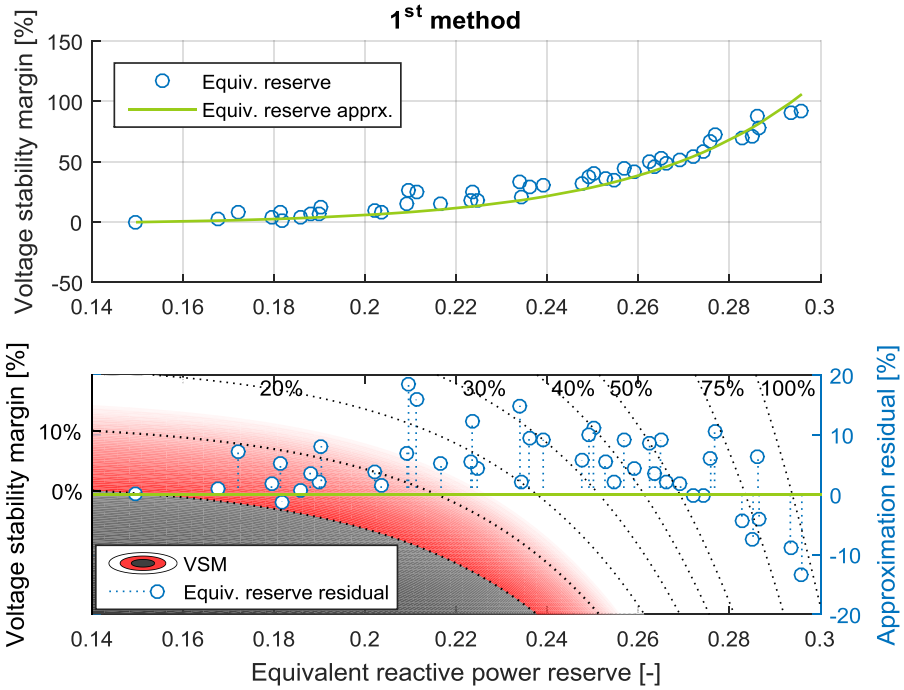

Figure 4-28 Approximation of equivalent reactive power reserve obtained with method no. 1

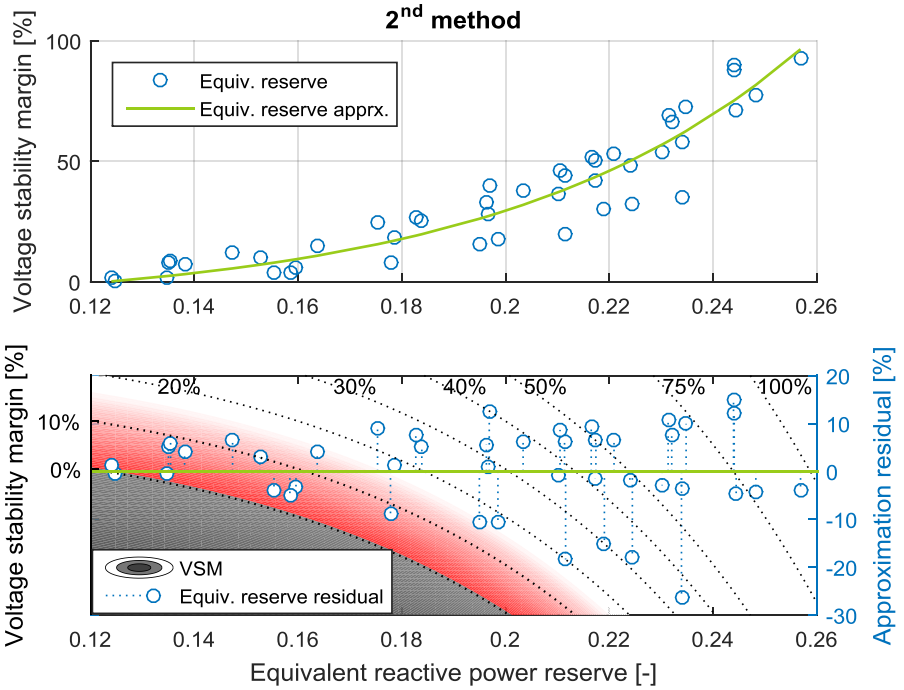

Figure 4-29 Approximation of equivalent reactive power reserve obtained with method no. 2

The upper plots of Figure 4-28 and Figure 4-29 contain data points representing the equivalent reactive power reserve according to equation Eq. 4-22. The difference between the two figures is the way that the points representing particular reactive power reserves were mapped into their equivalents. The first method, with arbitrarily defined weighting factors and selected voltage stability margin thresholds, overcame the difficulties stemming from the distortion of points (see Figure 4-27), whereas the second method managed to suppress this only to a limited extent.

The green curve visible in these plots is the final function describing the correlation between equivalent reactive power reserve and voltage stability margin. It has been derived by means of approximation as described in Case 1 with two minor modifications in order to assure that the errors inherent to the approximation are handled securely:

A. Weighted approximation is used, i.e. several points with the lowest VSM are assigned with higher weighting factors in such a way that the point with lowest VSM receives the highest weight. In this way it is assured that the error of the approximation is minimized for a zero VSM and the whole curve is slightly shifted downwards.
B. In order to be able to perform operation described above, a modification of approximation function is needed. A simple shifting term *c* is sufficient:

$$y = ae^{bx} - c \qquad \text{Eq. 4-23}$$

The lower plots reveal the quality of approximation in terms of the residual values expressed in percentage of voltage stability margin. From this plot it is evident that neither the approximation function nor the original points are in the area for which VSM is negative (dark grey area). Negative residuals mean too optimistic system stability evaluation, however if they do not reach the grey area, the situation is safe and therefore the approximation is acceptable. This visualization method also allows for informative depiction of low VSM level (e.g. red area to about 15%).

Case 3: system load, system generation

The two methods are validated for the most generic conditions, in which the whole load in the power system is increased and increased demand is covered by all generators. Figure 4-30 shows the distribution of operating points for this case. The largest sensitivity to load changes is exhibited by generator 1.10, the smallest by generator 2.11, but on the other hand generator 2.11 is the least prone to contingencies and generator 1.10 is the most. Generator 1.9 is in the middle with respect to the two factors.

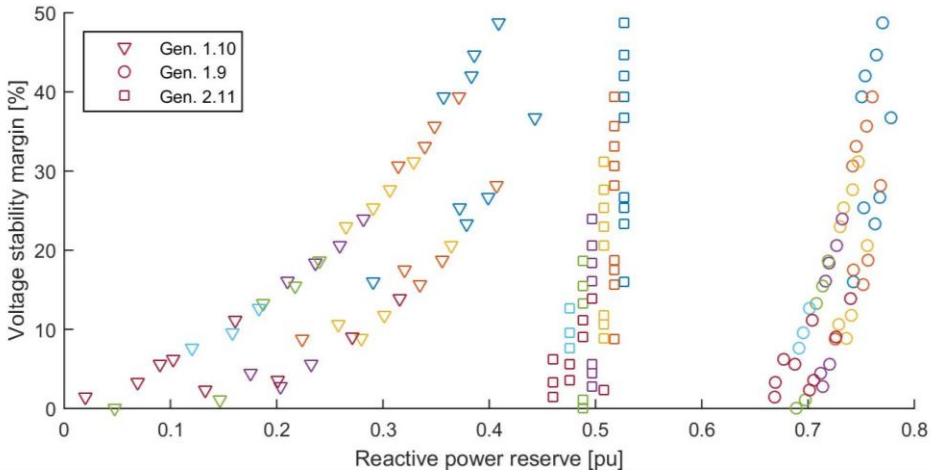

Figure 4-30 Distribution of operating points for increasing system load level; each load level is marked with different color starting from top blue

The two methods described in Case 2 are applied to the data above. From the results presented in Figure 4-31 it stems that:

- the proposed methods of voltage stability assessment work for changes of system load, which means that reactive power reserves of distributed generators can be used as observables of voltage stability margin in a quantitative way;

- the methods can handle contingencies resulting in large power flow deviations from base case scenario and large changes in operational point of the generators;
- the remaining differences are addressed by applying larger weighting factors to those points of the equivalent reactive power reserve which correspond to the lowest VSM; in this way the approximation error is shifted towards the safe direction and security of operation is assured.

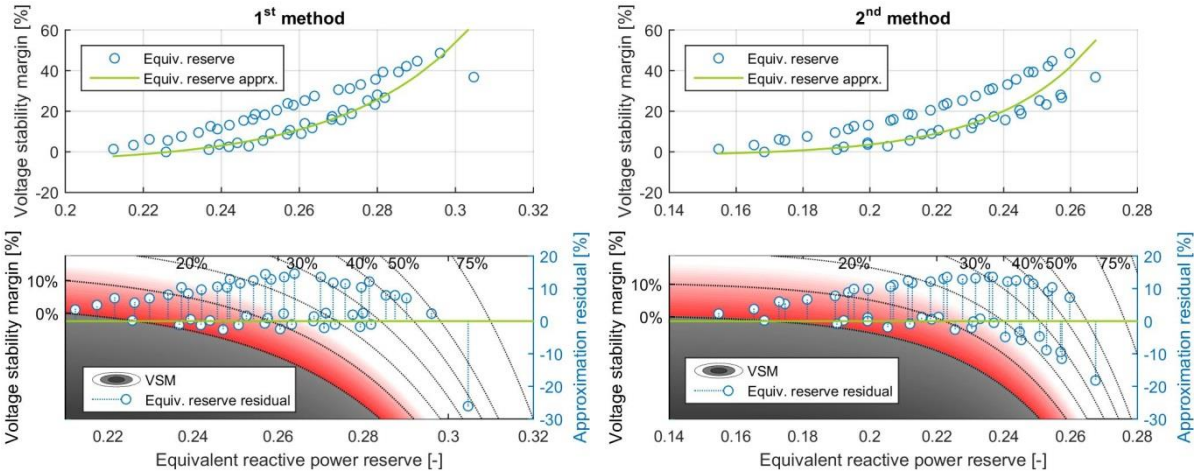

Figure 4-31 Comparison of the two approximation methods for system-wide changes of load

4.4.2 Application to the Web-of-Cell concept

Adaptation of the method

In principle each cell in the Web-of-Cell concept [55] should be designed in such a way that it is self-reliant in case of a communication breakdown with other cells. Losing information about reactive power reserves in the neighbouring cells, or relevant cells in general, is a critical example for the analysed observable. Therefore, considering a case of a cell operating in an interconnected WoC system, however with a limited access to information from outside the cell, other available observables should be used. Reactive power flow in the tie lines is a natural candidate.

Depending on flow direction, the cell can be a reservoir of reactive power if the power flows out of the cell or a sink if the power flows into the cell. In the former case the external power system can be substituted by an equivalent generator (Figure 4-32a) whose reactive power reserve Q_{res}, in terms of reactive power limit Q_{lim} that the system can provide, is expressed as:

$$Q_{Reserve} = |Q_{Lim} - Q| \qquad \text{Eq. 4-24}$$

In the latter case, the external power system can be regarded as an additional load connected to the cell. Then the reactive power flow Q is negative with respect to the cell's balance, reactive power limit Q_{lim} to the power that the cell can provide is also negative, therefore Eq. 4-24 can also be used to express cell reactive power reserves on the interface to the interconnected power system (Figure 4-32b).

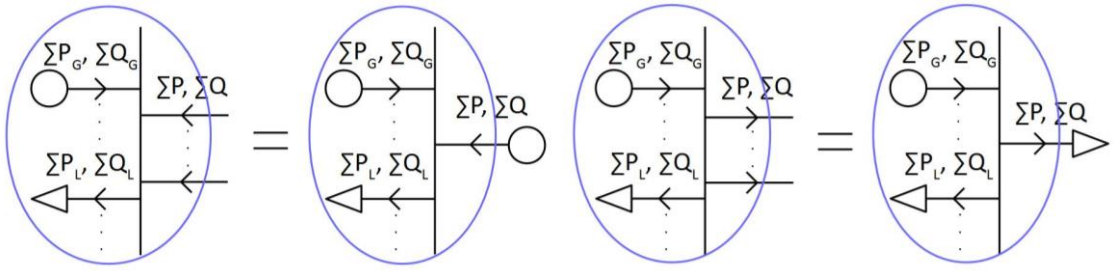

a) b)

Figure 4-32 Conversion of the external power system into (a) equivalent generator or (b) equivalent load for reactive power reserve calculation

A case where a cell is in equilibrium, meaning no reactive power exchange with external power system, and only provision of reactive power to cover lines' losses, is out of interest since it does not provide valuable insight into correlation between reactive power flow and VSM. In such case its weighting factors should be zero.

In the Pan-European system model Cell 1 represents a typical power production area where generation is in surplus over the demand, whereas the contrary is true for Cell 2. These two examples are used to verify the elaborated voltage stability assessment concept with limitations as described above, i.e. only own reactive power reserves and tie line flows are observed. The total reactive power flow of the interface between these cells and remaining part of the power system for the same set of contingencies are shown in Figure 4-33. The right-hand side of the figure depicts data transformed by Eq. 4-24 to a useful form for the algorithm calculating the equivalent reactive power reserve.

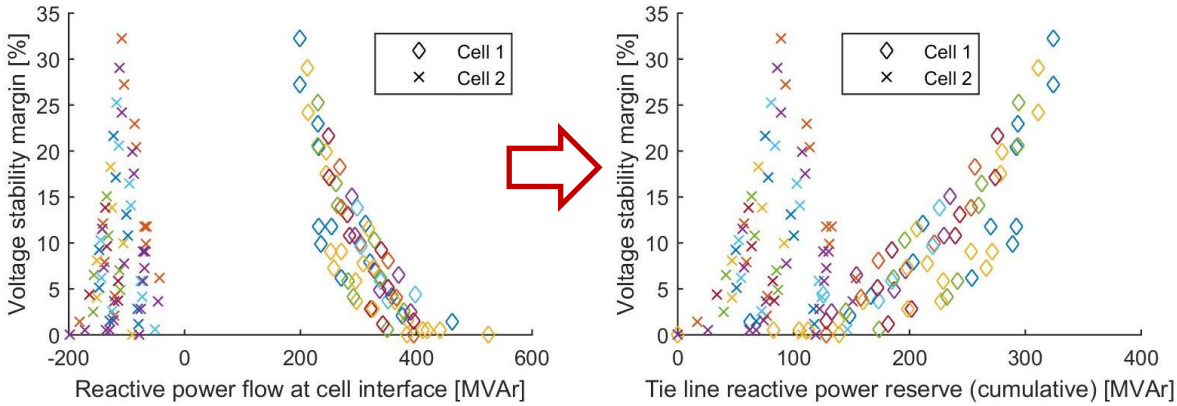

Figure 4-33 Reactive power flow at cell interface (sum of all tie-lines) and reactive power reserve provided via the tie-line interface by the cell (in case of cell 1) or by the power system (in case of cell 2)

Assessment of voltage stability margin with use of observables available within Cell 1 is presented in Figure 4-34. The optimization algorithm (2nd method) assigned weighting factors of 0.05, 0.2 and 1.2 to reactive power reserve of generator 1.10, reactive power reserve of generator 1.9 and reactive power reserve of cell 1 interface respectively. The resulting curve linking equivalent reactive power reserve and VSM allows for direct evaluation of the VSM based on current reserves with a maximum error of 10.15%. However, if unprocessed data of reactive power reserves was used (left-hand side plot in Figure 4-34) the error would be in the range of 25%.

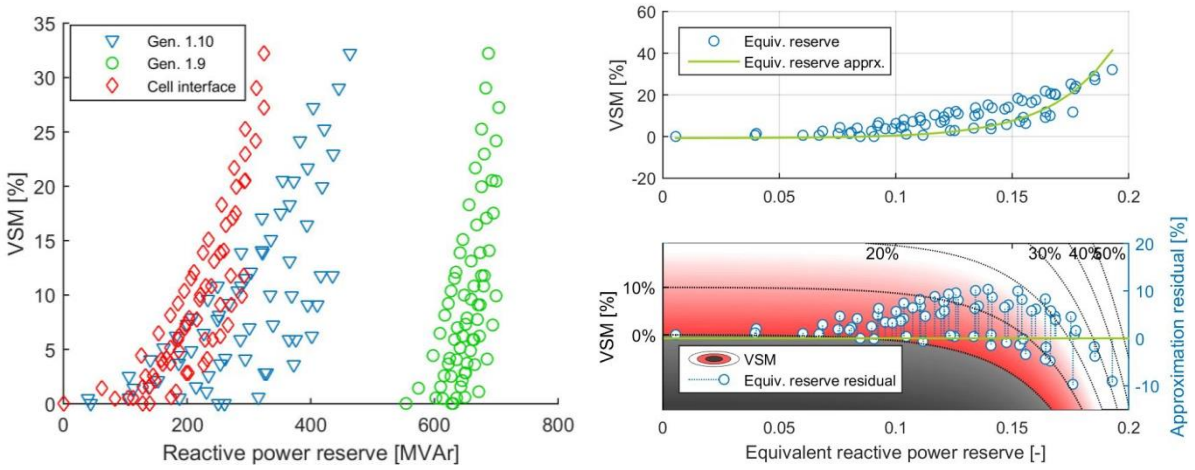

Figure 4-34 Cell 1 observables (left-hand side) used in the calculation of equivalent reactive power reserve for VSM estimation

As far as Cell 2 is concerned, there are only two available observables, namely reactive power reserve of generator 2.11 and cell interface reserve. It is the generator reserve that was assigned a high weighting factor (1.95 compared to 0.11 for cell interface reserve) due to its smaller gradient with respect to the VSM, so the equivalent reserve in this case is predominantly dependent on the generator reserve. This implies that the approximation error is in similar range as the spread of operational points of the generator, which is 10% of the VSM.

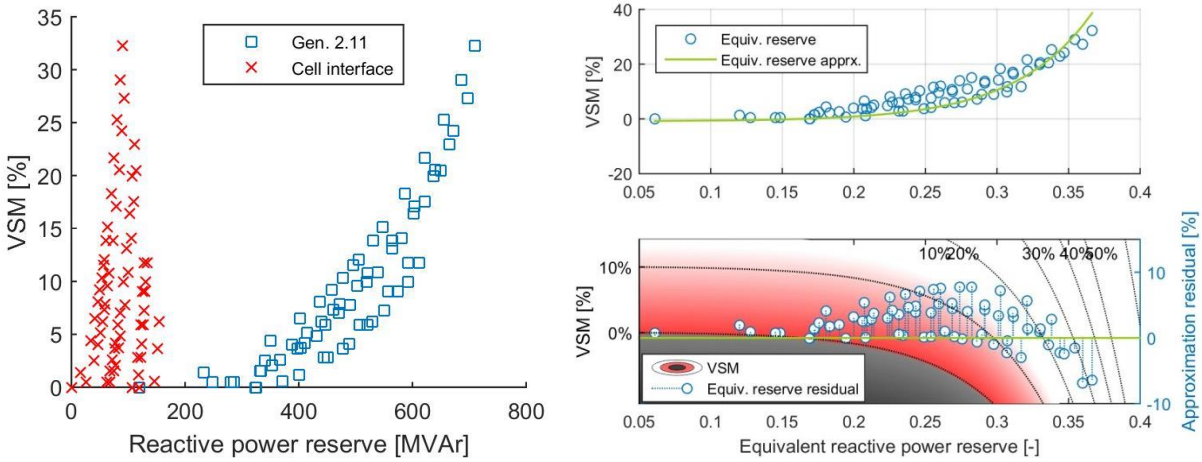

Figure 4-35 Cell 2 observables (left-hand side) used in the calculation of equivalent reactive power reserve for VSM estimation

Evaluation of the method on the Pan-European power system model

Application of the proposed method for system observability is extended to cover converter-interfaced generation. For this purpose four scenarios with varying level of wind generation (WG), i.e. 0%, 25%, 50% and 75% are analysed in the Pan-European power system model. It was assumed that each generation presented symbolically in Figure 3-1 (buses 9, 10, 11, 12) consists of 2 units (one SG and one WG) generating active power accordingly to scenario definition. Increasing demand in the VSM calculation was covered by generators proportionally to their active

power generation. The results from voltage stability analysis are presented in Figure 4-36, where synchronous generation is marked in black and wind generation is indicated in green.

The difference between SG and WG in both the magnitude of reactive power reserve and the shape of distribution of points visible in the figure results from different reactive power generation capability of the two types of sources. For WG V-shaped capability curve with a nominal cosφ equal to 0.95 was applied. Contrary to SG, reactive power capability of WG rises as active power production is increased, and consequently the distribution of points is more vertical. Nonetheless, the amount of reactive power supplied by WG is not significant until it achieves predominance in the system (75% case) which also leads to reduced total VAr resources and lower values of VSM.

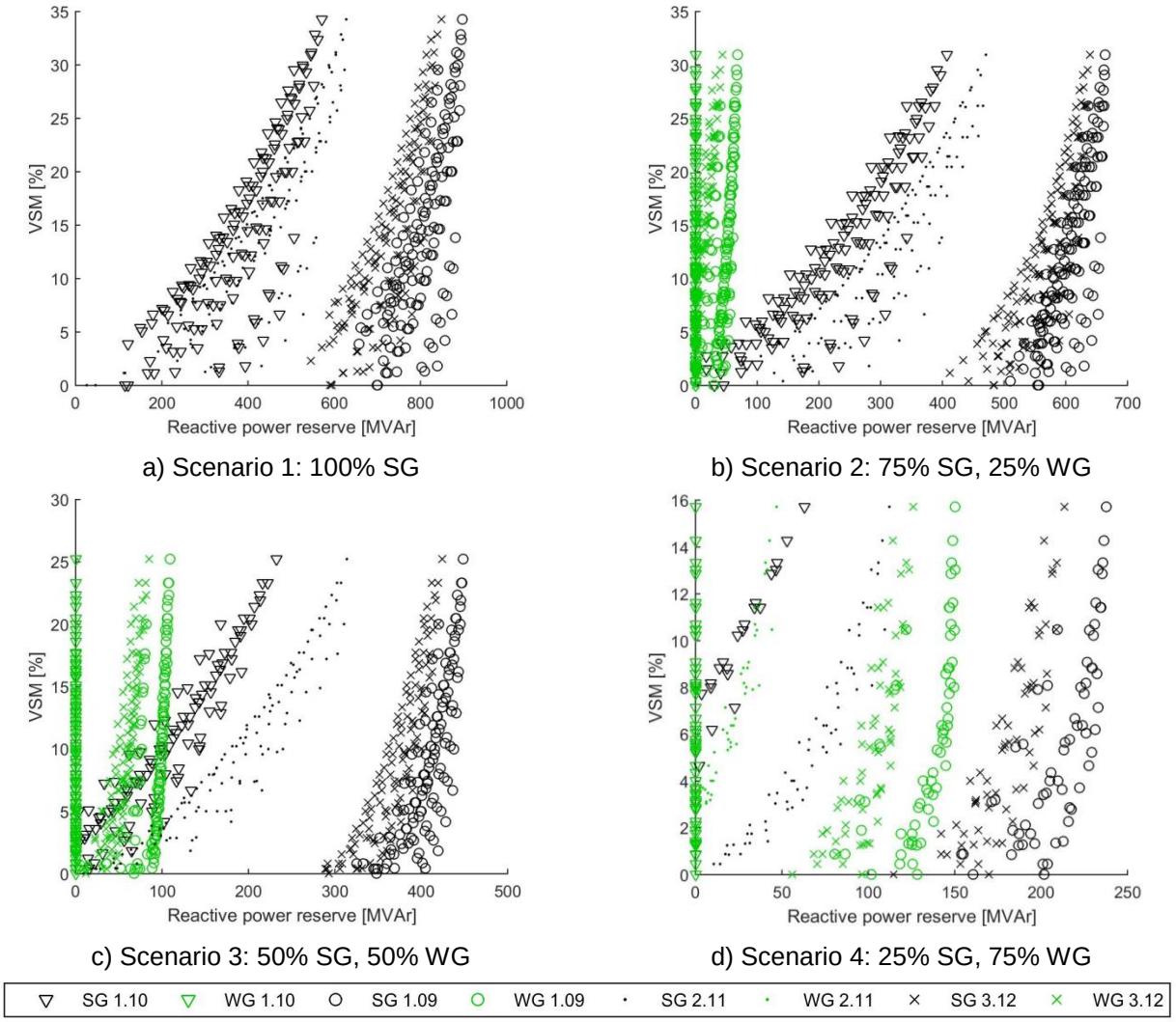

Figure 4-36 Reactive power reserves in the Pan-European model used for the calculation of equivalent reactive power reserve for VSM estimation in four different scenarios

Table 4-10 presents the summary of the results (achieved by application of the 2nd type method) for four scenarios and four types of observables used for calculation of equivalent reactive power reserve. Observables “SG+WG comb.” mean that reactive power reserves of SG and WG connected to the same bus were added together before using in the optimization algorithm, whereas in “SG+WG sep.” method these reserves were considered separately. R^2 is a measure of approximation accuracy and “$Res_{min/max}$” denote the highest negative and positive residual of the approximation. For each scenario the best selection of observables was marked in green and

presented in Figure 4-37. These indicators show that inclusion of reactive power reserve from WG improves the overall performance of the method, in particular in scenarios where WG predominates over SG (compare plots in Figure 4-38).

Table 4-10 Summary of results for analysed observables and scenarios

Scenario	Observables	R^2	*a*	*b*	*c*	w_1	w_2	w_3	w_4	w_5	w_6	w_7	w_8	Res_{min}	Res_{max}
1: 100% SG	SG only	2244	3.85	0.012	4.671	0.078		0.000		0.219		0.000		-13.6	5.1
2: 75% SG + 25% WG	SG only	4412	0.01	0.036	2.243	0.085		0.098		0.092		0.122		-11.9	3.0
	WG only	5220	0.90	0.186	3.411		0.100		0.145		0.100		0.145	-6.1	10.4
	SG+WG comb.	1024	5.00	0.014	5.333	0.118		0.000		0.196		0.000		-10.7	3.2
	SG+WG sep.	1537	2.87	0.022	3.201	0.052	0.100	0.000	0.204	0.158	0.100	0.002	0.166	-10.2	2.7
3: 50% SG + 50% WG	SG only	230	1.94	0.026	5.177	0.071		0.005		0.133		0.100		-5.3	1.7
	WG only	2235	0.00	0.088	-0.319		0.100		0.633		0.000		0.633	-4.6	9.5
	SG+WG comb.	181	5.82	0.036	7.527	0.055		0.001		0.084		0.015		-5.2	1.4
	SG+WG sep.	116	1.71	0.004	3.283	0.014	0.100	0.000	1.862	1.168	0.013	0.003	1.063	-4.1	1.5
4: 25% SG + 75% WG	SG only	60	4.01	0.001	4.103	3.200		0.087		8.286		0.008		-1.3	1.7
	WG only	191	156.66	0.005	159.429		0.100		0.033		0.372		0.005	-2.5	1.9
	SG+WG comb.	53	1.44	0.019	2.726	0.127		0.121		0.523		0.007		-2.7	1.0
	SG+WG sep.	12	102.92	0.001	103.352	1.370	0.100	0.000	0.096	1.102	2.580	0.000	0.000	-1.2	0.5

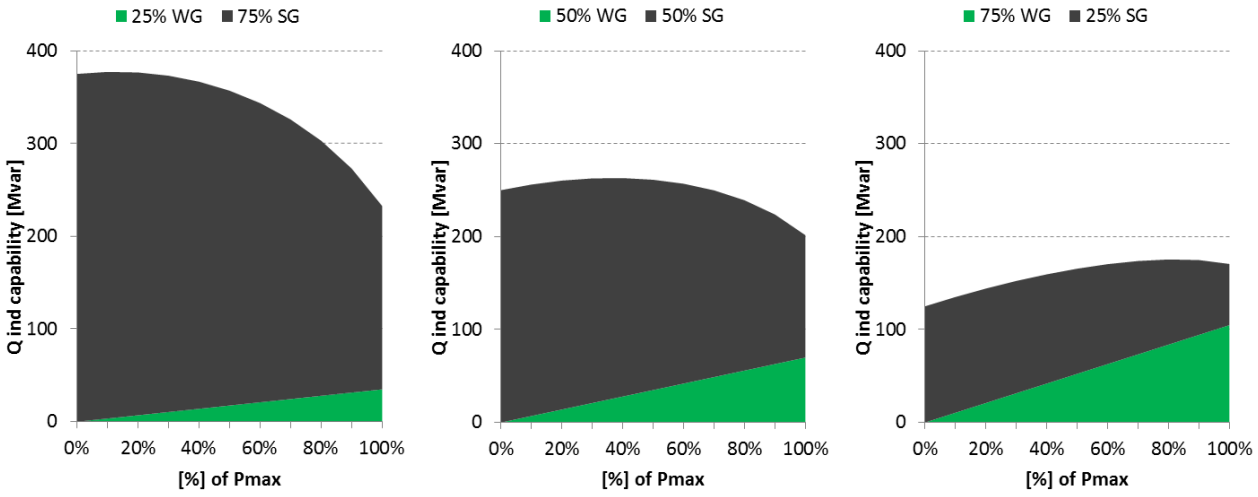

Figure 4-37 Cumulated inductive reactive power reserves of WG and SG units in case of 25%, 50% and 75% of WG share

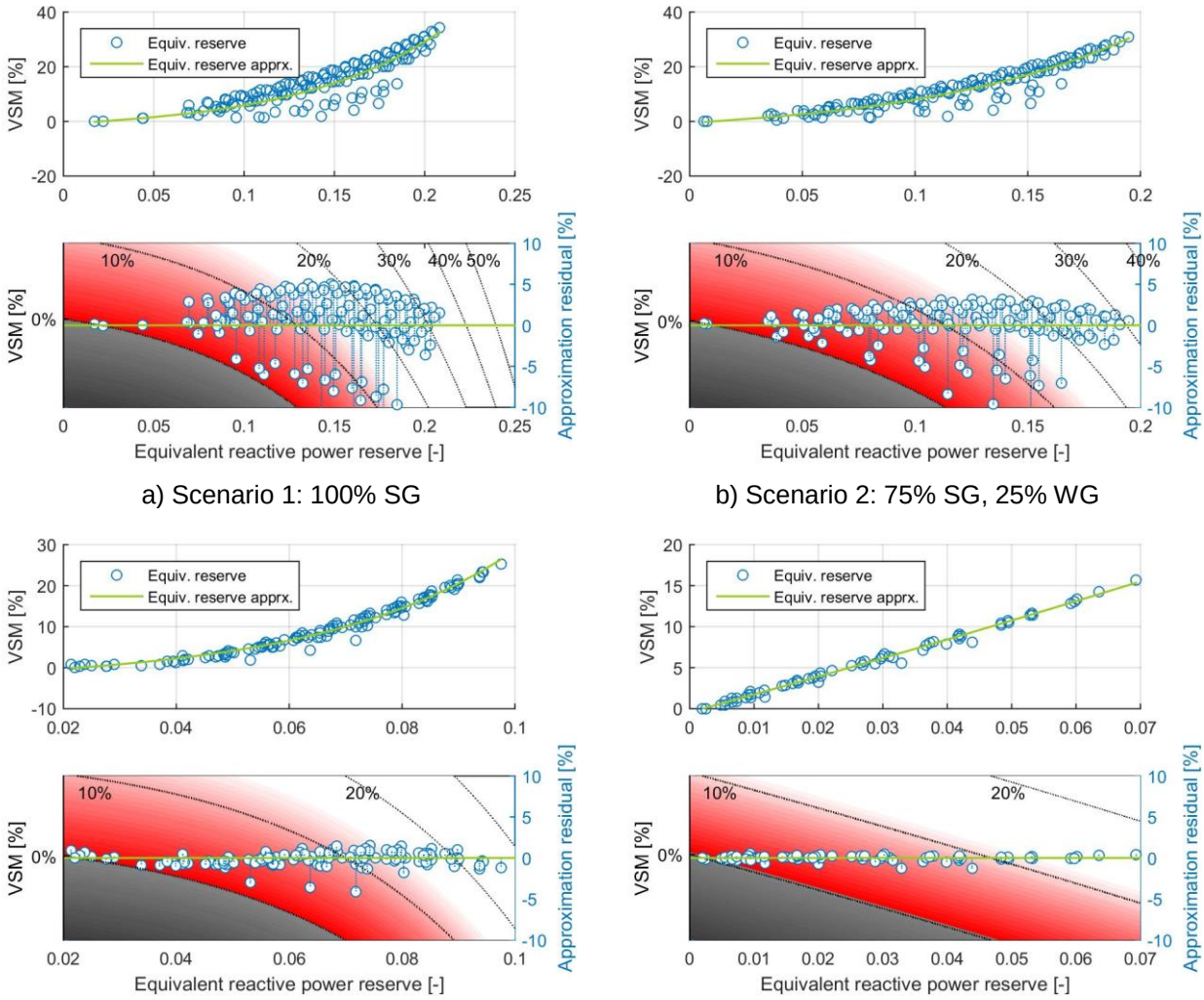

a) Scenario 1: 100% SG

b) Scenario 2: 75% SG, 25% WG

c) Scenario 3: 50% SG, 50% WG

d) Scenario 4: 25% SG, 75% WG

Figure 4-38 VSM estimation by the equivalent reactive power reserve in scenarios with different WG level

4.4.3 Summary

There are various indices and methods evaluating voltage stability [51][52] but it seems that a most comprehensive approach is described in publications [8][53] provided by a group of researchers who have implemented their ideas into commercial available software tools. But even the best analytical tools must be well incorporated into the system planning and operation best practices to be used effectively. For example the blackout in the USA and Canada in 2003 was not prevented despite availability of an adequate voltage stability assessment software since the middle of 1990's. The report [54] analysing its causes and giving recommendations stated that:

As reported in previous chapters, the blackout on August 14, 2003, was preventable. It had several direct causes and contributing factors, including:

- **Failure to maintain adequate reactive power support**
- **Failure to ensure operation within secure limits**
- Inadequate vegetation management
- Inadequate operator training

- **Failure to identify emergency conditions and communicate that status to neighbouring systems**
- **Inadequate regional-scale visibility over the bulk power system**.

Presented methodology not only uses experience of [8][53] but also tries to comply with those findings (marked bolded) through constant observation of reserves of VAR resources and alternative observables related to VARs (in case data from VAR generation is not available or illegible) and immediate indication how far from stability limit the system might fall in case of contingency. Presented approach can be incorporated into SCADA environment following the steps depicted in Figure 4-39.

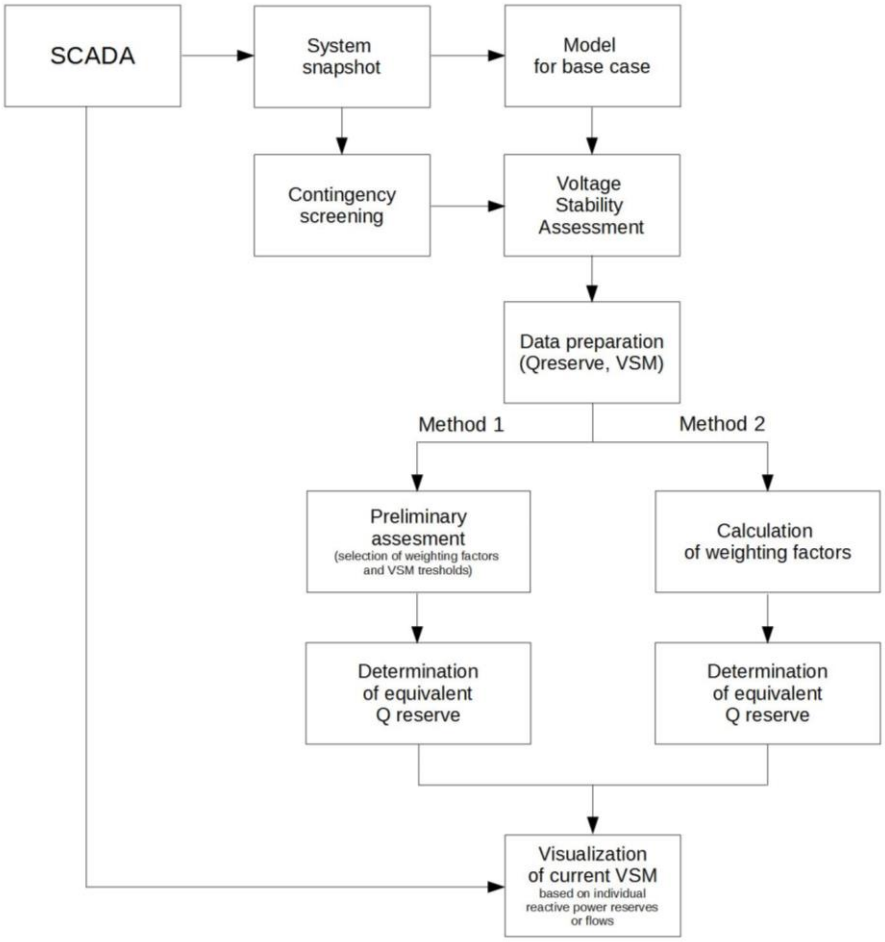

Figure 4-39 Flow chart of voltage stability assessment based on the proposed methodology

4.5 Topic 5: Inter-cell loop flows

In this chapter, observables for identifying and avoiding inter-cell loops flows are investigated. The necessity of new observables depends on the control method and control level. The Use Cases do not specify how the power flow between cells should be controlled. The BRC and BSC set the active power set point of the production and export/import for a cell and the PPVC optimize the power flow inside a cell. No Use Case controls the power flow and voltage setpoints on an overall cell level since the PPVC should not contain a CTRL-3 level. However, a voltage cooperation between the cells are stated in the PPVC Use case: “The CSO will manage the voltage set-points of the cell nodes inside and, as a result, also in the border nodes with neighbouring cells. The

neighbouring cells will be required to maintain those voltages in the interconnection points, previously agreed with the CSO for the establishment of operational security limits in terms of voltage ranges and reactive (active) power exchanges across the borders tie-lines."

4.5.1 Optimal power flow and load flow simulations

Optimal Power Flow (OPF) has been simulated on three different cases on the DTU-Pan European circuit to study how the OPF works on this system. The simulation has been performed in PowerFactory. The losses are minimized by the OPF, as defined by the PPVC. In order to be able to run an OPF, some changes have to be made in the model:

- Generators replace PWM modules since PWM converters do not support OPF function in PowerFactory. Reactive power limits are set such as the converters and the sum of active power of the converters equals the production of the offshore wind farm.
- The grid is divided into 4 islands (one for each cell) for cases with individual OPF.

Other assumptions:

- Restrictions of the bus voltages in the OPF are between 0.92 pu and 1.03 pu. A new OPF should be triggered if any bus voltage is below 0.9 pu or above 1.05 pu.
- The Case 5 in the SRPS DTU Pan-European grid based on the CIGRÉ MV EU grid is used for all simulations in this chapter.

The results from three different cases are presented below.

1. **An overall OPF without any restrictions of power flow between the cells**

In this case, the losses are minimized for the whole grid, and this case therefore gives the lowest total losses for the grid. Since there are no restrictions on power flow between the cells, the OPF converges with no problems. The results from the OPF and the load flow are shown in Figure 4-40. The tap settings of the transformers, number of connected stages in parallel of the SVC's and voltage set points of the generators from the OPF are used as inputs to the load flow. Figure 4-40c shows the deviation between the OPF and the load flow. In this case, the load flow equals the results from the OPF.

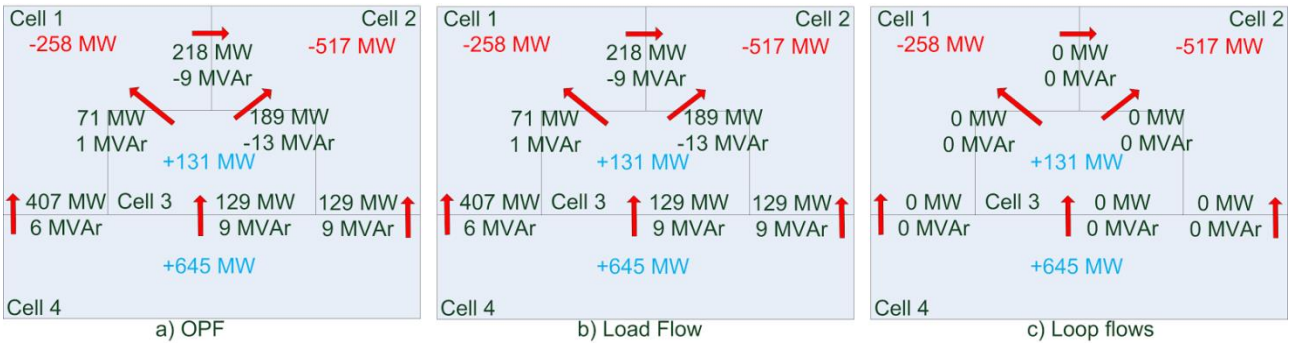

Figure 4-40 Active and reactive power flow between cells when using an overall OPF a) Results from the OPF, b) Results from the load flow, c) Loop flows (deviation between OPF and load flow)

2. An overall OPF with restrictions of active power flow between cells

In the second case, restrictions of active power flow between the cells are added. The cells are still connected and the minimum losses are found for the entire grid. Solutions on the OPF problem are found if restrictions of power the active power flow is near the results found in Case 1 and for the active power flow found in Figure 4-40a. However, no solutions are found with the restrictions shown in Figure 4-41a and Figure 4-41b. These restrictions of the power flow are defined from what seems natural when looking at production surplus/deficit in each cell.

Between Cell 1, Cell 2 and Cell 3 there is a triangle of power lines on the same voltage level and no transformers are part of this triangle. As seen from Figure 4-41a, Cell 3 should deliver 131 MW to Cell 1; however, there should be no active power flow between Cell 3 and Cell 2 and between Cell 2 and Cell 1. The power flow will naturally be divided, some power will go directly from Cell 3 to Cell 1 and the rest will go through Cell 2 causing a power loop. The only way to affect this is to control the reactive power production in Cell 2; however, this will have very limited impact on the active power flow. This explains why solutions of the OPF only are found if the power flow is near the results found in Case 1.

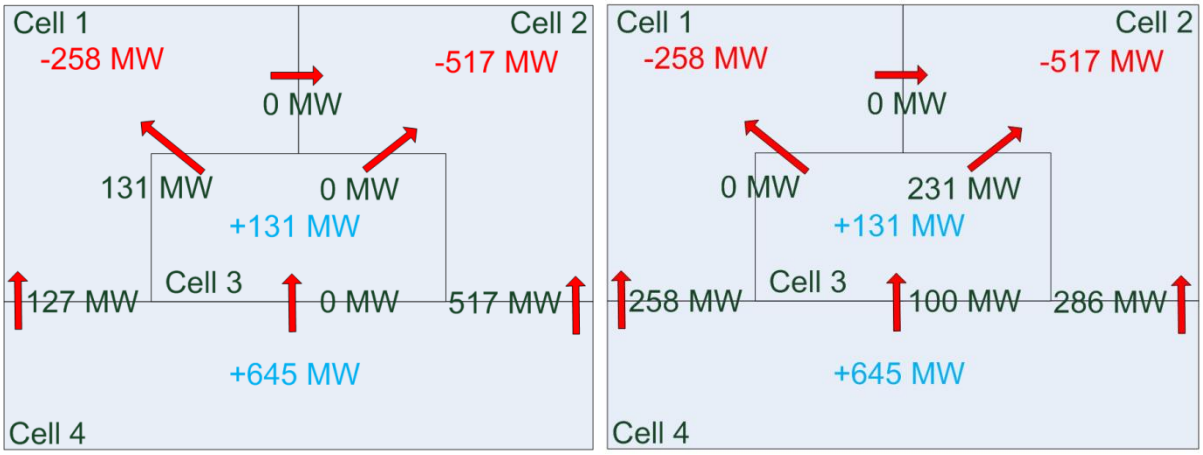

Figure 4-41 Active power flow set points defined by BRS/BRC a) Case 2A, b) Case 2B

3. One Individual OPF per cell with restrictions of power flows (P and Q) between cells

In Case 3, the grid is split into the four cells. At each connection point between the grids, a synchronous generator with restrictions on active and reactive power represents the neighbour grid. The cells are decoupled in this way to ensure that the OPF finds a minimum loss for each cell, independent of the results from the OPF in the other cells.

Solutions of the OPF are found for a large range of restrictions of active and reactive power flows. However, the voltage of the connection point between the cells in the different OPF does not match. The result from a power flow simulation on the whole grid with the settings achieved from the OPF will in most cases differ from the power flow results from the OPF, and power loops will occur.

In Cell 2, the line between Bus 2.4 and Bus 2.5 could not deliver enough power to the load on Bus 2.5. Therefore, Cell 2 is depending on import from Cell 1.

Figure 4-42 and Figure 4-43 show two different cases (Case 3A and 3B) with different restrictions in active and reactive power flows between the cells. Figure 4-42a shows the solution of the OPF

for Case 3A. The tap settings of the transformers, number of connected stages in parallel of the SVC's and voltage setpoints of the generators from the OPF are used as inputs to the load flow shown in Figure 4-42b. The loop flows, the deviation between OPF and load flow, are shown in Figure 4-43c. There are two main loop flows; one between Cell 1, Cell 3 and Cell 2 of approximately 12 MW, and one between Cell 2, Cell 3 and Cell 4 of approximately 60 MW. In addition, the reactive power flow also differs from the OPF.

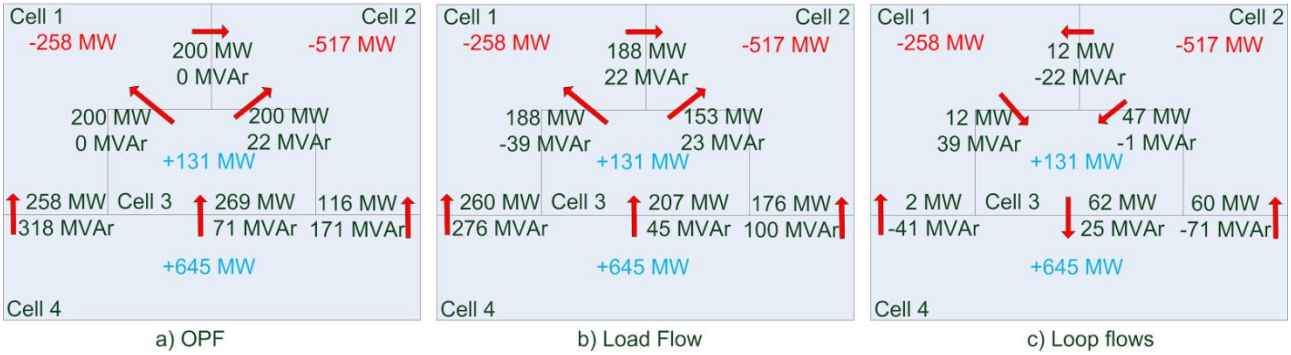

Figure 4-42 Active and reactive power flow between cells when using individual OPFs (Case 3A) a) Results from the OPF, b) Results from the load flow, c) Loop flows (deviation between OPF and load flow)

Figure 4-43 shows the results from Case 3B. The same loops flows are identified; one between Cell 1, Cell 3 and Cell 2 of approximately 10 MW and one between Cell 2, Cell 3 and Cell 4 of approximately 65 MW. In addition, the reactive power flow also differs from the OPF.

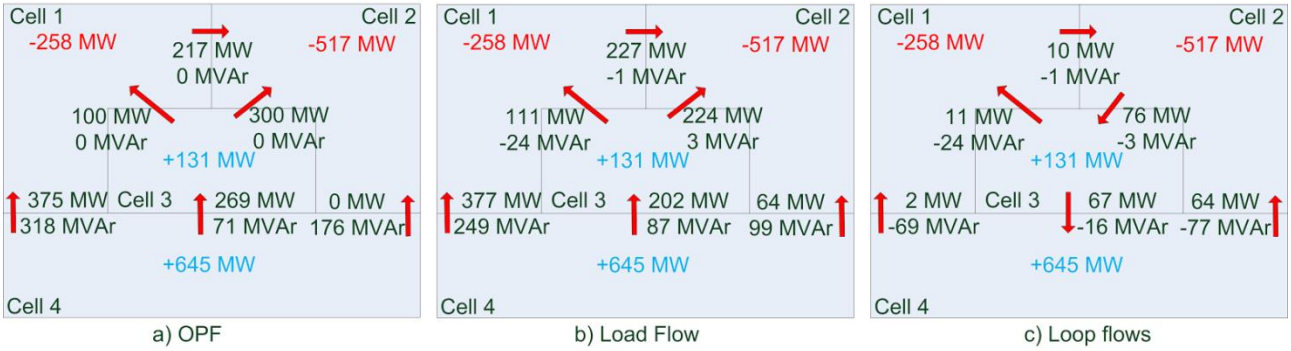

Figure 4-43 Active and reactive power flow between cells when using individual OPFs (Case 3B) a) Results from the OPF, b) Results from the load flow, c) Loop flows (deviation between OPF and load flow)

Table 4-11 and Table 4-12 show respectively the power flow between the cells and the losses; in each cell and the total losses. The losses is lowest for Case 1; the overall OPF. If individual OPFs are used, as in Case 3A and 3B, the losses increase by 0.4 to 0.5%.

Table 4-11 Power flow between cell in Case 1 and Case 3

		Overall OPF Case 1		Individual OPF's: Case 3A		Individual OPF's: Case 3B	
		OPF	LF	OPF	LF	OPF	LF
Cell 1-2	MW	218	218	200	188	217	227
	MVAr	-9	-9	0	22	0	-1
Cell 3-1	MW	72	72	200	188	100	111

	MVAr	1	1	0	-39	0	-24
Cell 3-2	MW	189	189	200	153	300	224
	MVAr	-13	-13	22	23	0	3
Cell 4-1	MW	407	407	258	260	375	377
	MVAr	6	6	318	276	318	249
Cell 4-2	MW	110	110	116	176	0	64
	MVAr	80	80	171	100	176	99
Cell 4-3	MW	129	129	269	207	269	202
	MVAr	9	9	71	45	71	87

Table 4-12 Losses in Case 1 and 3

		Overall OPF Case 1		Individual OPF's: Case 3A		Individual OPF's: Case 3B	
		OPF	LF	OPF	LF	OPF	LF
Loss Cell 1	MW	12.18	12.18	15.80	15.25	18.72	20.18
Loss Cell 2	MW	17.47	17.47	21.02	23.22	22.02	17.73
Loss Cell 3	MW	8.11	8.11	16.66	13.90	9.89	7.74
Loss Cell 4	MW	4.86	4.86	2.16	3.18	4.11	6.55
Loss Total	MW	42.62	42.62	55.64	55.55	54.74	52.20
Total loss	%	1.61	1.61	2.10	2.09	2.06	1.97

4.5.2 Observables and solutions for avoiding inter-cell loop flows

Three different solutions for avoiding inter-cell loop flows are suggested:

1) Overall OPF

In this case, an overall control runs a simplified OPF for the whole grid or large parts of the grid as illustrated in Figure 4-44. The reactive power flow between the cells and the voltage of the connection points between cells are set by the overall OPF. The overall OPF could also reschedule power flow through other cells. In special cases, the overall OPF could also reschedule production (P and Q) in order to avoid power loops and overloaded lines. The individual OPFs optimize the power flow inside each cell with the restrictions given by the overall OPF.

By using an overall OPF, the total losses will probably be lower than using individual cell OPFs.

An overall OPF implies CTRL 3; inter cell control layer. However, in ELECTRA it is decided that the PPVC should not contain a CTRL 3.

A topology reduction method for identifying loops and loop flows is been developed in T8.2 and T8.3. This topology reduction could be used for simplifying an overall OPF.

Observables in this case will probably be:

- Active and reactive power in tie-lines
- Voltage magnitude and angle in connection points
- Deviation between active and reactive power set points and actual values in tie-lines
- Deviation between voltage magnitude and angle set points and actual values in connection points

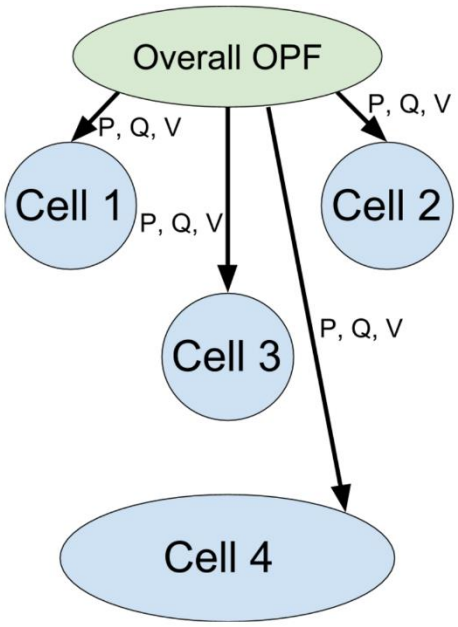

Figure 4-44 Sequence diagram for an overall OPF

2) Consensus-based Distributed Optimal Power Flow

An individual OPF is performed in each cell. The result is communicated to the neighbour cells and the OPF's use data from the neighbour cells in the next iteration step as illustrated in Figure 4-45. The goal is to convert the OPF towards a solution where the state of the interface to the neighbour cells is the same in the OPF's of both cells. The states of interface are:

- Active power in tie line(s) between the cells,
- Reactive power in tie line(s) between the cells,
- Voltage magnitude and angle at connection point(s) between the cells

The bus voltages (real and complex) of the related busses in the neighbour cells are communicated to the neighbour cell between each iteration of the OPF. The voltage difference to the (filtered) solution from the previous step in the neighbour cell is included in the OPF function that should be minimized. The difference is multiplied with a parameter deciding how important this part of the minimization function is. The parameter could be increased when the iteration numbers increases to reduce the voltage mismatch between the OPF's in the neighbour cells. A similar solution is presented in [51] (Liu). In this paper, the local minimization function for bus i is written as

$$\min_{\mathrm{P_i^G},Q_i^G,e_i,f_i,e_{j(i)},f_{j(i)}} F\left(P_i^G\right) + \rho_i \sum_{i\sim j}\left(\left|\left|e_{j(i)}-\hat{e}_{j(i)}\right|\right|^2+\left|\left|f_{j(i)}-\hat{f}_{j(i)}\right|\right|^2+\left|\left|e_i-\hat{e}_{i(j)}\right|\right|^2 + \left|\left|f_i-\hat{f}_{i(j)}\right|\right|^2\right) \quad \text{Eq. 4-25}$$

where $\mathrm{P_i^G}$ and Q_i^G are the active and reactive generation power at bus i, $i>0$ is a large number selected as a penalty factor in order to make sure that the estimation errors are minimized with a

higher priority, $V_i = e_i + jf_i$ is the bus voltage, $V_{j(i)} = e_{j(i)} + jf_{j(i)}$ is the bus voltages of the neighbour bus j and $e_{j(i)}$ and $f_{j(i)}$ are a pair of consensus variables defined as

$$\hat{\boldsymbol{e}}_{\boldsymbol{j(i)}}(\boldsymbol{k}+\boldsymbol{1}) = \hat{\boldsymbol{e}}_{\boldsymbol{j(i)}}(\boldsymbol{k}) + \boldsymbol{\gamma}\left(\boldsymbol{e}_{\boldsymbol{j}}(\boldsymbol{k}) - \hat{\boldsymbol{e}}_{\boldsymbol{j(i)}}(\boldsymbol{k})\right) \quad \text{Eq. 4-26}$$

$$\hat{\boldsymbol{f}}_{\boldsymbol{j(i)}}(\boldsymbol{k}+\boldsymbol{1}) = \hat{\boldsymbol{f}}_{\boldsymbol{j(i)}}(\boldsymbol{k}) + \boldsymbol{\gamma}\left(\boldsymbol{f}_{\boldsymbol{j}}(\boldsymbol{k}) - \hat{\boldsymbol{f}}_{\boldsymbol{j(i)}}(\boldsymbol{k})\right) \quad \text{Eq. 4-27}$$

where $0 < \gamma < 1$ is the consensus gain and k is the iteration step. The bus voltage used in optimization of other cells is send through this consensus filter. If $\gamma = 1$, the filter is bypassed, and the previous calculated value is used directly. The iteration stops when the difference $||e_j(k) - \hat{e}_{j(i)}(k)|| < \epsilon$ is small enough.

This method for distributed OPF can be transferred to the Web-of-Cells methodology by using one local OPF per cell instead of one per bus. The minimization function will therefore try to minimize the total production in the cell (or minimize the losses) and the voltage differences between the voltage in the connection point(s) to neighbour cell(s) and the voltage obtained by the OPF(s) of neighbour cell(s).

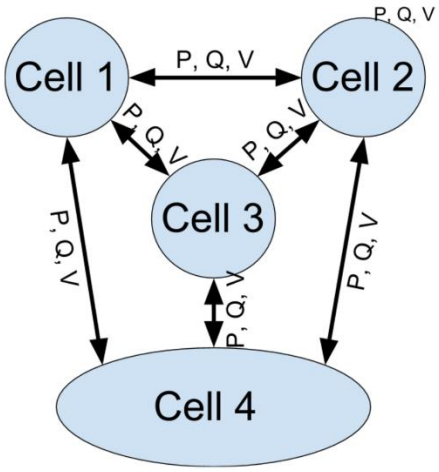

Figure 4-45 Sequence diagram for consensus-based Distributed Optimal Power Flow

The minimizing function could not be modified in PowerFactory. The OPF must therefore be performed in another simulation tool, for instance MATPOWER (Zimmerman) [52]. However, the reactive power production curve of the synchronous generators and PWM's must be simplified.

The voltage different parts of the minimization function could also be used to reschedule active and reactive power flow through other cells. If the minimization functions do not converge after n iterations, this can be caused by restrictions in power flow between the cells. The voltage difference at the connection point between neighbour cells will show how the power flow can be rescheduled to obtain convergence. This is illustrated in Figure 4-46. In this case, the active power is scheduled to 100 MW from Cell 1 to Cell 2, the other active power flows are scheduled to 0 MW, and all reactive power flows between cells are scheduled to 0 MVAr.

The OPF will minimize the losses in each cell; however, it is not able to limit the voltage difference in the connection point of two connected cells. The OPF in Cell 1 will calculate a too low voltage e compared to the corresponding voltage calculated by the OPF in Cell 2. At the same time, the voltage difference will be opposite between Cell 1 and Cell 3 and between Cell 3 and Cell 2. All three cells will observe that a reschedule of power flow through Cell 2 will be beneficial and will reduce the voltage difference at the connection points obtained by the OPF of two connected cells.

The neighbour cells must agree on a rescheduling of the power flow based on this information before each cells are running a new OPF.

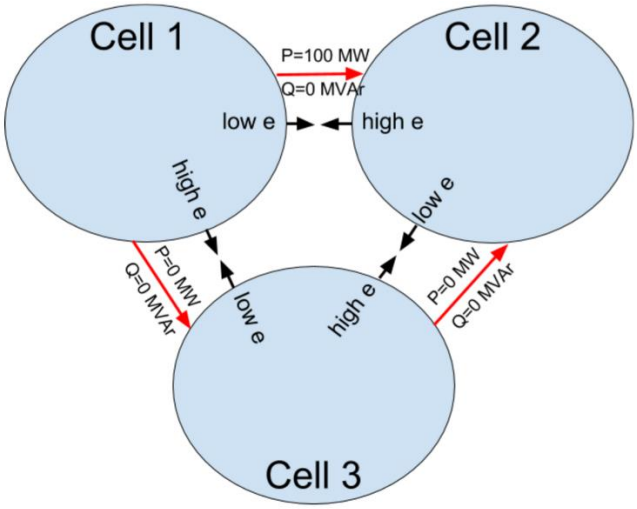

Figure 4-46 Illustration of the necessity to reschedule the power flow

Observables in this case will probably be:

- Active and reactive power in tie-lines between cells
- Voltage magnitude and angle in connection points between cells, or real and imaginary voltages $V_{j(i)} = e_{j(i)} + j_{f(i)}$
- Consensus variables $e_{j(i)}$ and $f_{j(i)}$ (option)
- Deviation between active and reactive power set points and actual values in tie-lines
- Deviation between voltage and voltage angle set points and actual values in connection points

PMU's should be used as measurement devices since both voltage magnitude and angle measurements are included in the minimization function. The sampling rate does not need to be higher than 50 Hz since the measurement is only used when the PPVC is triggered.

3) Token Ring distributed control for OPF

PPVC is performed in a Token Ring. The first cell is performing an OPF, sending the setpoints for the voltage and optionally the reactive power flow in the tie line at the connections further to the next cell, as illustrated in Figure 4-47. This cell performs an OPF with the input from the previous cells. This sequence is repeated until it converges.

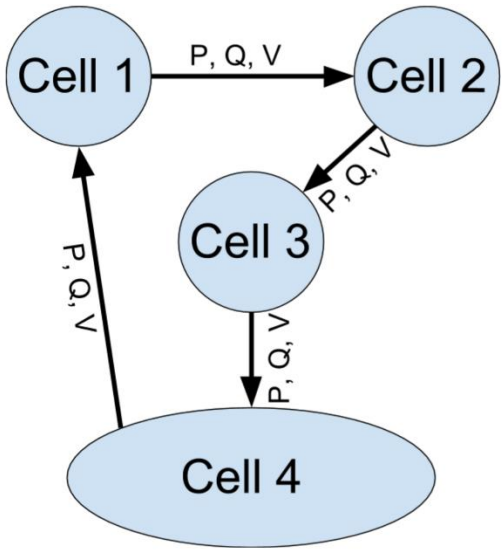

Figure 4-47 Sequence diagram for Token Ring distributed control for OPF

The Token Ring distributed control will probably be slow because the OPF needs to be run in series for all cells, many times.

Observables in this case will probably be:

- Active and reactive power in tie-lines
- Voltage magnitude and angle in connection points between cells
- Deviation between active and reactive power set points and actual values in tie-lines
- Deviation between voltage and voltage angle set points and actual values in connection points

PMU's should be used as measurement devices since both voltage magnitude and angle measurements are included in the minimization function. The sampling rate does not need to be higher than 50 Hz since the measurement is only used when the PPVC is triggered.

4.6 Topic 6: HVDC operation (trip/runback)

The proposed methodology for identification of observables important from the slant of HVDC operation was described in Section 2.7. Its main assumption was to identify key differences in the behaviour of the HVDC schemes and their interaction with the AC power system between a traditionally controlled power system and the one operating in the WoC environment. Converter trip was selected as a typical disturbance in operation of the HVDC system in order to trigger a set of different phenomena, affecting virtually all of the control systems governing the operation of the power system. Since HVDC converters are able to control both active and reactive power flow, converter trip and resulting interruption of power flow was meant to be an ultimate benchmark for the novel control systems under development in this project.

However, due to a delay in delivery of developed, programmed and verified use cases ready to be incorporated into the simulation environment elaborated within this task, the proposed methodology had to be changed. Because of lack of ability to perform simulations relevant observables are proposed based on the results of the analysis carried out in the other topics of this task as well as referring to state-of-the-art literature.

An interruption of active power flow transferred by the HVDC system will trigger the use cases responsible for balance and frequency control. The subsequent phenomena will be related mainly to transient stability, which has been investigated in Section 4.1. The proposed observable based on voltage angle can be used to assess the severity of disturbance caused by HVDC converter trip. The phase angle differential can also be used for control of embedded HVDC systems. This approach is used in the recently commissioned VSC scheme between France and Spain in order to provide active power setpoints in such a way that the scheme emulates an AC line [63]. AC line emulation based on phase angle measurement can also be used in emergency schemes. For example when a rapid phase angle change between the terminals is detected, an automatic runback order can be issued to the power control loop of the HVDC controller in order to limit the transfer and prevent from causing subsequent disturbances [64].

Regarding voltage stability, as discussed in Section 4.4, the VSC converters have reactive power control capability and if operated in active voltage control mode can be regarded as reactive power reserves of the power system. As shown, these reserves are suitable to be used as observables for voltage stability with particular application in PPVC.

From the viewpoint of the stability and reliability of operation of HVDC systems, observables related to frequency have particular importance. As pointed out in Section 4.3, lower inertia caused by predominating generation from renewables will manifest itself in higher ROCOF and frequency nadir. As ROCOF can be measured it could be indirectly used to assess system strength, which in turn is a factor determining basic operational properties and hardcoded parameters of controllers of the HVDC schemes, both LCC and VSC. In the highly fluctuating power system in terms of energy balance and generation portfolio, particularly if accompanied by low SCR level, an adaptation system could be devised, in which ROCOF measurement would be used to adjust parameters such as PLL gains or recovery delays used in the re-energization process [49]. However, there are situations in which this observable could not be used universally – for example in locations where short circuit power is limited primarily by grid topology, as it is in long radial connections.

Small-signal stability with particular focus on low frequency oscillations as another area where HVDC systems can improve stability provided that proper signals are measured and additional control schemes are used. Auxiliary systems for oscillation damping are available and come in standard because in principle they do not require any additional devices or measurements on top of what is necessary for normal operation. However, along with the development of WAMS and WADC systems the utilization of HVDC for damping purposes will be extended and improved.

Point-to-point HVDC links are also used for mitigation of loop flows in the power system. For instance, it has been a standard procedure agreed between TSOs from Germany, Denmark, Sweden and Poland to use the existing links for sending back a part of excessive power generated by WG installed in Germany, but flowing through the Polish, Czech and Austrian grids back to Germany [65][65]. The observables used in this case were power flows in the tie lines. Also embedded links could be used for this purpose.

5 Conclusions and lessons learned

Task 5.4 focused on deriving power system observables for high voltage systems. An overview of the relevant system-wide topics to be analysed has been presented, highlighting the link with the need for increasing observability. The main characteristics of the reference grid adopted for the investigations have been thoroughly described and the model has been made available in both tools PowerFactory and SimPowerSystem for research purposes.

The different observables have been derived by analysing traditional instability phenomena typical of large power systems and the findings are here summarized. The conducted studies were focused on novel observability concepts at the system-wide scale: observables necessary for the novel WoC-based control methods have been developed, to enable proper operation both within cells and at inter-cell level. The main results obtained can be summarized as follows.

An approach to assess transient stability on a system-wide level and visualize the results appropriately was introduced. Transient stability is assessed by means of observed voltage angles rather than rotor angles and, therefore, the method can also be applied under presence of high share of converter based generation. The results are presented in a bar plot with dedicated colouring in order to facilitate the visual examination. Future work will concern determining the most critical buses to be analysed and define preventive actions to resolve potential stability issues.

The proposed method for small signal cell stability assessment, with focus on inter-cell oscillations, is based on real-time mode damping estimation of voltage angle differences between cells, using Prony's Method. Derived observables, as oscillation mode amplitude, frequency, damping and energy could be used for providing power system control room operators with adequate indicators of the stress of their network and prevent power system swing with proper actions. The results are presented for three examples with different low-frequency mode behaviour. However, additional work has to be done regarding “dominant inter-cell oscillation path” determination, a concept based on the notion of interaction paths. These dominant inter-cell oscillation paths are deterministic and algorithms for their identification using both models and measurements are available. Signals from the dominant path are the most observable and have the highest content of inter-cell modes. This suggests that by using well-selected dominant path signals for wide-area control, adequate damping performance can be achieved.

A reduced amount of mechanical inertia causes fast and wide balancing, and therefore frequency, variations. This calls for the need of measuring not only the frequency, but also its time derivative i.e. the ROCOF, which is a new observable. Prompt control actions (synthetic inertia) in each cell can be introduced based on the local ROCOF measurement. Measurement performance requirements in terms of acquisition and elaboration latency and of output precision have to be considered, in order to have correct frequency and ROCOF estimates for effective (and possibly fast) control purposes as well as avoid inadvertent protection system interventions. Both at cell and inter-cell level, the amount of available inertia also has to be monitored, as a further new observable, and cells have to procure sufficient reserves - from resources endowed with physical inertia and/or synthetic inertia - in order to support short-term frequency stability.

The proposed method for voltage stability margin (VSM) assessment is based on reactive power reserves monitoring. For the best VSM estimation all available VAR resources, i.e. reactive power resources, are monitored and equivalent reactive power reserve is calculated, assigning each

resource a calculated weighting factor. In case distant measurements are not available (cell perspective) VAR measurements of inter-cell lines substitute them providing necessary information for VSM calculation.

An inter-cell loop flow is a physical phenomenon that occurs when there is a difference between commercial schedules and physical flows of power between the producers and the customers. OPF simulations on the Pan-European circuit in PowerFactory show that inter-cell loop flows could be avoided by using an overall OPF (on the whole Woc). In this case, the minimum total losses are obtained. However, the PPVC in ELECTRA should not contain a CTRL-3 (inter-cell) level, and the OPF must be performed at a cell level, causing higher losses and inter-cell loop flows. By exchanging observables, like active and reactive power in tie-lines between neighbour cells and voltage magnitude and angle at the connection point, between each iteration of the OPF, the neighbour cells could agree on the voltage at the connection points and power flow in the lines, avoiding inter-cell loop flows. Two methods are suggested: “consensus-based distributed OPF” and “Token Ring distributed control for OPF”.

6 References

[1] C. Caerts, et al. “Specification of Smart Grids high level functional architecture for frequency and voltage control”. ELECTRA Deliverable D3.1: WP3 Scenarios and case studies for future power system operation. 2015.

[2] A.Z. Morch, et al. ”Adaptive Assessment of Future Scenarios and Mapping of Observability Needs”. ELECTRA Deliverable D5.1: WP 5: Increased Observability. 2015.

[3] K. Visscher, M. Marinelli, A. Morch, and S. H. Jakobsen, “Identification of observables for future grids – the framework developed in the ELECTRA project”, PowerTech, 2015 IEEE, pp.1-6, Eindhoven, 29 Jun – 2 Jul. 2015.

[4] A. Morch, S. H. Jakobsen, K. Visscher, and M. Marinelli, “Future control architecture and emerging observability needs”, Power Engineering, Energy and Electrical Drives (POWERENG), 2015 International Conference on, pp. 1-5, Riga, 11-13 May 2015.

[5] M. Marinelli, M. Pertl, M. Rezkalla, M. Kosmecki, S. Canevese, A. Obushevs, A. Morch, “The Pan-European Reference Grid Developed in the ELECTRA Project for Deriving Innovative Observability Concepts in the Web-of-Cells Framework”, *Universities Power Engineering Conference (UPEC),* 2016 Proceedings of the 51st International, pp. 1-6, Coimbra, 6-9 Sep. 2016.

[6] CIGRÉ Working Group C4.601 on Power System Security Assessment, “Review of on-line dynamic security assessment tools and techniques”, CIGRE Technical Brochure No. 325, June 2007.

[7] P. Kundur, J. Paserba, V. Ajjarapu, G. Andersson, A. Bose, C. Canizares, N. Hatziargyriou, D. Hill, A. Stankovic, C. Taylor, T. Van Cutsem, and V. Vittal, "Definition and classification of power system stability IEEE/CIGRE joint task force on stability terms and definitions”, *Power Systems, IEEE Transactions on*, vol.19, no.3, pp.1387-1401, Aug. 2004.

[8] P. Kundur, “Power System Stability and Control”, McGraw-Hill, 1994.

[9] M. Pavella, D. Ernst, and D. Ruiz-Vega, “Transient Stability of Power Systems A Unified Approach to Assessment and Control”, Kluwer Acad. Publ., pp. 1–254, 2000.

[10] C. Dai, “Direct methods for power system transient stability analysis using BCU method”, Austin, 2013.

[11] V. Knazkins, “Stability of Power Systems with Large Amounts of Distributed Generation”, Stockholm, 2004.

[12] J. C. Boemer, M. Gibescu, and W. L. Kling, “Dynamic models for transient stability analysis of transmission and distribution systems with distributed generation: an overview”, in *PowerTech, 2009 IEEE Bucharest*, pp. 1–8, 2009.

[13] Y. Omagari and T. Funaki, “Numerical study of transient stability criteria for an inverter-based distributed generator”, in *Power Electronics for Distributed Generation Systems (PEDG), 2012 3rd IEEE International Symposium on*, pp. 865–871, 2012.

[14] J. Alipoor, Y. Miura, and T. Ise, “Power System Stabilization Using Virtual Synchronous Generator With Alternating Moment of Inertia”, *IEEE J. Emerg. Sel. Top. Power Electron.*, vol. 3, no. 2, pp. 451–458, Jun. 2015.

[15] Q.-C. Zhong, P.-L. Nguyen, Z. Ma, and W. Sheng, “Self-Synchronized Synchronverters: Inverters Without a Dedicated Synchronization Unit”, *IEEE Trans. Power Electron.*, vol. 29, no. 2, pp. 617–630, Feb. 2014.

[16] G. Delille, B. François, and G. Malarange, “Dynamic frequency control support: A virtual inertia provided by distributed energy storage to isolated power systems”, in *Innovative Smart Grid Technologies Conference Europe (ISGT Europe), 2010 IEEE PES*, pp. 1–8, 2010.
[17] A.M. Lyapunov, “Stability of Motion”, English translation, Academic Press, Inc., 1967.
[18] L. L. Grigsby, “Power System Stability and Control. The Electric Power Engineering Handbook”, CRC Press/IEEE Press, 2001.
[19] H. Breulmann, E. Grebe, M. Lösing, W. Winter, R. Witzmann, P. Dupuis, M.P. Houry, T. Margotin, J. Zerenyi, J. Dudzik, J. Machowski, L. Martín, J. M. Rodríguez, E. Urretavizcaya, Analysis and Damping of Inter-Area Oscillations in the UCTE/CENTREL Power System, CIGRÉ Session 2000, Paper 38-113.
[20] M. Klein, G. J. Rogers, and P. Kundur, “A fundamental study of inter-area oscillations in power systems”, IEEE Trans. Power Syst., vol. 6, no. 3, pp. 914–921, 1991.
[21] V. Knap, R. Sinha, M. Swierczynski, D.-I. Stroe, and S. Chaudhary, "Grid inertial response with Lithium-ion battery energy storage systems”, in *Industrial Electronics (ISIE), 2014 IEEE 23rd International Symposium on*, pp.1817-1822, 1-4 June 2014.
[22] G. Lalor, A. Mullane, and M. O’Malley, “Frequency control and wind turbine technologies”, IEEE Transactions on Power Systems, vol. 20, no. 4, Nov. 2005.
[23] A. Ulbig, T.S. Borsche, G. Andersson, “Impact of Low Rotational Inertia on Power System Stability and Operation”, in IFAC World Congress 2014, Capetown, South Africa, 2014. 22 December 2014 revised version online: http://arxiv.org/pdf/1312.6435v4.pdf (accessed 30 September 2015).
[24] M. Marinelli, S. Massucco, A. Mansoldo, and M. Norton, “Analysis of inertial response and primary frequency power control provision by doubly fed induction generator wind turbines in a small power system”, 17th Power System Computation Conference (PSCC), pp. 1-7, Stockholm, 22-26 Aug. 2011.
[25] P. Tielens and D. Van Hertem, “Grid Inertia and Frequency Control in Power Systems with High Penetration of Renewables”, Young Researchers Symposium in Electrical Power Engineering, Delft, vol. 6, April 2012, KU Leuven, Leuven, Belgium, 2012. Online: https://lirias.kuleuven.be/bitstream/123456789/345286/1/Grid_Inertia_and_Frequency_Control_in_Power_Systems_with_High_Penetration_of_Renewables.pdf (accessed 30 September 2015).
[26] ENTSO-E, "Supporting document for the network code on operational security”, Technical Report, 2nd Edition Final, 24 September 2013. Online: https://www.entsoe.eu/fileadmin/user_upload/library/resources/OS_NC/130924-AS-NC_OS_Supporting_Document_2nd_Edition_final.pdf (accessed 12 October 2015).
[27] A. Gomex Exposito, et al. "Algorithms for State Estimation of ETN", Deliverable D2.1 – Part 1, *PEGASE (Pan European Grid Advanced Simulation and State Estimation) European FP7 Project (Grant Agreement Number 211407)*, 14 April 2011. Online: http://www.fp7-pegase.com/pdf/D2.1_part1_algorythm.pdf (accessed 30 September 2015).
[28] Website of the PEGASE (Pan European Grid Advanced Simulation and State Estimation) European FP7 Project, http://www.fp7-pegase.com/domain-simulation.php (accessed 6 October 2015).
[29] A. Gómez-Expósito, A. de la Villa Jaén, C. Gómez-Quiles, P. Rousseaux, and T. Van Cutsem, "A Taxonomy of Multi-Area State Estimation Methods", *Electric Power Systems Research*, Vol. 81, Issue 4, pages 1060-1069, April 2011.
[30] A. Gómez-Expósito, Ali Abur, P. Rousseaux, A. de la Villa Jaén, and C. Gómez-Quiles, "On the Use of PMUs in Power System State Estimation", in *17th Power Systems Computation*

Conference (PSCC), Stockholm, Sweden, August 22-26, 2011. Online: http://www.pscc-central.org/uploads/tx_ethpublications/fp211.pdf (accessed 30 September 2015).

[31] P. Yang, Z. Tan, A. Wiesel, and A. Nehora, "Power System State Estimation Using PMUs With Imperfect Synchronization", *IEEE Transactions on Power Systems*, vol.28, no.4, pp.4162-4172, Nov. 2013.

[32] K. Visscher, et al., "Functional description of the monitoring and observability detailed concepts for the Distributed Local Control Schemes". ELECTRA Deliverable D5.2: WP 5: Increased Observability.

[33] W. Bignell, H. Saffron, T.T. Nguyen, and W. Derek Humpage, "Effects of machine inertia constants on system transient stability", *Electric Power Systems Research*, Volume 51, Issue 3, 1 September 1999, pp. 153-165.

[34] D. Wu, M. Javadi, and J. N. Jiang, "A preliminary study of impact of reduced system inertia in a low-carbon power system", *Journal of Modern Power Systems and Clean Energy (Special Issue on Low-Carbon Electricity)*, vol. 3, issue 1, pp. 82–92, March 2015. Online: http://link.springer.com/article/10.1007%2Fs40565-014-0093-8 (accessed 29 September 2015).

[35] R. Kumar, "Assuring voltage stability in the smart grid", in *Innovative Smart Grid Technologies (ISGT), 2011 IEEE PES*, 2011, pp. 1–4.

[36] J. Machowski, J. W. Białek, J. R. Bumby, "Power System Dynamics Stability and Control", Second Edition, John Wiley & Sons, Ltd. 2008.

[37] THEMA Consulting Group, "Loop flows - Final advice", prepared for the European Commission https://ec.europa.eu/energy/sites/ener/files/documents/201310_loop-flows_study.pdf (accessed 23.10.15).

[38] CIGRÉ Working Group B4.37, "VSC Transmission". CIGRÉ Report 269, 2005.

[39] CIGRÉ Working Group 14.07 / IEEE Working Group 15.05.05, "Guide for Planning DC Links Terminating at AC System Locations Having Low Short-circuit Capacities I", CIGRÉ Report 68, 1992.

[40] AD Hansen, F. Iov, P. Sørensen, N. Cutululis, C. Jauch, F. Blaabjerg. "Dynamic wind turbine models in power system simulation tool DIgSILENT". Danmarks Tekniske Universitet, Risø Nationallaboratoriet for Bæredygtig Energi. (Denmark. Forskningscenter Risoe. Risoe-R; No. 1440(ed.2)(EN)) http://orbit.dtu.dk/files/7703047/ris_r_1400_ed2.pdf, 2007.

[41] M. Marinelli, "Wind Turbine and Electrochemical Based Storage Modeling and Integrated Control Strategies to Improve Renewable Energy Integration in the Grid", Ph.D. thesis, University of Genova, pp.1-130, Mar 2011.

[42] S. Grillo, M. Marinelli, and F. Silvestro, "Wind Turbines Integration with Storage Devices: Modelling and Control Strategies", Wind Turbines, Ibrahim Al-Bahadly (Ed.), ISBN: 978-953-307-221-0, InTech, DOI: 10.5772/15101.

[43] CIGRÉ Report "Benchmark Systems for Network Integration of Renewable and Distributed Energy Resources", CIGRE Task Force C6.04.02, July 2009.

[44] ENTSO-E. "Documentation on Controller Tests in Test Grid Configurations". Tech. Report, 2013.

[45] K. Sun. "Power System Operations & Planning - Load Modeling". 2015.

[46] M. Pertl, M. Rezkalla, M. Marinelli, "A Novel Grid-Wide Transient Stability Assessment and Visualization Method for Increasing Situation Awareness of Control Room Operators", *Innovative Smart Grid Technologies (ISGT Asia), 2016 IEEE PES International Conference and Exhibition on*, pp.1-6, Melbourne, 28 Nov - 01 Dec 2016.

[47] Commission Regulation (EU) 2016/631 of 14 April 2016 establishing a network code on requirements for grid connection of generators.
[48] Commission Regulation (EU) 2016/1447 of 26 August 2016 establishing a network code on requirements for grid connection of high voltage direct current systems and direct current-connected power park modules.
[49] J. Z. Zhou and A. M. Gole, "VSC transmission limitations imposed by AC system strength and AC impedance characteristics", in AC and DC Power Transmission (ACDC 2012), 10th IET International Conference on, 2012, pp. 1–6.
[50] L. Bao, Z. Huang, and W. Xu, "Online voltage stability monitoring using var reserves", IEEE Transactions on Power Systems, vol. 18, no. 4, pp. 1461–1469, Nov. 2003.
[51] J. Machowski, J. Bialek, and J. R. Bumby, "Power system dynamics and stability", John Wiley & Sons, 1997.
[52] C. W. Taylor, "Power system voltage stability", McGraw-Hill, 1994.
[53] Gao, B., et al. "Towards the development of a systematic approach for voltage stability assessment of large-scale power systems". IEEE Transactions on Power Systems 11.3 (1996): 1314-1324.
[54] U.S.-Canada Power System Outage Task Force, "Final Report on the August 14, 2003 Blackout in the United States and Canada: Causes and Recommendations", April 2004.
[55] L. Martini, L. Radaelli, H. Brunner, C. Caerts, A. Morch, S. Hanninen, and C. Tornelli, "ELECTRA IRP Approach to Voltage and Frequency Control for Future Power Systems with High DER Penetration", in 23rd International Conference on Electricity Distribution (CIRED), (Lyon), pp. 1–5, 2015.
[56] J. Liu, M. Benosman, and A. Raghunathan, "Consensus-based distributed optimal power flow algorithm". In Innovative Smart Grid Technologies Conference (ISGT), 2015 IEEE Power Energy Society (Feb 2015), pp. 1–5.
[57] R. D. Zimmerman, C. E. Murillo-Sánchez, and R. J. Thomas, "MATPOWER: Steady-State Operations, Planning and Analysis Tools for Power Systems Research and Education", Power Systems, IEEE Transactions on, vol. 26, no. 1, pp. 12-19, Feb. 2011.
[58] ENTSO-E, "Future System Inertia", Report of the Nordic Analysis Group, Future System Inertia project. Online: https://www.entsoe.eu/Documents/Publications/SOC/Nordic/Nordic_report_Future_System_Inertia.pdf (accessed 02.12.16).
[59] H.P. Asal, B. Madsen, H.W. Weber, E. Grebe, "Development in Power-Frequency Characteristic and Droop of the UCPTE Power System and Proposals for new Recommendations for Primary Control", CIGRE 1998, Group 39. Online: https://www.eeh.ee.ethz.ch/fileadmin/user_upload/eeh/studies/courses/power_system_dynamics_and_control/Documents/UCPTE_Power_Freq_Paper.pdf (accessed 02.12.16).
[60] ENTSO-E, "Network Code on Load-Frequency Control and Reserves", 28 June 2013, to be included in the System Operation Guideline awaiting validation by the European Parliament and Council. Online: https://www.entsoe.eu/fileadmin/user_upload/library/resources/LCFR/130628-NC_LFCR-Issue1.pdf (accessed 02.12.16).
[61] ENTSO-E, "Frequency Stability Evaluation Criteria for the Synchronous Zone of Continental Europe – Requirements and impacting factors", RG-CE System Protection & Dynamics Sub Group, March 2016. Online: https://www.entsoe.eu/Documents/SOC%20documents/RGCE_SPD_frequency_stability_criteria_v10.pdf (accessed 02.12.16).
[62] DNV-GL, "RoCoF Alternative Solutions Technology Assessment", Final Report, Phase 1, Report No.: 16011111, Rev. 004, 23/06/2015. Online: http://www.eirgridgroup.com/site-

files/library/EirGrid/RoCoF-Alternative-Solutions-Technology-Assessment-Phase-1-DNV-GL-Report_.pdf (accessed 02.12.2016).
[63] J. Bola, et al., “Operational experience of new Spain-France HVDC interconnection”, CIGRÉ 2016, Paris, September, 2016.
[64] M. Marz, et al., “Mackinac HVDC Converter Automatic runback utilizing locally measured quantities”, 2014 CIGRÉ Canada Conference, Toronto, September 22-24, 2014.
[65] J.M. Birkebæk, A. Jäderström, R. Paprocki, O. Ziemann, “Using HVDC links to cope with congestions in neighbouring ac networks”, 17th Power Systems Computation Conference, Stockholm, August 22-26, 2011.
[66] S. Canevese, A. Gatti, M. Rossi, “Analisi di perturbazioni sulla rete continentale a partire da misure di frequenza” (Analysis of perturbations on the continental network, starting from frequency measures), RdS technical report n°16001371, 29 February 2016.
[67] K. Visscher, et al., “Numerical Algorithms for determination of identified observables in ELECTRA Use Cases”, Annex to ELECTRA Deliverable D5.2.
[68] S. Canevese, E. Ciapessoni, A. Gatti, M. Rossi, “Monitoring of Frequency Disturbances in the European Continental Power System”, AEIT International annual conference, Capri, 5-7 October 2016.
[69] N. Zhou, J. Pierre, D. Trudnowski, and R. Guttromson, “Robust RLS methods for online estimation of power system electromechanical modes”, IEEE Trans. Power Syst., vol. 22, no. 3, pp. 1240–1249, Aug. 2007.
[70] R. W. Wies, J. W. Pierre, and D. J. Trudnowski, “Use of ARMA block processing for estimating stationary low-frequency electromechanical modes of power systems”, IEEE Trans. Power Syst., vol. 18, no. 1, pp. 167–173, Feb. 2003.
[71] J. Pierre, D. Trudnowski, and M. Donnelly, “Initial results in electromechanical mode identification from ambient data”, IEEE Trans. Power Syst., vol. 12, no. 3, pp. 1245–1251, Aug. 1997.
[72] Z. Tashman, H. Khalilinia, and V. Venkatasubramanian, “Multi-dimensional Fourier ringdown analysis for power systems using synchrophasors”, IEEE Trans. Power Syst., vol. 29, no. 2, pp. 731–741, Mar. 2014.
[73] J. Rueda, C. Juarez, and I. Erlich, “Wavelet-based analysis of power system low-frequency electromechanical oscillations”, IEEE Trans. Power Syst., vol. 26, no. 3, pp. 1733–1743, Aug. 2011.
[74] L. Vanfretti. “Estimation of electromechanical modes in power systems using synchronized phasor measurements and applications for control of inter-area oscillations”, A contribution to CIGRE WG B5-14 “Wide Area Protection and Control Technologies, 2013.
[75] J. de la O Serna, J. Ramirez, A. Z. Mendez, and M. Paternina, “Identification of electromechanical modes based on the digital Taylor-Fourier transform”, IEEE Trans. Power Syst., vol. 31, no. 1, pp. 206–215, Jan. 2016.
[76] IEEE Publications, "Identification of Electromechanical Modes in Power Systems”, IEEE Power & Energy Society, Special publication TP462, June 2012.
[77] Y. Chompoobutrgool and L. Vanfretti, ”On the Persistence of Dominant Inter -Area Oscillation Paths in Large-Scale Power Networks”,' IFAC Symposium on Power Plants and Power Systems, Toulouse, France, September 2-5, 2012.
[78] J.F. Hauer, W.A. Mittelstadt, K.E. Martin, J.W. Burns, and H. Lee, ”Integrated Dynamic Information for the Western Power System: WAMS Analysis in 2005”,' Chapter 15 in Power System Stability and Control: The Electric Power Engineering Handbook, L.L. Grigsby (Ed.), CRC Press: Boca Raton, FL, 2007.

[79] Y. Chompoobutrgool and L. Vanfretti, ”Identification of Power System Dominant Inter -Area Oscillation Paths”,' available for early access, IEEE Transactions on Power Systems, 2013.
[80] L. Vanfretti, S. Bengtsson, and J. O. Gjerde, “Preprocessing synchronized phasor measurement data for spectral analysis of electromechanical oscillations in the Nordic Grid”, in press, European Transactions on Electrical Power, 2013.
[81] David B. Percival and Andrew T. Walden, ”Spectral Analysis for Physical Applications - Multitaper and Conventional Univariate Techniques'', Cambridge University Press 1998.
[82] L. Vanfretti, V. Peric, and J. O. Gjerde, ”Estimation of Electromechanical Oscillations in the Nordic Grid using Ambient Data Analysis”, Invited Paper, Panel Session on Identification of Electromechanical Modes in Power Systems, IEEE PES General Meeting 2013.

7 Disclaimer

The ELECTRA project is co-funded by the European Commission under the 7th Framework Programme 2013.

The sole responsibility for the content of this publication lies with the authors. It does not necessarily reflect the opinion of the European Commission.

The European Commission is not responsible for any use that may be made of the information contained therein.

8 Annex I - Pan European network detailed information

8.1 Static data

In the following table the main technical specification concerning generators, loads, static compensators, AC and DC lines, transformers and PWM-based converters are reported. The load flow set points for zero wind power generation are given in Table 8-1.

Table 8-1 Specifications of the elements of the Pan-European simulation model

Element Name	Type	Specifications	Terminal Node 1	Terminal Node 2	Load flow set point @ Terminal 1 [MW+j MVAr]
Base-SG 1.9 (1) & (2)	Generator	Snom=500 [MVA]; Vnom=20 [kV]; cosphinom=0.85 [1]; Connection YN ; Inertia 2H=10 [s]; Node type = PV 2 parallel machines	Bus 1.9		325
Base-SG 1.10 (1) & (2)	Generator	Snom=500 [MVA]; Vnom=20 [kV]; cosphinom=0.85 [1]; Connection YN ; Inertia 2H=10 [s]; Node type = PV 2 parallel machines	Bus 1.10		325
Base-SG 2.11 (1) & (2)	Generator	Snom=500 [MVA]; Vnom=20 [kV]; cosphinom=0.85 [1]; Connection YN ; Inertia 2H=10 [s]; Node type = Slack 2 parallel machines	Bus 2.11		Slack
Base-SG 3.12 (1) & (2)	Generator	Snom=500 [MVA]; Vnom=20 [kV]; cosphinom=0.85 [1]; Connection YN ; Inertia 2H=10 [s]; Node type = PV 2 parallel machines	Bus 3.12		325
Base-Wind Park 4.8	Generator	Snom=1500 [MVA]; Vnom=400 [kV]; cosphinom=0.8 [1]; Node type = PQ	Bus 4.8		0
Base-Load 1.2	Load	Snom=500+j164 [MVA]; Vnom=220 [kV]; Cosphinom=0.95; Connection D; P-ZIP (V)=[0 1 0]; Q-ZIP (V)=[0 0 1];	Bus 1.2		500+j164
Base-Load 1.3	Load	Snom=500+j164 [MVA]; Vnom=220 [kV]; Cosphinom=0.95; Connection D; P-ZIP (V)=[0 1 0]; Q-ZIP (V)=[0 0 1]	Bus1.3		500+j164
Base-Load 2.3	Load	Snom=400+j131 [MVA]; Vnom=220 [kV]; Cosphinom=0.95; Connection D; P-ZIP (V)=[0 1 0];	Bus 2.3		400+j131

		Q-ZIP (V)=[0 0 1];			
Base-Load 2.4	Load	Snom=400+j131 [MVA]; Vnom=220 [kV]; Cosphinom=0.95; Connection D; P-ZIP (V)=[0 1 0]; Q-ZIP (V)=[0 0 1];	Bus 2.4		400+j131
Base-Load 2.5	Load	Snom=400+j131 [MVA]; Vnom=220 [kV]; Cosphinom=0.95; Connection D; P-ZIP (V)=[0 1 0]; Q-ZIP (V)=[0 0 1];	Bus 2.5		400+j131
Base-Load 3.6	Load	Snom=400+j1131 [MVA]; Vnom=220 [kV]; Cosphinom=0.95; Connection D; P-ZIP (V)=[0 1 0]; Q-ZIP (V)=[0 1 0];	Bus 3.6		400+j131
Base-Shunt 2.5	Capacitor bank	Shunt_max=240 [MVAr]; num of Caps=12 [1]; Q_Cap=20 [MVAr]; 2 parallel shunts	Bus 2.5		j0 (cap)
Base-Shunt 3.6	Capacitor bank	Shunt_max=240 [MVAr]; num of Caps=12 [1]; Q_Cap=20 [MVAr];	Bus 3.6		j0 (cap)
Base-Line 1.1-1.2	Overhead Line	Impedance=0.0659+j*0.398 [Ohm/km]; C=8.5 [nF/km]; Length=100 [km];	Bus 1.1	Bus 1.2	
Base-Line 1.2-2.5a	Overhead Line	Impedance=0.0659+j*0.398 [Ohm/km]; C=8.5 [nF/km]; Length=300 [km];	Bus 1.2	Bus 2.5	
Base-Line 1.2-2.5b	Overhead Line	Impedance=0.0659+j*0.398 [Ohm/km]; C=8.5 [nF/km]; Length=300 [km];	Bus 1.2	Bus 2.5	
Base-Line 1.7-4.1a	Overhead Line	Impedance=0.0732+j*0.312 [Ohm/km]; C=5.73 [nF/km]; Length=150 [km];	Bus 1.7	Bus 4.1	
Base-Line 2.4-2.4.8	Overhead Line	Impedance=0.0659+j*0.398 [Ohm/km]; C=8.5 [nF/km]; Length=100 [km];	Bus 2.4	Bus 2.4.8	
Base-Line 2.4-3.6	Overhead Line	Impedance=0.0659+j*0.398 [Ohm/km]; C=8.5 [nF/km]; Length=100 [km];	Bus 2.4	Bus 3.6	
Base-Line 2.4-2.5	Overhead Line	Impedance=0.0659+j*0.398 [Ohm/km]; C=8.5 [nF/km]; Length=100 [km];	Bus 2.4	Bus 2.5	
Base-Line 2.8-4.3a	Overhead Line	Impedance=0.0732+j*0.312 [Ohm/km]; C=5.73 [nF/km]; Length=300 [km];	Bus 2.8	Bus 4.3	
Base-Line 2.8-4.3b	Overhead Line	Impedance=0.0732+j*0.312 [Ohm/km]; C=5.73 [nF/km]; Length=300 [km];	Bus 2.8	Bus 4.3	
Base-Line 3.6-3.7	Overhead Line	Impedance=0.0659+j*0.398 [Ohm/km]; C=8.5 [nF/km];	Bus 3.6	Bus 3.7	

		Length=100 [km];			
Base-Line-DC 4.4-4.5	Overhead Line	Impedance=0.1+j*0 [Ohm/km]; C=0 [nF/km]; Length=100 [km];	Bus 4.4	Bus 4.5	
Base-Line-DC 4.4-4.7	Overhead Line	Impedance=0.1+j*0 [Ohm/km]; C=0 [nF/km]; Length=100 [km];	Bus 4.4	Bus 4.7	
Base-Line-DC 4.4-4.8	Overhead Line	Impedance=0.1+j*0 [Ohm/km]; C=0 [nF/km]; Length=300 [km];	Bus 4.4	Bus 4.8	
Base-Line-DC 4.5-4.6	Overhead Line	Impedance=0.1+j*0 [Ohm/km]; C=0 [nF/km]; Length=100 [km];	Bus 4.5	Bus 4.6	
Base-Line-DC 4.6-4.7	Overhead Line	Impedance=0.1+j*0 [Ohm/km]; C=0 [nF/km]; Length=100 [km];	Bus 4.6	Bus 4.7	
Base-Line a 2.4-2.3	Overhead Line	Impedance=0.0659+j*0.398 [Ohm/km]; C=8.5 [nF/km]; Length=100 [km];	Bus 2.4	Bus 2.3	
Base-Line b 2.4-2.3	Overhead Line	Impedance=0.0659+j*0.398 [Ohm/km]; C=8.5 [nF/km]; Length=100 [km];	Bus 2.4	Bus 2.3	
Base-Trafo 1.1-1.7	Transformer	Snom=1000 [MVAr]; V1=220 [kV]; V2=400 [kV]; uk=15 [%]; X/R=150 [1]; Windings YNyn0 ;	Bus 1.1	Bus 1.7	
Base-Trafo 1.2-1.10	Transformer	Snom=1000 [MVAr]; V1=220 [kV]; V2=22[kV]; uk=12 [%]; X/R=240 [1]; Windings YNd0 ;	Bus 1.2	Bus 1.10	
Base-Trafo 1.9-1.1	Transformer	Snom=1000 [MVAr]; V1=22[kV]; V2=220[kV]; uk=12 [%]; X/R=240 [1]; Windings YNd0 ;	Bus 1.9	Bus 1.1	
Base-Trafo 1.2-1.3	Transformer	Snom=1000 [MVAr]; V1=220[kV]; V2=400[kV]; uk=12 [%]; X/R=150 [1]; Windings YNyn0 ;	Bus 1.2	Bus 1.3	
Base-Trafo 2.3-2.11	Transformer	Snom=1000 [MVAr]; V1=220 [kV]; V2=22[kV]; uk=12 [%]; X/R=150 [1]; Windings YNd0 ;	Bus 2.3	Bus 2.11	
Base-Trafo 2.3-2.8	Transformer	Snom=1000 [MVAr]; V1=220 [kV]; V2=400 [kV]; uk=15 [%]; X/R=150 [1]; Windings YNyn0 ;	Bus 2.3	Bus 2.8	
Base-Trafo 2.4-2.8	Transformer	Snom=1000 [MVAr]; V1=220 [kV]; V2=400 [kV]; uk=15 [%]; X/R=150 [1];	Bus 2.4	Bus 2.8	

		Windings YNyn0 ;			
Base-Trafo 3.7-3.12	Transformer	Snom=1000 [MVAr]; V1=220 [kV]; V2=22[kV]; uk=12 [%]; X/R=240 [1]; Windings YNd0 ;	Bus 3.7	Bus 3.12	
Base-Trafo 4.2-3.6	Transformer	Snom=1000 [MVAr]; V1=400 [kV]; V2=220 [kV]; uk=15 [%]; X/R=150 [1]; Windings YNyn0 ;	Bus 4.2	Bus 3.6	
Base-PWM 1.2	PWM converter	Modulation: Sinusoidal PWM Snom=500 [MVA]; Vacnom=400 [kV]; Vdcnom=725 [kV]; Control Mode: Vac-P 2 parallel converters	Bus 1.8	Bus 1.3	0
Base-PWM 4.1	PWM converter	Modulation: Sinusoidal PWM Snom=500 [MVA]; Vacnom=400 [kV]; Vdcnom=725 [kV]; Control Mode: Vac-P	Bus 4.4	Bus 4.1	0
Base-PWM 4.2	PWM converter	Modulation: Sinusoidal PWM Snom=500 [MVA]; Vacnom=400 [kV]; Vdcnom=725 [kV]; Control Mode: Vac-P	Bus 4.5	Bus 4.2	0
Base-PWM 4.3	PWM converter	Modulation: Sinusoidal PWM Snom=500 [MVA]; Vacnom=400 [kV]; Vdcnom=725 [kV]; Control Mode: Vac-Vdc	Bus 4.6	Bus 4.3	Master (controls Vdc and Vdc)
Base-PWM 4.8	PWM converter	Modulation: Sinusoidal PWM Snom=1500 [MVA]; Vacnom=400 [kV]; Vdcnom=725 [kV]; Control Mode: Vac-phi	Bus 4.7	Bus 4.8	Controls magnitude and angle of Vac at wind bus (4.8)

8.2 Dynamic models

8.2.1 Conventional units

Gas turbine governor (GOV_GAST): it represents the principal dynamic characteristics of industrial gas turbines driving generators connected to electric power systems. The model consists of a forward path with governor time constant and a combustion chamber time constant, together with a load-limiting feedback path. The load limit is sensitive to turbine exhaust temperature, and the time constant to represent the exhaust gas measuring system is considered.

Excitation system (AVR_EXAC1): 1981 IEEE type AC1

These models are applicable for simulating the performance of Westinghouse brushless excitation systems. They model a field-controlled, alternator-rectifier excitation system consisting of an alternator main exciter with non-controlled rectifiers. The exciter does not employ self-excitation and the voltage regulator power is taken from a source not affected by external transients. The diode characteristic in the exciter output imposes a lower limit of zero on the exciter output voltage.

8.2.2 Hydro units

Hydraulic turbine governor (HYGOV): Represents a straightforward hydroelectric plant governor, with a simple hydraulic representation of the penstock with unrestricted head race and tail race, and no surge tank.

Excitation system (AVR_EXAC1): 1981 IEEE type AC1

8.2.3 HVDC converters

The Pan-European model includes a multi-terminal HVDC (MT-HVDC) grid with five Voltage Source Converters (VSC). A suitable control strategy has to be implemented in order to control the converters of a MT-HVDC grid properly. The implemented control strategy is referred to as master/slave-control which basically consists of three different controllers:

- The master VSC converter controls the DC and the AC voltage at its terminals.
- The slave VSC converters control their active power flow and the AC voltage at their terminals.
- The converter connected to the wind farm controls the AC voltage and the frequency at the AC terminal, i.e. where the wind farm is connected.

Vdc-Vac control (master controller)

The Vdc-Vac controller is used to control the DC and the AC voltage at its terminals. The converter PWM 4.3 is operated in this control mode. DC and AC voltages are measured and compared with their set points and the id/iq current reference of the PWM converter is set accordingly.

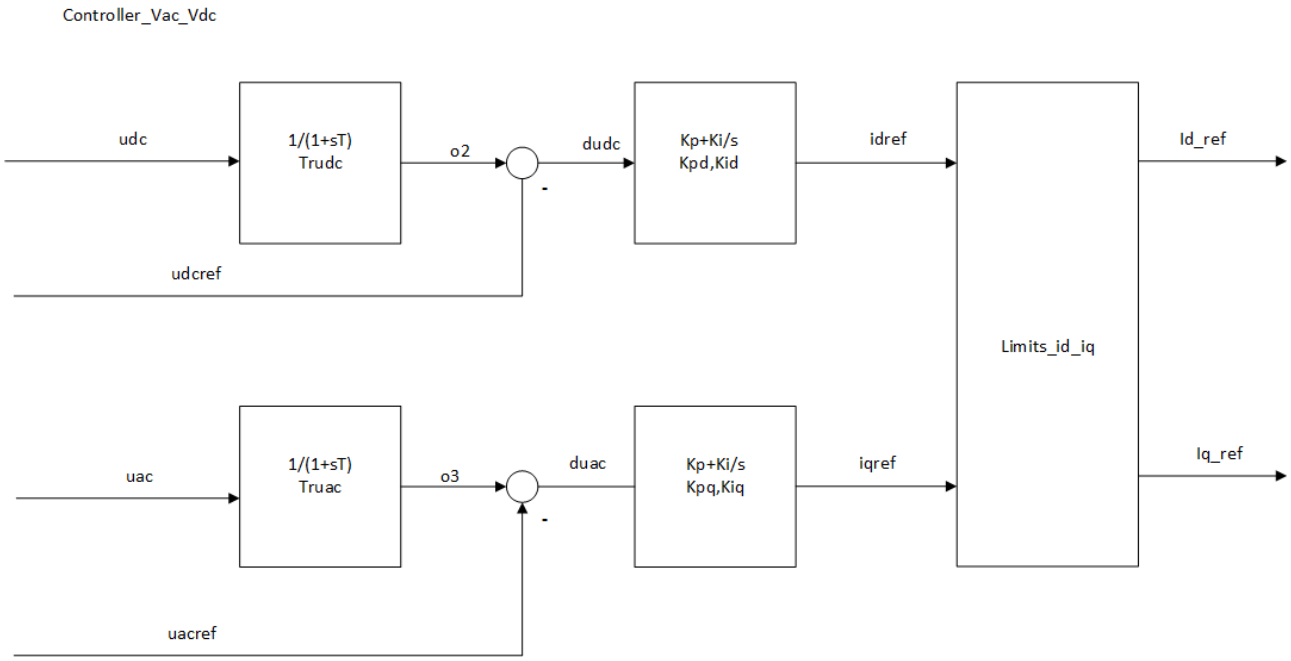

Figure 8-1 Vdc-Vac controller.

P-Vac control (slave controller)

The P-Vac controller is used to control the active power flow and the AC voltage at its terminal. The converters PWM 1.2, 4.1 and 4.2 are operated in this control mode. Active power and AC voltage are measured and compared with their set points and the id/iq current reference of the PWM converter is set accordingly.

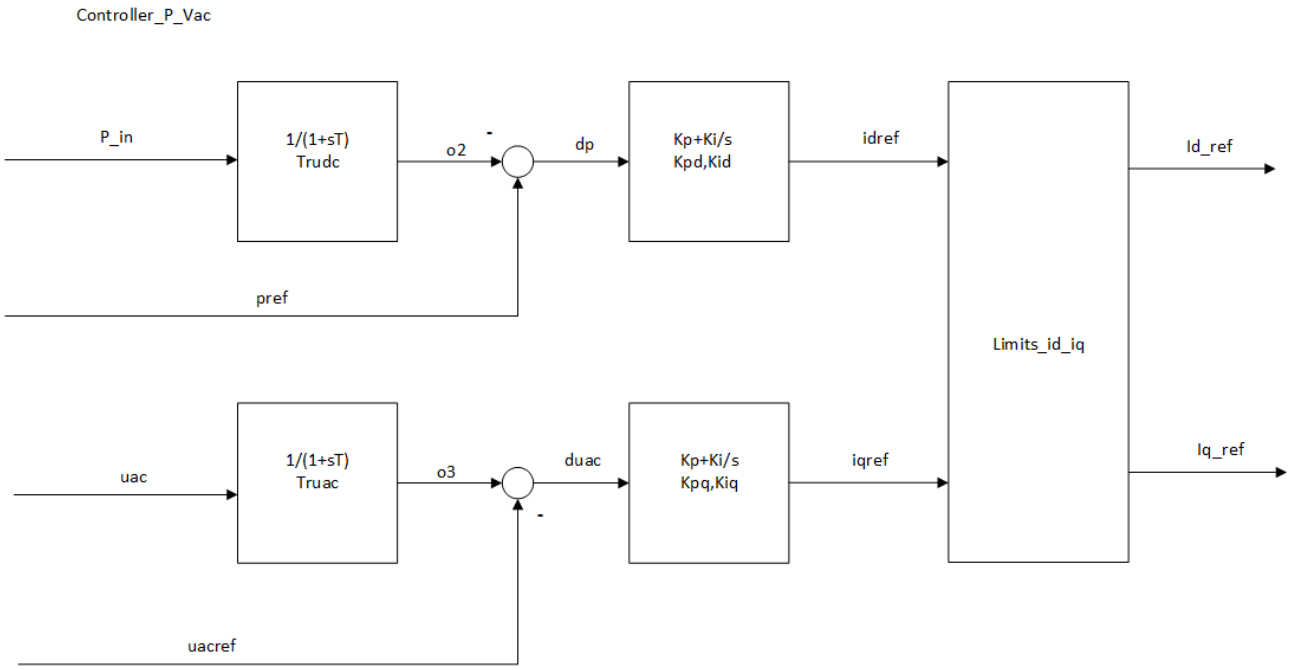

Figure 8-2 P-Vac controller.

Since the Vdc-Vac and P-Vac controllers control the id/iq currents of the PWM converters the maximum allowed current has to be limited. The maximum current is limited to 1.1 p.u. and the relation between id and iq current is shown in Figure 8-3.

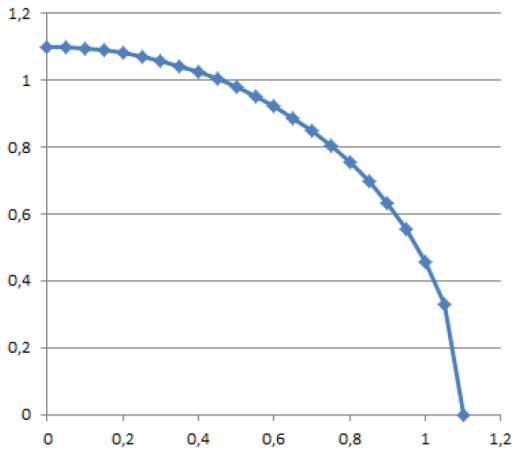

Figure 8-3 Current limit characteristic of the master/slave controllers.

Vac-frequency control

This type of control is usually used for offshore PWM converters which connect power plants (typically wind farms) with the DC grid. The AC voltage and frequency of the offshore AC grid are being controlled by the converter using a measurement of the AC voltage and comparing it to the set point and changing the iq reference current accordingly. The DC voltage is measured as well and gives another input to the controller since the AC and DC voltages are not completely decoupled from the modulation index a relation between them has to be considered.

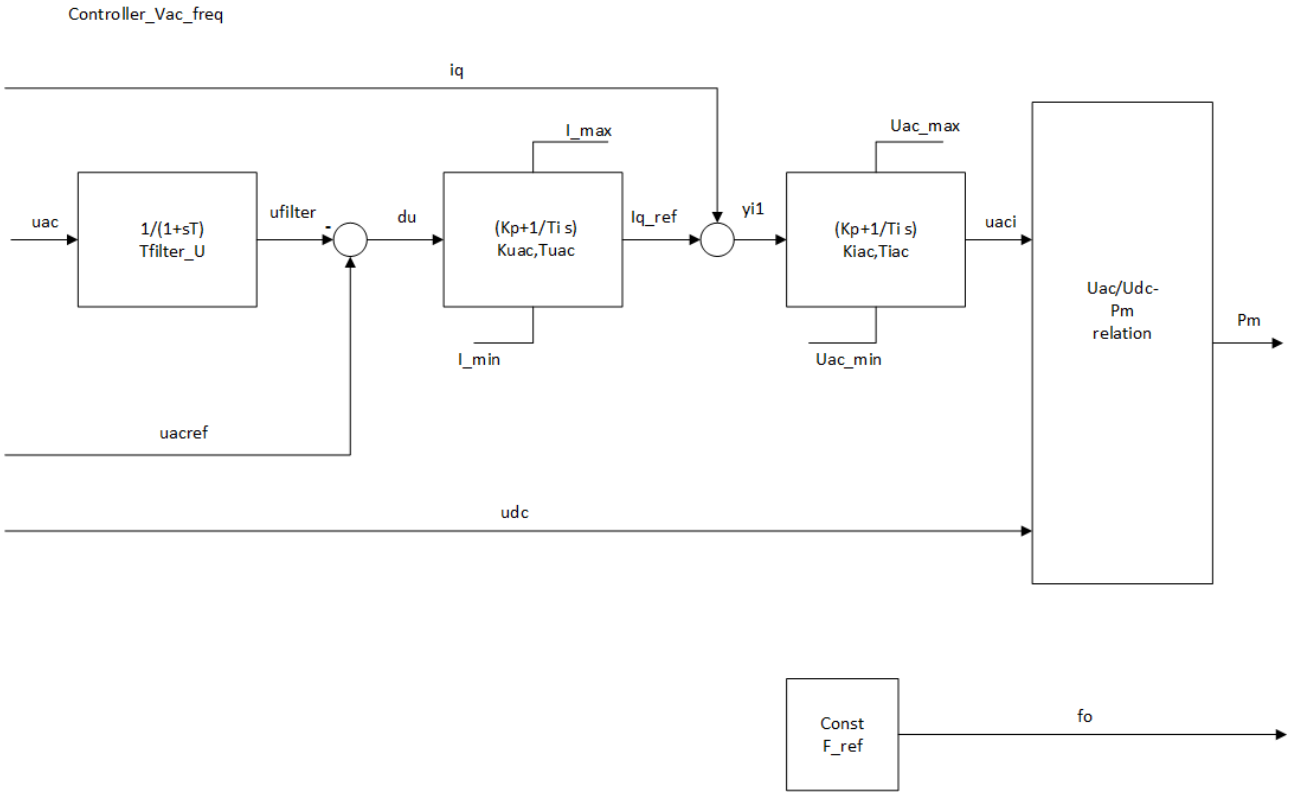

Figure 8-4 Vac-frequency controller.

The relation between the AC/DC voltage to the modulation index is shown in Figure 8-5. This relation is considered in the wind park connected controller shown above.

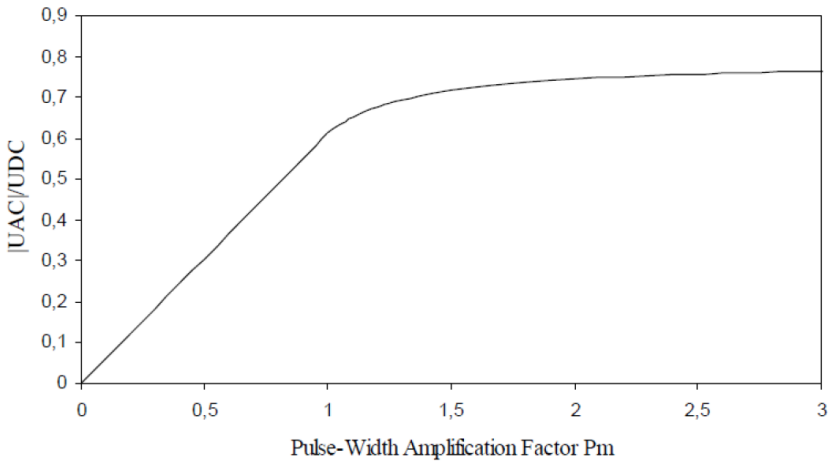

Figure 8-5 Uac/Udc - Pm relation.